Polyurethanes from Renewable Resources

Lewis Karl Williams

Department of Chemistry, University of Sheffield, Sheffield, S3 7HF, UK.

Supervisor: Prof. Anthony J. Ryan

Declaration

The work described in the present thesis was undertaken at the University of Sheffield between October of 2008 and January of 2012 under the supervision of Professor Anthony J. Ryan. Unless otherwise stated, it is the work of the author and has not been submitted in whole or in part for any other degree at this or any other Institute.

Lewis Williams

Department of Chemistry

The University of Sheffield

February 2013

Abstract

A series of polyurethane (PU) and polyurethane-urea (PUU) elastomers derived from a renewable source have been synthesised and characterised extensively. Comparisons have been made to analogous series of elastomers utilising petroleum derived diisocyanates.

The renewable elastomers utilised a difuranic diisocyanate (DFDI) derived from furfural, a readily available raw material synthesised from agricultural waste. DFDI was synthesised using a modified version of a published procedure, utilising triphosgene for the formation of the diisocyanate.

The reaction kinetics of the diisocyanates used were compared using an adiabatic temperature rise technique in both catalysed and uncatalysed reactions, showing that DFDI reacts at approximately one fifteenth the rate of MDI with primary alcohols.

The polyurethane series comprised MDI/DFDI and 1,4-butanediol (BD) hard segments (HS) and polytetrahydrofuran (PTHF) soft segments (SS) at 1, 2 and 2.9 kDa molecular weights. The PUU series utilised the 2kDa PTHF SS and the amine precursor to the diisocyanate, in effect simulating the HS produced in a water blown (polyurethane-urea) foam.

In all PU elastomers the DFDI variants displayed much greater degrees of phase separation as evidenced by lower soft segment (SS) Tgs observed by both DSC and DMTA measurements, greater invariants observed in SAXS frames, more SS crystallinity observed in WAXS data and a much more clearly defined morphology observed in tapping mode AFM images. Crystallinity within the SS was found to be much higher in DFDI based elastomers, whereas crystalline hard segments were only observed in MDI based PU elastomers and was more pronounced at higher HS contents and at lower SS molecular weights.

The PUU elastomers showed very clear morphologies in AFM images but were found to possess a lower degree of phase separation overall, agreeing with previous literature suggesting that the stronger hydrogen bonding of urea groups can hinder phase separation.

Acknowledgements

Firstly I would like to thank Tony Ryan for the opportunity to carry out a PhD in his group. His limitless enthusiasm and knowledge helped to find solutions to the most difficult aspects of this research. I would also like to thank Patrick Fairclough for advice and support throughout. Thanks are also owed to John Stanford for helpful discussions on the research and to EPSRC for funding.

Cheers to the early morning Chemistry gym team Jon, Mike and Rick for being great friends. You guys helped keep me motivated through the years.

Thank you to the doctors of the group; Andy, Christine, Linge, Pierre, and Shaomin for helping with various aspects of this research, and especially Sasha for dumbing down SAXS enough for me to understand. Andy (again) and Chris for teaching me and allowing me to use the large scale reactor.

Thanks also to:

Co-founder of the Bill Withers power hour, Adam Blanazs. Fellow members of the Ryan/Fairclough group Amy, Anne-Cecile, Babs, Chris, Gary, Josh, Masayuki, Matt, Obed, Sarah, Susi and honorary member of the group Zoë, for swinging the research/tea-drinking balance in the wrong direction.

Andy Parnell, Nic Mullin and Joe Smerdon for helping with the acquisition and processing of AFM images; Richard Wilkinson for maintaining the SAXS and WAXS machines; Dan Jackson for making multiple reactors in the glass workshop; Brian Taylor and Sue Bradshaw for keeping the NMR machines running; Rob Hanson for help acquiring DSC data; Les Morton for running DMTA experiments and Chris Hill for helping with SEM images.

I also wish to thank Emily for your patience during this endeavour, you were a welcome distraction throughout.

Finally, I owe a great deal of thanks to my family for inspiring me. I am perpetually grateful to be part of such a loving and supportive family. This thesis is for you.

Glossary of symbols and acronyms

$\langle N_n \rangle$	Number average segment length
$\langle N_w \rangle$	Weight average segment length
δ	Solubility parameter
η	Viscosity
η_x	Electron density of fraction x
φ	Volume fraction
χ	Interaction parameter
θ	Scattering angle
λ	Wavelength
ε_{12}	Energy of the interaction between species 1 and 2
1,4BD	1,4-butanediol
A_i	Molar concentration of species i
Cp	Specific heat capacity (constant pressure)
CE	Chain extender
d	Domain spacing
DFDA	Difurfuryldiamine
DFDD	Difurfuryldiamide
DFDI	Difurfuryldiisocyanate
DMTA	Dynamic Mechanical Thermal Analysis
DSC	Differential Scanning Calorimetry
E	Modulus (youngs)
E'	Storage modulus
E"	Loss modulus
EG	Ethylene Glycol (Ethane-1,2-diol)
f_n	Functionality
f_e	Weight average functionality of polyol
F	Free energy
FFA	Furfurylamine (Furan-2-ylmethanamine)
FFD	Furfurylamide

g_e	Weight average functionality of isocyanate
HDI	Hexamethylene Diisocyanate
HS	Hard segment
IPDI	Isophorone diisocyanate
k_B	Boltzmann constant
MDA	Methylene Dianiline
MDI	Methylene Diphenyldiisocyanate
M_n	Number average molecular weight
M_w	Weight average molecular weight
Mwt	Molecular weight
N_x	Repeat units of polymer x
NMR	Nuclear magnetic resonance
ODT	Order/Disorder transition
p_{NCO}	Isocyanate conversion
PEO	polyethyleneoxide
PPO	polypropyleneoxide
PSD	Power spectral density
PTHF	polytetrahydrofuran (aka. PTMEG)
PU	polyurethane
PUU	polyurethane-urea
Q	SAXS invariant
q	Heat (DSC) or Scattering vector (SAXS/WAXS)
$q_{1/2}$	Extent of reaction of chain extender (1) and polyol (2)
$s_{1/2}$	Molar ratio of chain extender (1) or polyol (2) to isocyanate
r	Stoichiometric imbalance
S	Entropy
SAXS	Small angle X-ray scattering
SPU	segmented polyurethane
SS	Soft segment
T	Temperature
t	time

tanδ	Loss factor
TDI	Toluene diisocyanate
TEA	Triethylamine
TEDA	Triethylaminediamine (DABCO)
Tg	Glass transition temperature
TGA	Thermogravimetric analysis
TPU	Thermoplastic polyurethane
U	Enthalpy
v_f	Free volume
WAXS	Wide Angle X-ray Scattering
z	Number of neighbouring sites in a lattice model

Table of Contents

Chapter 1. Introduction

Polyurethanes

Polyurethanes were discovered by Otto Bayer in Leverkusen, Germany in 1947 whilst searching for alternatives to natural rubber[1]. It was found that the polymers formed from a step growth polymerization of polyester polyols and diisocyanates could be created simply and without unwanted by-products, a distinct advantage compared to other synthetic polymers available at the time.

Since BASF and Dow introduced polyether polyols in 1957, and silicone surfactants in 1958, polyurethane became industrially viable on a large scale due to the "one-shot technology"[2]. The two component nature of the raw materials gives polyurethane an advantage over thermoplastic polymers as manufacturing costs are greatly reduced, with high pressure moulding equipment not being required.

Polyurethanes are one of the most versatile groups of polymers available. A wide range of properties can be achieved and as such polyurethanes are used to manufacture parts for many different industries. Rigid foams for insulation are produced in large volumes for the construction industry; flexible foams are commonly used in the furniture, automotive and aviation industries; elastomers, duromers, integral skin and other classes find use in many other industries.

Segmented polyurethanes (SPU) are block copolymers composed of alternating blocks of polyol and hard segment (HS) units with the general formula $-(AB)_n$, where A is a polyol residue and B is HS.

Isocyanates

Isocyanates are molecules containing the N=C=O functional group, the carbon atom is highly electron deficient due to delocalisation of electrons onto the electronegative heteroatoms (scheme 1). Isocyanates can react with any molecule containing an 'active' hydrogen atom[3] including amines, alcohols and carboxylic acids. The reactivity of the isocyanate group however can cause problems in the synthesis of diisocyanates[4], as the reaction between the amine precursor and the isocyanate product is fast.
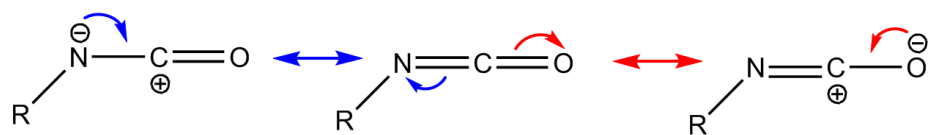
Scheme 1: The resonance forms contributing to the reactivity of the isocyanate group.

There are four popular isocyanates used industrially (as displayed in figure 1), all are diisocyanates and all are petroleum derived. Worldwide, the production of isocyanates exceeds 4 million tonnes per year; methylene diphenyl diisocyanate (MDI) accounts for >60% of the global market[5].
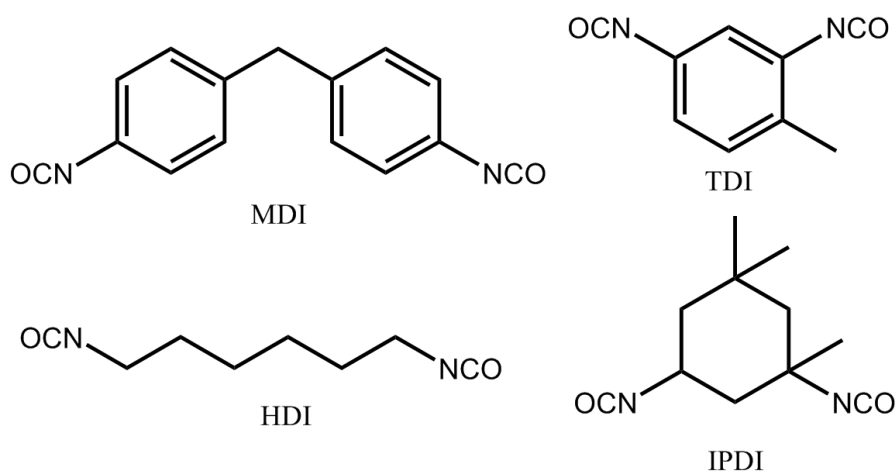
Figure 1: Structures of the most commonly used diisocyanates.

MDI is the preferred diisocyanate industrially, favoured over toluene diisocyanate (TDI) which has a higher vapour pressure. Hexamethyl diisocyanate (HDI) and isophorone diisocyanate (IPDI) are the most common aliphatic diisocyanates and are used in applications where ultraviolet stability is especially important, polyurethanes made from aromatic diisocyanates have a tendency to yellow with prolonged exposure to UV light. The colour is due to a photo-fries rearrangement of the urethane group around the aromatic ring leading to a quinone-imide structure[6].

Polyols

There are two main types of polyols used in polyurethane systems; polyetherols are preferred for most applications as polyesterols are more susceptible to hydrolysis[7]. Polyesters are used mainly in high performance elastomers as the extra carbonyl groups allow for a more polar matrix with higher intermolecular forces and the potential for strain induced crystallisation.

Polyetherols are generally manufactured by the base catalysed polymerization of ethylene oxide or propylene oxide, with low molecular weight glycols and polyols used as initiators. In the example shown in scheme 2, glycerol is used as the initiator. Potassium hydroxide deprotonates the hydroxyl groups turning them into strong nucleophiles and increasing the rate of reaction with ethylene oxide.
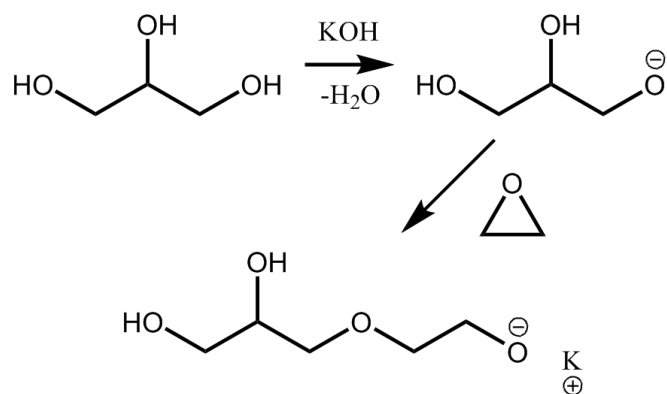
Scheme 2: Example synthesis of polyether polyols.

Another common polyether polyol used in the literature and industrially in high performance elastomers is polytetrahydrofuran (PTHF aka. PTMEG and polyTHF)[8], a polyether polyol formed from the ring opening polymerization of tetrahydrofuran. PTHF is the only common polyol from a renewable source (see scheme 3); although most of the world's supply of tetrahydrofuan is synthesised via the acid catalysed dehydration of 1,4-butanediol[9] which is predominantly petroleum derived.
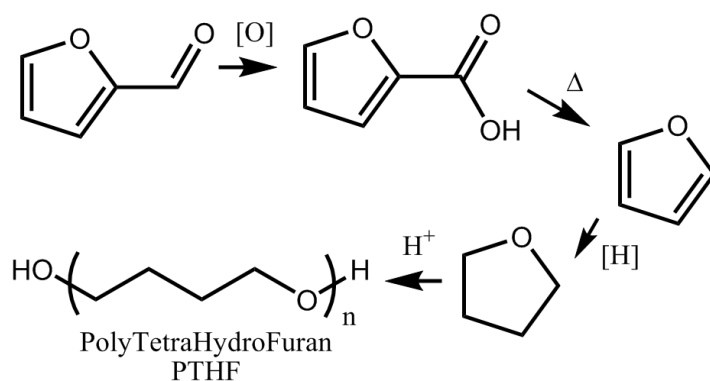
Scheme 3: Renewable source route to PTHF.

Chain extenders

Chain extenders (CE) are low molecular weight diols or diamines used to create a block

copolymer. The reaction of diisocyanate and chain extender forms the hard segment (HS) and it is the HS that gives the polyurethane its strength and modulus. The structure of hard and soft segments from a PTHF/MDI/BD elastomer are shown in figure 2.
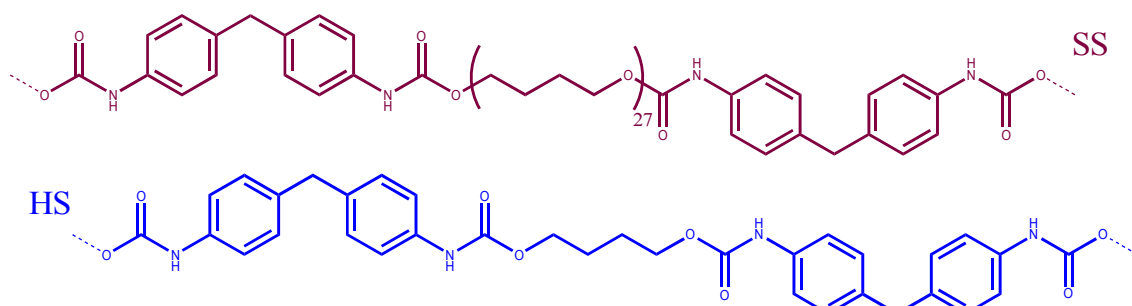
Figure 2: Hard and soft segments made of MDI and 1,4-BD (HS) and, MDI and PTHF (SS).

The HS are so called due to their Tg or Tm being well above ambient temperatures, leading to a hard glassy semicrystalline state; the SS has a sub ambient Tg leading to a softer rubbery state[10].

The HS and SS are immiscible due to difference in solubilities leading to phase separation. 1,4-butanediol (BD) and 1,2-ethanediol (EG) are two of the most common chain extenders; BD is more reactive than EG due to intramolecular H-bonding in EG, reducing the nucleophillicity[11].

Reactions

The relevant reactions of isocyanates with various reactants are outlined in figure 3. The reaction between an isocyanate and an alcohol produces a urethane bond (carbamate ester) and is catalysed by tertiary amines and organometallic compounds acting as Lewis bases. The reaction is exothermic, releasing 100 kJ mol^{-1} [12], the reaction of an isocyanate with water and subsequent reaction of a second isocyanate group with the amine product of carbamic acid decomposition (gas/blow reaction used in foams) releases 197 kJ mol^{-1} [2, 11].
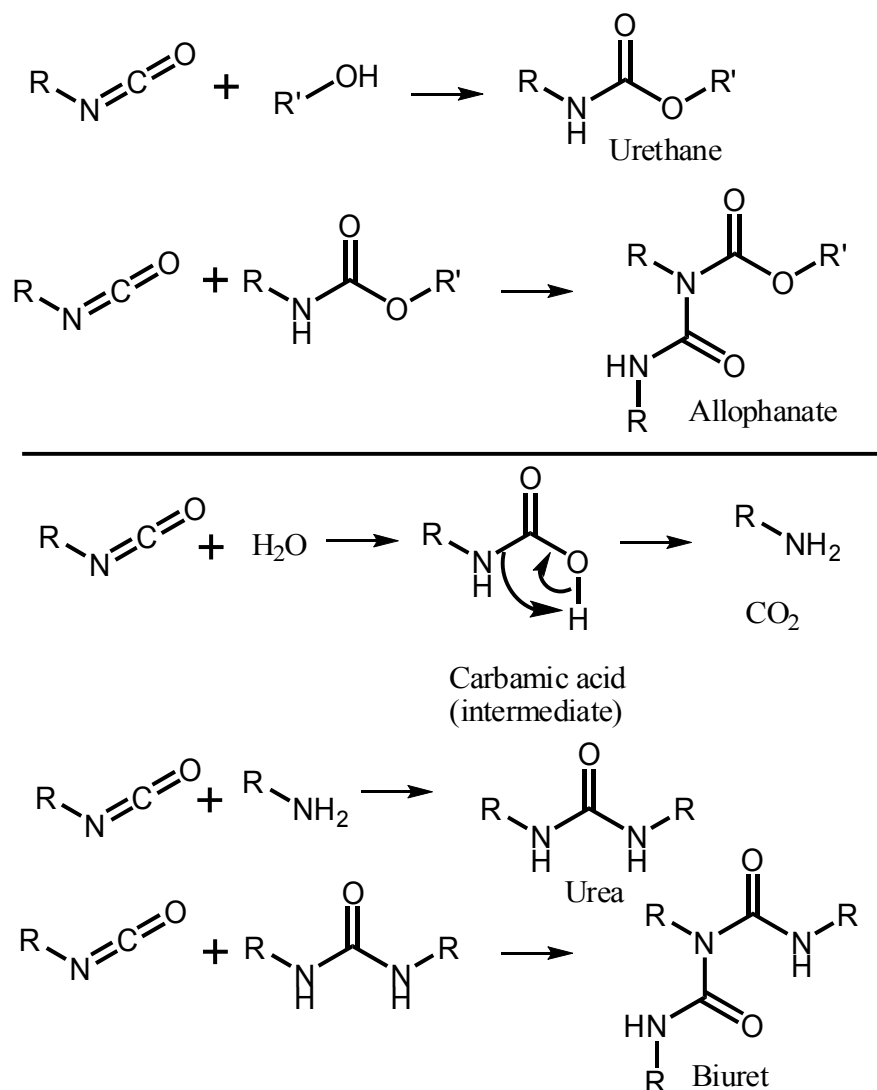
Figure 3: Multiple reaction schemes outlining the reactions of isocyanates with different reactants.

The first catalytic mechanism was proposed in 1947 by Baker and Holdsworth[13] and proceeds via reversible nucleophilic attack on the central carbon of the isocyanate to create an activated zwitterion intermediate (scheme 4). Farkas[14] proposed that the reaction proceeds via an amine activated hydrogen complex, as shown in scheme 5. Metal catalysts are thought to behave in a similar manner with mechanisms thought to involve either the formation of an activated hydroxyl or isocyanate group.
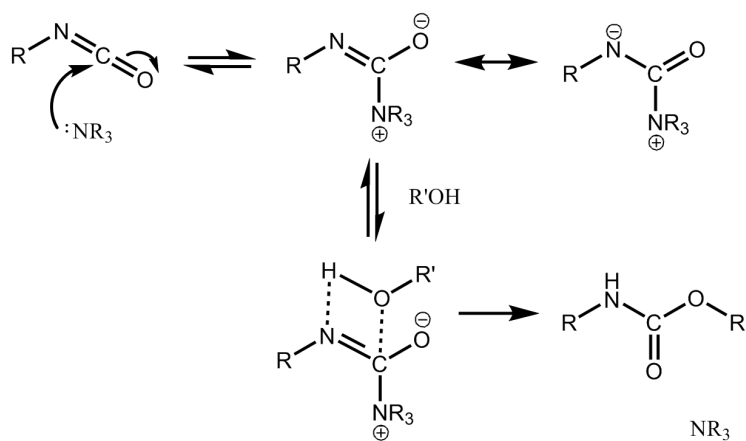
Scheme 4: Urethane formation catalysed by a tertiary amine forming a Zwitterion intermediate.
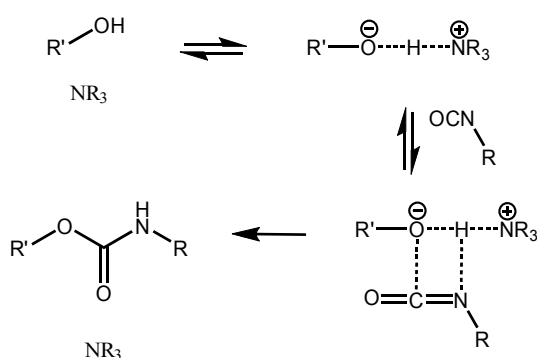
Scheme 5: Urethane formation via an amine active hydrogen complex.

A two step synthesis is utilised in the synthesis of SPU to produce a polymer with a narrower segment length distribution of hard blocks[15], which ultimately leads to a greater degree of phase separation.

In the first stage, a pre-polymer is formed by the reaction between a polyol and an excess of diisocyanate; for more efficient processing in industry, most two part polyurethane systems utilise isocyanate end-capped pre-polymers synthesised in advance on a large scale.

The second stage (known as chain extending) is when the polymer becomes a segmented block copolymer due to the reaction of chain extenders with pendant (and any monomeric) isocyanate groups to form hard segments.

Additives

PU foam is made by including a blowing agent (either chemical (water) or physical (low boiling solvents)) to create bubbles of gas which "blow" the forming polymer into

a foam during cure. Even PU systems containing no blowing agents often contain micro-bubbles formed from the reaction of small amounts of water with isocyanates to produce carbon dioxide. It is sometimes necessary to include a moisture scavenger such as zeolite powder to prevent any water present from reacting with the isocyanate.

Defoaming agents are often employed to inhibit nucleation of bubbles; defoamers are generally organically modified polysiloxanes and function due to their positive entering and spreading coefficients, making them enter the foam struts and spread, displacing any foam stabilizing surfactants present.

Renewable components

Throughout industry, most polymers are created using monomers derived from petroleum based feedstocks, the escalating use of oil for energy and other uses coupled with the knowledge that as a source it is finite has led to research in renewable sources of monomers[16].

Common renewable forms of polymers include natural rubber, shellac, amber and cellulose. While some oil derived synthetic polymers have incorporated natural components, the bulk of material continues to come from oil. Research into polymers based on renewable sourced monomers and oligomers has not been pursued with as much vigour as renewable sources of energy, despite the time frame of its validity as a method being the same.

Polyurethanes are for the most part produced from oil derived components. Castor oil, a triglyceride with three secondary hydroxyl groups per molecule has been used in some elastomer systems but its use is not widespread due to a low hydroxyl number and the low reactivity of secondary hydroxyls.

The research into vegetable oils in segmented PU began in the 1960's[17], since then many oils have been considered including safflower, sunflower, soybean and castor oils. Work carried out in this lab[18] using a natural oil polyol from soybeans has produced feasible elastomers and flexible foams.

Some triglycerides like those from castor oil naturally have hydroxyl groups on the fatty acid chain, others must be converted chemically. Common methods of introducing hydroxyl groups include epoxidation and hydroformylation of alkenes[18a, b] present in

unsaturated fatty acids as outlined in figure 4.
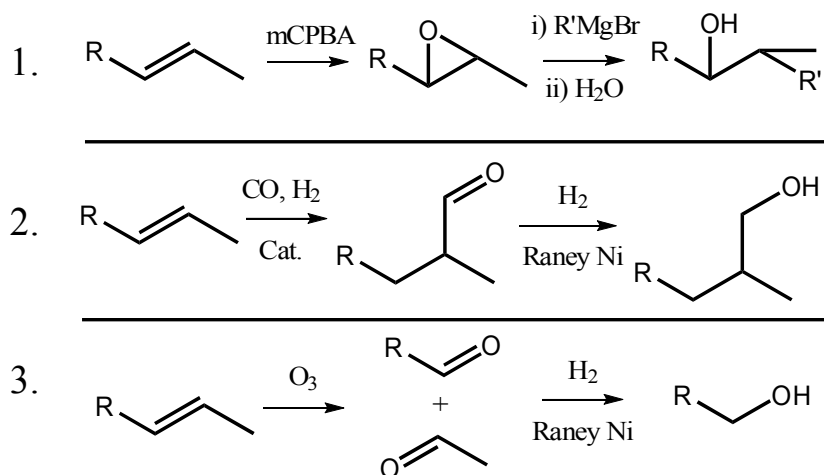
Figure 4: Methods of hyrdoxyl formation from alkenes by, 1. the epoxidation 2. hydroformylation and 3. ozonolysis routes[18a, b].

Research into furanic based monomers is a common theme in renewable polymers due to the availability and low cost of furfural, which may be obtained from boiling oat husks, corn cobs and other hemicellulose containing plant materials, with sulphuric acid.

Most of the research into using furanic monomers in PU has been carried out by two groups[19]. Much of the research into furanic polymers and renewable derived polymers in general within the last 20 years has been carried out by Gandini who published a review of furan containing polymers in 1997[20] and whose group has published many papers on renewable derived variants of common industrially used polymers[19c-f, 21].
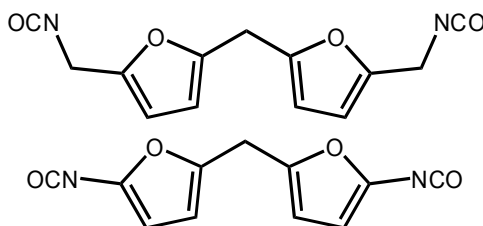
Figure 5: The structure of the diisocyanates synthesised by Cawse[19a, b].

Before Gandini began his work, Stanford and Cawse[19a, b, 22] had already pioneered the use of furanic monomers in polyurethane. The two diisocyanates synthesised and used in their research are shown in figure 5, and of these the topmost structure (5,5'-methylenebis(furan-5,2-diyl)dimethaneisocyanate, a difuranic diisocyanate and henceforth referred to as DFDI) is the subject of this research.

Cawse[19a] synthesised a range of segmented PU elastomers using these diisocyanates in 1984, preliminary studies found that polymers formed from these furanic diisocyanates were observed to gel approximately ten times faster than MDI based polymers. The furanic diisocyanate without the methyl group separating the NCO group from the furan ring (the bottom structure in figure 5) was found to be highly reactive and was not deemed viable for use in the synthesis of PU elastomers due to the tendency to form insoluble precipitates in the reaction mixture.

A study into the properties of elastomers based on these furanic diisocyanates and the kinetics of the isocyanate/alcohol reaction was published the same year[19b]. Kinetics were studied based on the method of Burkus and Eckert[23] in which polymerizations were carried out in toluene at 40°C using triethylamine (TEA) or triethylenediamine (TEDA) as the catalyst. Reaction progress was monitored by quenching aliquots with dibutylamine and carrying out a standard back-titration with HCl to determine NCO content. DFDI was reported to have reactivity between that of conventional alkyl and aryl diisocyanates, with the rational being that the methyl separation from the furan ring was not enough to completely shield the isocyanate group from the electron withdrawing effects of the aromatic ring. Elastomers were synthesised using a PTHF SS and a BD chain extender, producing polyurethane (potentially) solely derived from a single natural source material.

Gandini's group[19e] synthesised a range of furanic monomers (both hydroxyl and isocyanate functional) including a variant of DFDI synthesised using acetone in the ring fusing step (more detail on this later in chapter 3), leading to double methyl substitution on the bridging methyl group. Polyurethanes synthesised using these monomers were studied and the kinetics of the various NCO/OH reactions were assessed. In agreement with previous work, the disubstituted version of DFDI was found to have reactivity between that of common aromatic and aliphatic diisocyanates.

Molecular weight growth

The extent of reaction (p) and the stoichiometric ratio (r) (defined in equations 1 and 2) can be used to calculate the chain length and therefore molecular weight of polymers formed from the step growth polymerisation of diisocyanates and polyols[24].

$$p = \frac{[NCO]_0 - [NCO]_t}{[NCO]_0} \tag{1}$$

$$r = \frac{[NCO]_0}{[OH]_0} \tag{2}$$

Flory[25] and Stockmayer[26] were the first to derive expressions to calculate the number average molecular weight (M_n) of polymer systems, though intramolecular reactions were not considered.

Macosko and Miller[27] later derived expressions (equations 3 and 4) to predict the number average and weight average (M_w) molecular weight of a polymer, accounting for intramolecular reactions by approaching the problem using probability arguments and taking into account the recursive nature of the system.

$$M_n = \frac{rM_1 + M_2}{1 + r - 2rp} \tag{3}$$

$$Mw = \frac{r(1 + rp^2)M_1^2 + (1 + rp^2)M_2^2 + 4rp\, M_1 M_2}{r(M_1 + M_2)(1 - rp)^2} \tag{4}$$

Where $M_{1/2}$ is the molecular weight of the species involved.

When crosslinking species (functionality (f_n) greater than two) are involved the expression may be modified to take account of branching and remains valid so long as all groups (i.e. all OH groups on an f_n functional polyol) are equally reactive[27], to give:

$$Mw = \frac{r(1 + (f_n - 1)rp^2)M_1^2 + 2(1 + rp^2)\dfrac{M_f^2}{f_n} + 4rp\, M_1 M_f}{\left(rM_1 + \dfrac{2M_f}{f_n}\right)(1 - (f_n - 1)rp^2)} \tag{5}$$

Where f_n is the functionality of the polyol species and M_1/M_f are the molecular weights

10

of the isocyanate and polyol (multifunctional) species respectively. The denominator causes divergence at the gel point due to the term $1-(f-1)rp^2$, as $(f-1)rp^2$ exceeds 1 later in the reaction.

Based on that understanding, simplified relations to predict the gel point of a system may then be found. For systems utilising pure A and B components:

$$(rp^2)_g = \frac{1}{f-1}$$

$$p_g = \sqrt{\frac{1}{r(f-1)}}$$

(6)

and for systems where blended components are used (ie. real systems where the polyol component is likely to contain polyols of different functionalities):

$$(rp^2)_g = (p_{NCO} p_{OH})_g = \frac{1}{(f_e-1)(g_e-1)}$$

$$p_g = \sqrt{\frac{1}{r(f_e-1)(g_e-1)}}$$

(7)

Where f_e and g_e are the weight average functionalities of the polyol and isocyanate components found by:

$$f_e = \frac{\sum f_i^2 A_{fi}}{\sum f_i A_{fi}}$$

(8)

Where f_i and A_{fi} are the functionality and molar concentration of component i.
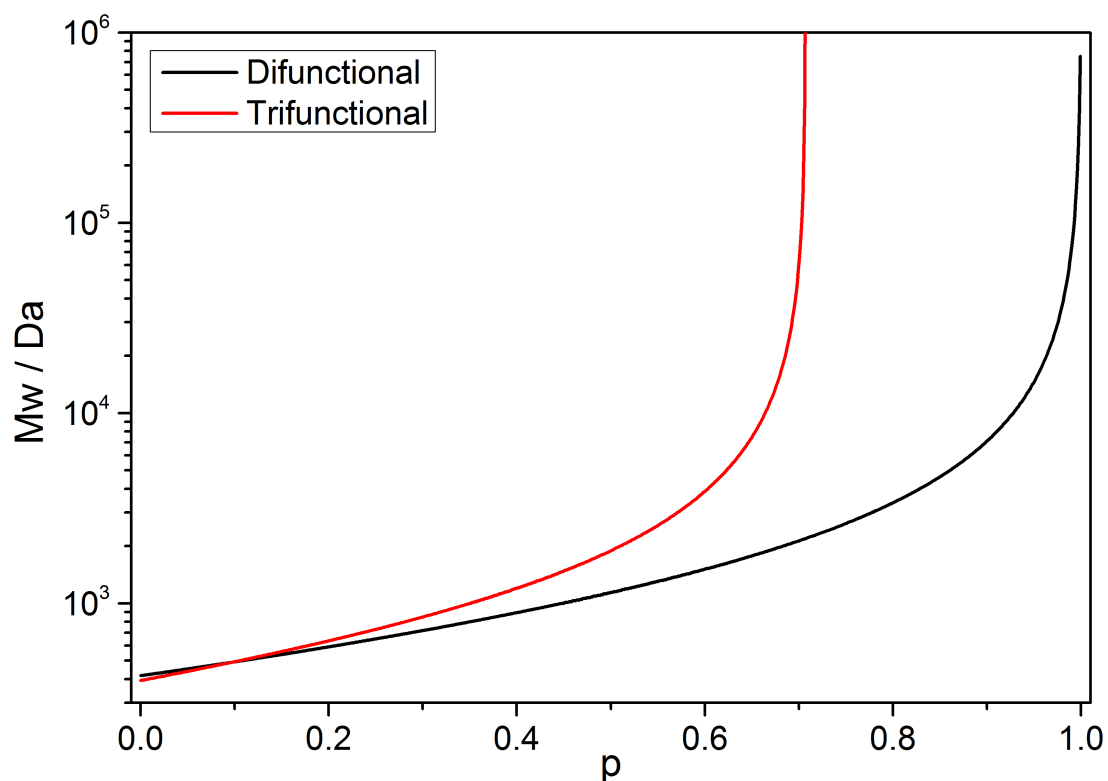
Figure 6: Weight average molecular weight growth for a 500 Da diol and triol based systems as calculated by equations derived by Macosko and Miller[24] when r=1.

Figure 6 shows calculated weight average molecular weights for 500Da diol and triol soft segment systems reacted with MDI (Mwt =205.25) against isocyanate conversion. Note that M_w is dominated by the low number of high Mwt species whereas M_n is dominated by the greater number of lower Mwt oligomers.

Segment length

The segment length is an important value to consider when investigating the structure and structure property relations of block copolymers.

The segment length (number and weight average) can be calculated with equations derived by Lopez-Serrano et. al.[28] based on two assumptions.

1. Functional groups are equally reactive, and

2. Rates of reaction of CE and polyol are equal.

The molar ratio of CE to diisocyanate, and extent of CE reaction then become the only variables.

$$\langle Nn_{HS}\rangle = \frac{1}{1-s_1 q_1^2} \qquad \langle Nw_{HS}\rangle = \frac{1+s_1 q_1^2}{1-s_1 q_1^2}$$

$$\langle Nn_{SS}\rangle = \frac{1}{1-s_2 q_2^2} \qquad \langle Nw_{SS}\rangle = \frac{1+s_2 q_2^2}{1-s_2 q_2^2}$$

(9)

Where $\langle Nn\rangle$ and $\langle Nw\rangle$ are the number and weight average segment lengths, respectively, s_1 and s_2 are the molar ratios of chain extender to isocyanate and polyol to isocyanate, respectively, and q_1 and q_2 are the extents of hydroxyl reaction of chain extender and the extent of polyol hydroxyl reaction, respectively.

Isocyanate functional group conversion p can then be found from the sum:

$$p = s_1 q_1 + s_2 q_2$$

(10)

The isocyanate conversion can be followed experimentally using a variety of techniques, but q_1 and q_2 are not as simple to determine due to the similarity in structures of polyols to common chain extenders used. Estimations can however be made using known rate constants for the monomers used.

Phase separation

Segmented polyurethanes have long been known to possess a phase separated morphology[29] driven by the difference in solubility of the hard and soft segments. Both continuous soft and hard segment phases have been reported; the discrete phases formed are usually in the order of tens of nanometres, with spacing being governed by the length of the blocks.

The fact that morphology is observed is evidence that thermodynamic equilibrium is not achieved. The resulting structure is a product of thermodynamics fighting against unfavourable kinetics[30]. Although microphase separation does occur in PU, materials with a regular structure over more than five morphological repeats are not observed[31]. This is due to the high viscosity of the system which limits mobility of the macromolecules.

In the pre-polymer route, hard segments are initially soluble in the SS matrix; but as the segment length increases (addition of more chain extender and isocyanate monomer units) so does the immiscibility.

Phase separation is arrested at the Berghmans point, which is the point of gelation and is a consequence of molecular weight growth, crosslinking and interactions between sections of the polymer backbone (including π-π stacking interactions if an aromatic isocyanate or chain extender is used and hydrogen bonds which are stronger in urea HS). A sharp increase in viscosity at the gel point (η increases from approximately 10 to 10^4 Pa s) will directly result in a rapid decrease in the rates of diffusion and therefore further association of HS into HS rich phases[32].

Tri and higher functionality polyols result in a partially restricted microphase separation due to gelation occurring sooner as seen in figure 6 (p12). Any present biuret or allophanate also results in a chemical crosslink, which can disrupt ordering in hard segments[28b].

For separate phases, the free energy of a two component system (where components are A and B), is F_A+F_B. The free energy of mixing is therefore the difference between free energy of the mixed system (F_{A+B}), and the unmixed components[33].

$$F^m = F_{A+B} - \left(F_A + F_B \right)$$
(11)

For mixing to occur, the free energy of mixing (F^m) must be ≤ 0, and can be calculated by:

$$\Delta F^m = \Delta U^m - T \Delta S^m$$
(12)

Where ΔF^m is the change in internal energy associated with mixing, T is temperature, ΔU^m is enthalpy changeand ΔS^m is the change in entropy change associated with mixing.

Using the Boltzmann formula to predict the entropy per site in a lattice model when two types of moiety are present, it can be shown (assuming sites are independent) that[33]:

$$S^m = -k_B \left(\phi_A \ln \phi_A + \phi_B \ln \phi_B \right) \tag{13}$$

Where ϕ is the volume fraction (ϕ_A is therefore the probability that a site in a lattice model is occupied by a molecule of the A type) and k_B is the Boltzmann constant. Entropy is therefore governed by the volume fractions of the components and the probabilities involved with filling a lattice model with those components, as expected, a mixture approaching purity experiences a decrease in entropic benefit.

The internal energy takes into account the interactions between the components using the interaction parameter (χ). χ is defined as the energy change when one molecule of type A is introduced into an environment of pure B type. Thus energy of mixing is the product of χ and the volume fractions of A and B.

$$U^m = \chi \phi_A \phi_B \tag{14}$$

χ describes the strength of interaction between the different species relative to interactions with themselves.

$$\chi = \frac{z}{2k_B T} \left(2\epsilon_{AB} - \epsilon_{AA} - \epsilon_{BB} \right) \tag{15}$$

Where z is the number of neighbouring sites, and ϵ is the energy of interaction between two neighbouring species. The energy of interaction and the number of sites are constant in a system, χ can therefore be seen as a temperature dependent constant.

Combining equations 13 and 14 with equation 12, it can be seen that F_{mix} is dependent on concentration, temperature and χ, where χ is itself a function of temperature.

$$F_{mix} = \left(\phi_A \ln \phi_A + \phi_B \ln \phi_B + \chi \phi_A \phi_B \right) k_B T$$

$$\frac{F_{mix}}{k_B T} = \phi_A \ln \phi_A + \phi_B \ln \phi_B + \chi \phi_A \phi_B \tag{16}$$

A plot of free energy of mixing per site vs. volume fraction (from Eq 16) shows how

different compositions are likely to fare when mixed. For values of χ less than two (figure 8) there is a single trough at $\phi=0.5$, but for values of χ greater or equal to two (figure 7) there is a peak at $\phi=0.5$ and two troughs either side[33].
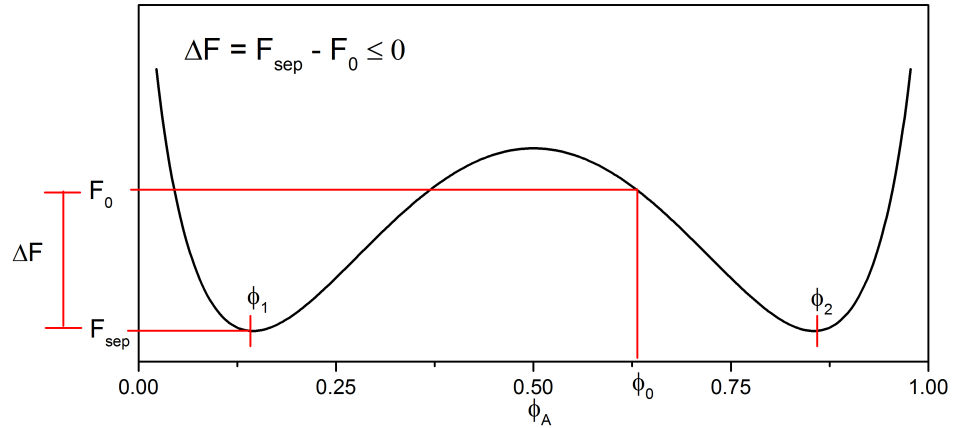
Figure 7: Free energy of mixing as a function of composition when $\chi=2.5$

Interpreting graphically, it is easy to understand how free energy governs phase separation. When $\chi \geq 2$ a mixture of initial concentration ϕ_0 can separate into two phases of concentrations ϕ_1 and ϕ_2, this is accompanied by a $\Delta F < 0$. However when $\chi < 2$, F_{sep} will always be higher than F_0 and ΔF will therefore be >0.

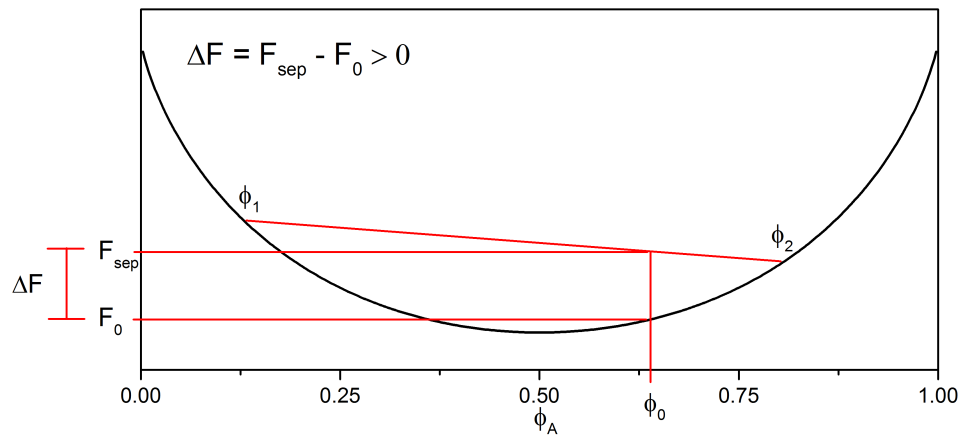*Figure 8: Free energy of mixing as a function of composition when $\chi= 1$*

Using the Flory-Huggins relation, the onset of phase separation with regards to chain length may be calculated[34].

$$X_c = \frac{1}{2}\left(\frac{1}{\sqrt{N_A}} + \frac{1}{\sqrt{N_B}}\right)^2$$

(17)

Where χ_c is the critical solubility parameter and N_x is the number of repeat units within a chain (normalised for the molar volume of one of those repeat units). Values of χ_c obtained from the Flory-Huggins relation are valid for dilute solutions, however modifications must be made to account for interactions in block copolymers. χ_c may then be compared to a value of the interaction parameter of the system, as calculated by using the Hildebrand-Scratchard equation.

$$\chi_{HS} = \frac{V_R}{RT}(\delta_A - \delta_B)^2$$

(18)

Where V_R is the molar volume and $\delta_{A,B}$ are the solubility parameters of the components.

In 1980, Leibler[35] published a "statistical theory of phase equilibria" in which the onset of phase separation within an AB copolymer was predicted using the product χN and f, the fraction of monomers on a chain.

Benoit and Hadziioannou[36] later developed a general theory to predict the scattering profiles of of multi-block copolymers. The curve for an $(AB)_n$ polymer when n=1, matches that derived by Leibler[35]. As n increases, the critical value of χN increases (less significantly so with each integer that n increases by).

As polymerization proceeds the increase in chain length corresponds to an increase in N, driving the separation from a homogeneous (disordered) to a microphase-separated (ordered) state (increasing the value of the ordinate). The morphology is determined by competition between kinetics of polymerization and phase separation[33].

Figure 9 may be used to roughly predict whether a polymer is likely to undergo phase separation. Using a series with a controlled HS% but an increasing SS Mwt (covered in chapter 5); compared to a 1kDa Mwt SS, the 2kDa Mwt PTHF SS has a significantly greater value of $\chi(N_A + N_B)$ due to the doubling of the N_A value. Fittingly, all results indicate a greater degree of phase separation exists in these polymers.
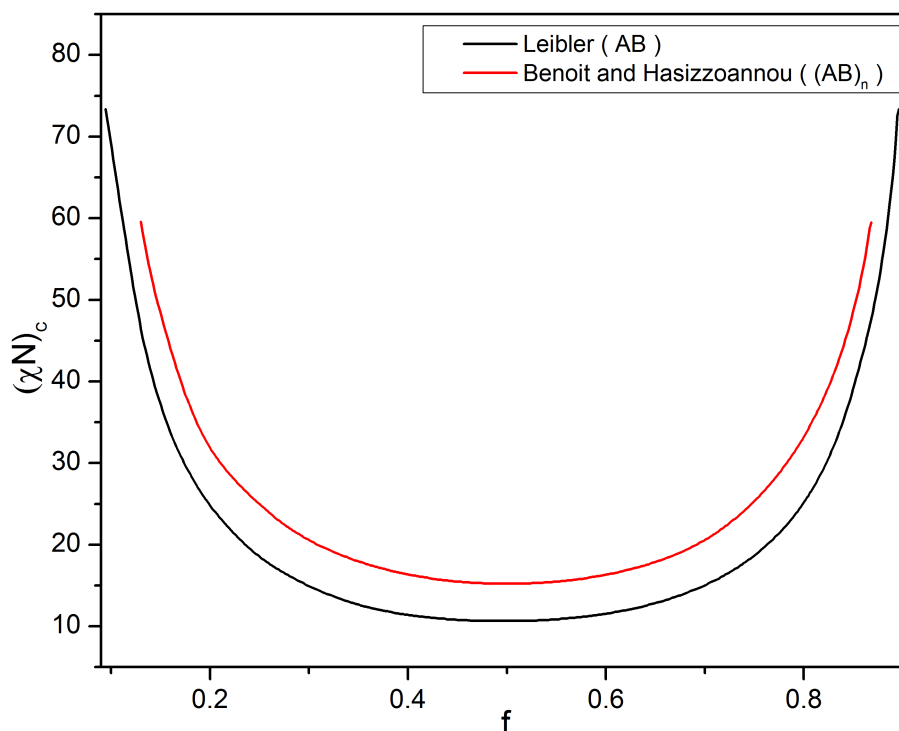
Figure 9: Critical χN products as derived by Leibler[35] (for AB); and Benoit and Hadziioannou[36] (for (AB)ₙ).

Other considerations

The reaction between amines and isocyanates form urea groups which are strongly hydrogen bonding and more immiscible with polyether SS than urethane groups[37]. Segmented polyurethane-ureas may display different degrees of phase separation depending on whether their cohesive hydrogen bonds have limited mobility within the system and hindered association of urea groups into hard domains. Using a polyester polyol SS generally leads to a lower degree of phase separation due to polar ester groups present in the soft segment reducing the interaction parameter (lower χ).

In 1995, Bras et. al.[38] sought to determine whether phase separation was driven by hydrogen bonding between hard segments or the thermodynamics of phase separation. Using simultaneous synchrotron SAXS and FT-IR spectroscopy, the time resolved structure development of polyurethane was studied. Isocyanate conversion monitored by IR showed 2nd order kinetics until 50 minutes. A peak observed in a (Lorentz-corrected) plot of intensity vs. q from the SAXS experiment showed a peak growing from 40 minutes onwards at $q^* = 0.053$ Å^{-1}. Tangents fitted to lines of relative invariant (SAXS) and relative absorbance (IR) showed the onset of microphase separation and hydrogen

bonding with the former preceding the latter by 4 minutes. The results showing clearly that two phase systems that can hydrogen bond are not necessarily in a single phase if no hydrogen bonding is observed by IR spectrometry. The driving force for structure development in polyurethanes is therefore the thermodynamics of phase separation rather than hydrogen bonding[38].

Aims

- Modify the synthesis of DFDI to increase the safety of the carbonylation step.

- Study the kinetics of Isocyanate reaction for DFDI, and compare to MDI.

- Prepare segmented polyurethanes utilising MDI/DFDI, PTHF and butanediol with varying SS Mwt and HS wt%.

- Prepare polyurethane-ureas utilising MDI/DFDI, PTHF and the diamine precursor to the diisocyanate.

- Investigate the structure-property relations in PU and PUU by carrying out AFM, DMTA, DSC, SAXS, WAXS and TGA.

Chapter 2. Theory and Experimental

Chemicals

Polyols

1000, 2000 and 2900 Da Mwt polytetrahydrofuran (Terathane from Invista) were purchased from Sigma. They were dried in a rotary evaporator at 80ºC for two hours and stored over 4Å molecular sieves to remove traces of water before use. Purity was assessed by ^{1}H-NMR and the equivalent weight was determined by end group analysis.

Isocyanates

Methylene diphenyl diisocyanate (MDI) (98%) was purchased from Sigma and used as-received. Purity was assessed via ^{1}H-NMR and melting point analysis.

The difuranic diisocyanate (DFDI) was synthesised, with a detailed account of reagents and conditions being reported in the following chapter.

For the synthesis of DFDI

Furfurylamine (≥99%) was purchased from Sigma and used as-received, older samples which had turned yellow were distilled before use. Purity was assessed by ^{1}H NMR.

Triphosgene was purchased from Fluorochem and used as-received. Purity was assessed by ^{1}H NMR (the absence of protons was indicative of a pure sample).

Chain extenders

1,4-butanediol was purchased from Sigma and stored over 4Å Molecular sieves prior to use, purity was assessed via ^{1}H-NMR.

MDA was purchased from Alfa-Aesar and used as-received, purity was assessed via ^{1}H-NMR.

DFDA was synthesised as an intermediate leading to the synthesis of DFDI, a detailed outline of synthesis and purification is given in chapter three.

Determination of polyol equivalent weight
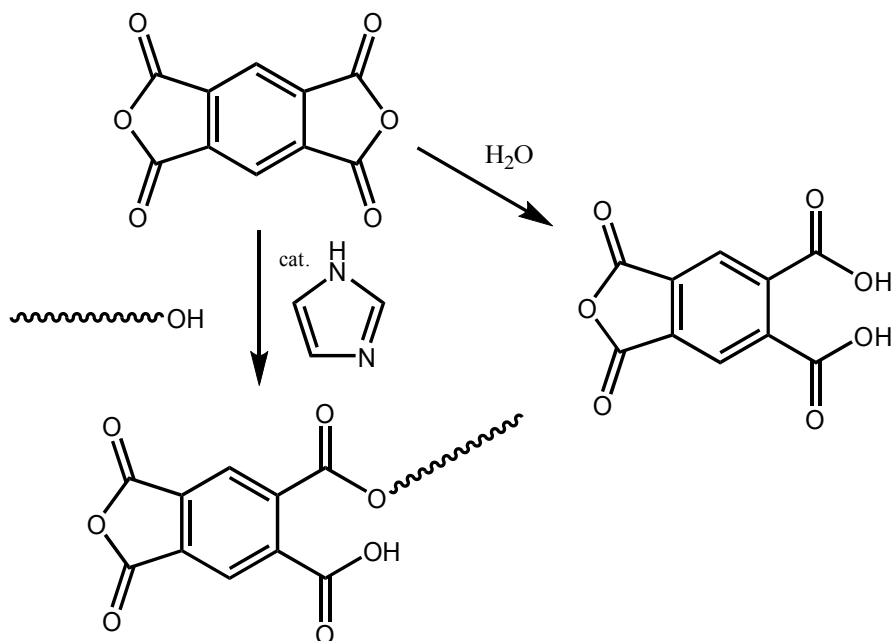
Scheme 6: Reaction scheme showing the formation of acid groups to titrate against.

The equivalent weight of hydroxyl-containing compounds was calculated based on the method described in the ASTM reference D4274-88[39]. Pyromellitic anhydride was used to esterify hydroxyl groups using imidazole as a catalyst (see scheme 6). The solution was then back titrated against NaOH to a phenolphthalein end-point.

Solutions of pyromellitic anhydride (PMA) and imidazole (1.54M) in dry DMF were prepared. The concentration of PMA depend upon the polyol being investigated (the excess of anhydride to hydroxyl groups should be approximately threefold), 2kDa PTHF called for a solution that was 0.23M in PMA.

PTHF (c.6g) was weighed into four conical flasks, 40ml and 10 ml of the PMA and imidazole solutions (respectively) were added to the four polyol flasks (and to four empty flasks that act as controls) using a graduated pipette, flasks were sealed with ground glass stoppers.

Solutions were heated to 80ºC and stirred with a magnetic stirrer for 15 minutes, after which 75cm³ of deionised water and ten drops of phenolpthalein solution (1% in MeOH) were added.

Solutions were titrated with 1M NaOH to a pink end-point (the pink colour can decay if solutions are not stirred and mixtures are non-homogeneous). Equivalent weights were

calculated using equation 19.

$$En_{poly} = \frac{1000\,m}{M(B-A)} \tag{19}$$

En_{poly} is the polyol equivalent weight (Mwt over functionality), M is molarity of the NaOH solution, B is the average titre of the background flasks and A is the titre value of the polyol containing flask. The reported equivalent weight is the average of three concordant results.

Pyromellitic anhydride, imidazole and HCl were purchased from Sigma Aldrich and used as-received.

Determination of NCO content
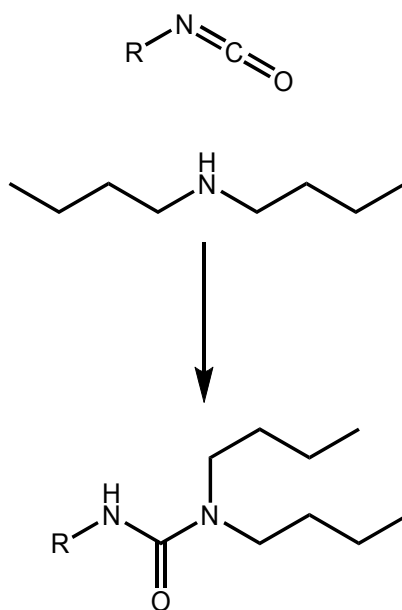
Scheme 7: Formation of urea groups and thus reduction of free base to titrate against.

The equivalent weight of the diisocyanates studied were determined by a back titration method commonly applied to isocyanates[28b] based on one of the test methods described in ASTM D5155[40]. Dibutylamine reacts with isocyanate (as seen in scheme 7) thus reducing the amount of free base.

Diisocyanate (c.0.3g) was accurately weighed into four conical flasks. 25cm^3 of a di-n-butylamine solution (3% in butanone) was added along with four portions into empty conical flasks (background flasks), all flasks were fitted with ground glass stoppers. The

flasks were stirred with a magnetic stirrer at room temperature for 30 minutes, after which 25cm^3 of isopropanol (IPA allows butanone and water to be miscible) and three drops of bromocresol green (1% in EtOH) were added.

Samples were titrated to a pale yellow end-point using 0.1M HCl. The equivalent weight was calculated using equation 20.

$$En_{ISO} = \frac{1000\,m}{M\,(B-A)}$$

(20)

Where En_{ISO} is the equivalent weight, m is the mass of diisocyanate, M is the molarity of HCl, B is the average titre of the background flasks and A is the titre value of the isocyanate containing flask. The reported equivalent weight is the average of three concordant results.

Di-n-butylamine, butanone, isopropanol and HCl concentrate (for making a 0.1M solution) were purchased from Sigma Aldrich and used as-received.

Synthesis of elastomers

Elastomers were formed via a standard pre-polymer route in order to give control over the hard segment segment length. This allowed the formation of strong, rubbery and phase separated elastomers[19b]. Polyol was chain extended in step one with all of the isocyanate required to react with the CE added in the second step (the product formed in this kind of reaction is sometimes referred to as a quasi-prepolymer in industry). The overall stoichiometry used in all reactions was one, with $n_{NCO}=n_{OH}$ and $n_{NCO}=n_{OH}+n_{NH}$.

In a two neck round bottomed flask, room temperature MDI flakes (or liquid RT DFDI) were accurately weighed, followed by molten PTHF. The polyol and isocyanate were mixed for two hours at 80°C (four hours at 80°C for DFDI elastomers) under an inert atmosphere using a magnetic stirrer (care was taken to use a strong magnet as viscosity can hinder stirring). The pre-polymer was poured into a disposable polyethylene cup with the new mass being used to calculate the amount of chain extender to be used (the high viscosity causes some pre-polymer to be lost in this step).

The chain extender was then accurately weighed onto the pre-polymer (viscosity hinders spontaneous mixing) and the mixture was subject to mechanical mixing

(c.1000rpm, 2.54cm diameter 3 bladed stirrer) for 30 seconds, care was taken to ensure thorough mixing was achieved. The forming polyurethane was then poured into a pre-warmed PTFE mould and cured in an oven at 70°C for 24 hours.

The urea elastomers were synthesised by following the same pre-polymer method, before dilution in dimethylformamide and adding the chain extender (in DMF) under rapid stirring. The modification was required to prevent gelation upon addition of the chain extender. Due to the reduction in concentration, samples were allowed two hours to complete chain extension. After which they were poured into PTFE moulds and placed in an oven at 60°C. The vacuum was increased slowly to prevent the formation of bubbles in the elastomer film and to allow a slow rate of evaporation enabling the PUU to settle into a phase separated state[41]. After 24 hours, the temperature was raised to 100°C and samples were left under full vacuum for five hours to remove all traces of solvent. IR spectroscopy was used to confirm the absence of solvent.

0% HS elastomers were cast by mixing molten PTHF and diisocyanate mechanically for 5 minutes, followed by degassing in a desiccator and curing in an oven at 70°C for 24 hours.

Pure hard segments were synthesised by combining dilute diisocyanate and chain extender in THF and stirring at room temperature until no more solid precipitated out of solution (c. one day for MDI-MDA and one week for DFDI-BD).

DMF and THF were purchased from Sigma Aldrich and dried with 4Å molecular sieves prior to use.

Analytical methods

Adiabatic temperature rise / Kinetics

An insulating foam (rigid polyurethane) box was constructed to hold the reaction vessel in an effort to reduce thermal transfer from the reaction mixture. A solution of isocyanate that was 0.7M in NCO groups was prepared in dry solvent and 6cm^3 was accurately measured into a HDPE container before being placed inside the insulating box. A 4.2M solution of the hydroxyl containing compound being used was prepared in the same solvent, the concentration was chosen so that the addition of 1cm^3 aliquot yielded an equal OH and NCO concentration, and therefore second order kinetics.

The isocyanate concentration was determined from previous experiments to find the maximum concentration of product that would not precipitate during the reaction. The highest usable concentration was sought to reduce errors associated with heat loss. This concentration was then kept constant for comparisons to be made within the series.

The temperature was determined using a J type thermocouple suspended through the reaction vessel lid into the solution, and a data-logger (National Instruments) using a half second resolution.

In order to calculate kinetic parameters, the temperature rise profiles were corrected for heat loss as per published procedure[10, 28b, 42].

When no reaction is taking place and there is no external source of heat:

$$\frac{dT}{dt} = -\frac{U}{\rho C_p}(T - T_{amb})$$

(21)

Where U is the global heat transfer coefficient per unit volume, ρ is the density, Cp is the specific heat capacity and T and T_{amb} are the temperatures of the system and at ambient.

Integration yields:

$$\ln(T_t - T_{amb}) = \ln(T_{t=0} - T_{amb}) - \frac{U}{\rho C_p}(t - t_0)$$

(22)

If the reaction is initiated when the system is at ambient temperature, the overall heat transfer coefficient ($U / \rho \, C_p$) can be determined from the slope of a plot of ln(ΔT) versus time for the portion of the graph after the maximum temperature has been reached (ie. the cooling phase) as seen in figure 10.
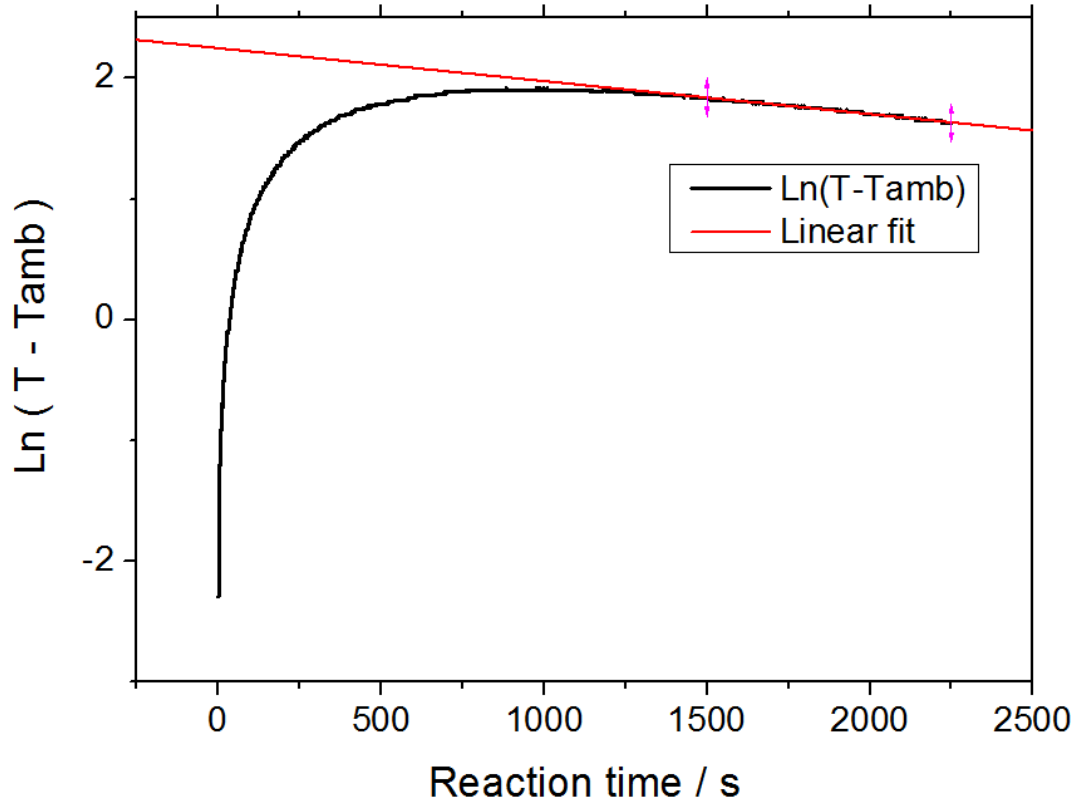
Figure 10: Linear fit to determine the overall heat transfer coefficient.

Using that slope and the integrated data from the same kinetics run, the corrected temperature can be found using equation 23 (an example of uncorrected and corrected temperature vs. time is given in figure 11):

$$T_{cor}(t) = T(t) + \frac{U}{\rho C_p} \int_{t_0}^{t} [T(t) - T_{amb}] \, dt \tag{23}$$

The conversion of isocyanate groups may then be found if the enthalpy of the NCO/OH reaction (ΔH), the system mass (m_T) and heat capacity (C_p) are known using[24]:

$$p_{NCO} = \frac{r(T_t - T_0) m_T C_p}{\Delta H} \tag{24}$$

Where r is the stoichiometry (defined by [NCO]/[OH], 1.0 in this case).

This is based on the following assumptions.

1. Isocyanates react with hydroxyls only, the only product being urethane groups.

This is a reasonable assumption based on previous reports[29, 43] that allophanate formation is slow and very much reversible at r values below 1.1 and temperatures below 100ºC.

2. The solution is homogeneous and well mixed.

3. The system has a constant heat capacity in the range being studied.

4. There are no external sources of heat.

An example of corrected temperature vs. time and isocyanate concentration calculated using equation 24 is given in figure 12. The characteristic stepwise nature of the curves is due to the 0.1ºC resolution of the temperature probe.
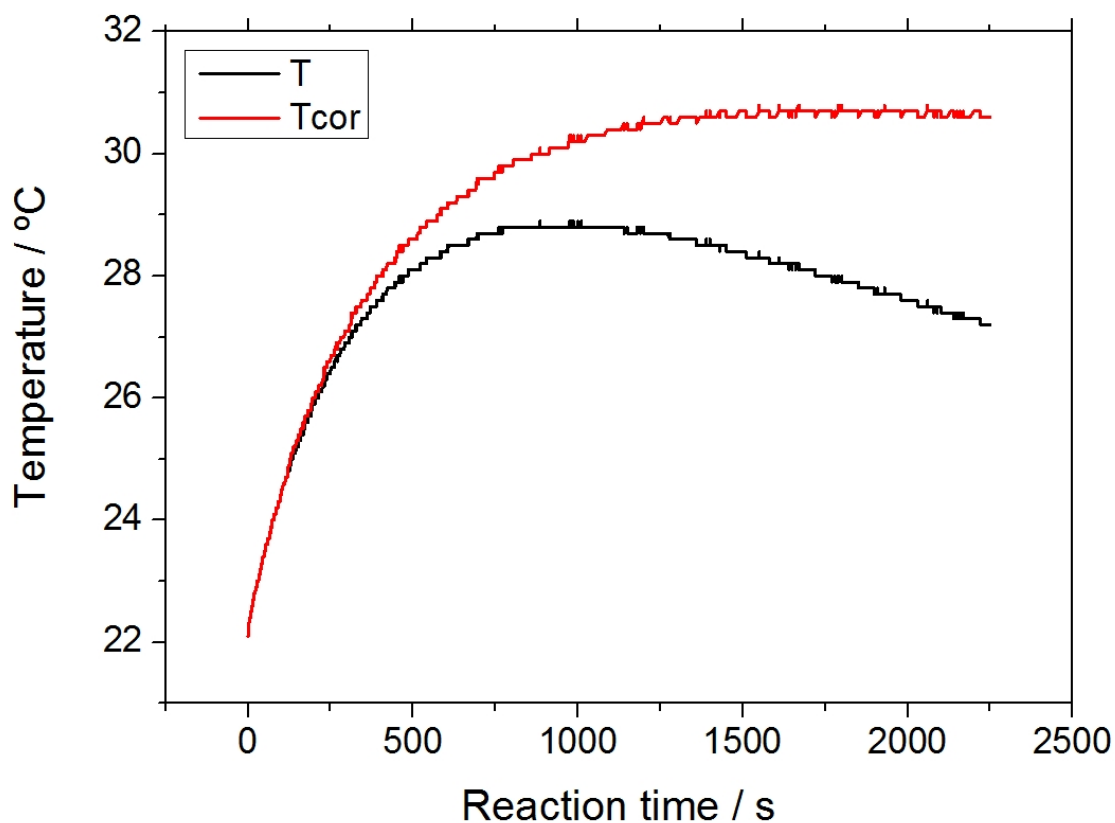
Figure 11: Plots showing T and T_{cor} for a typical kinetics run.
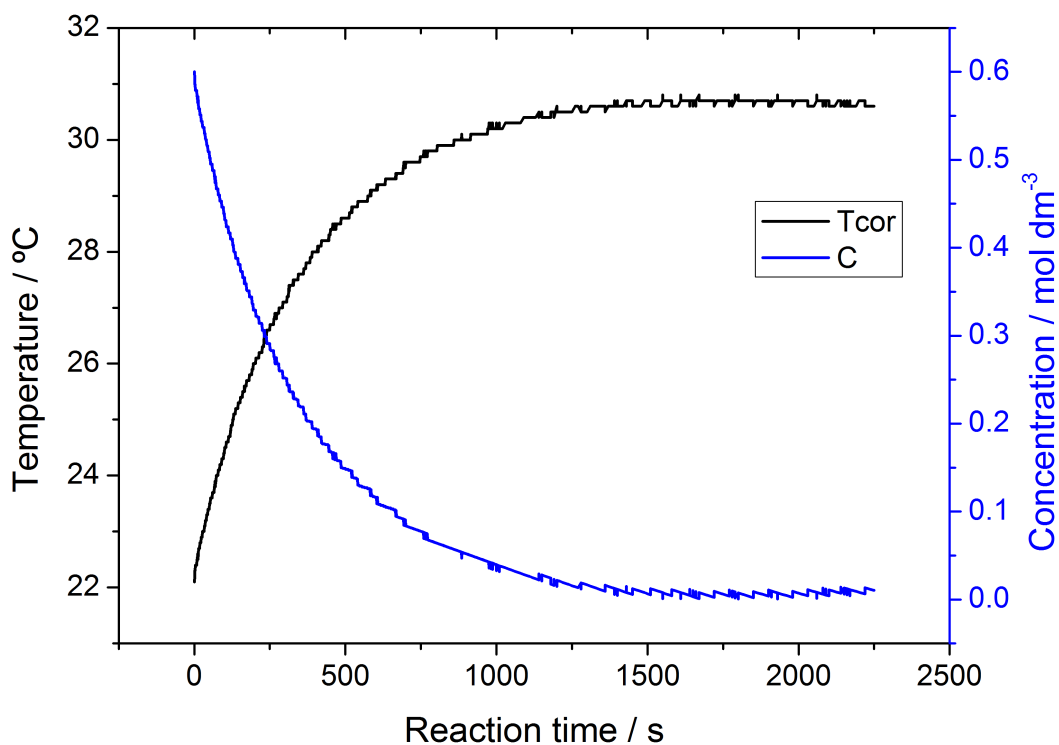
Figure 12: Plots showing T_c and concentration (C) vs. time.

NMR

Nuclear magnetic resonance (NMR) spectra were obtained using a Bruker ACF-400 MHz spectrometer. Compounds were dissolved at a concentration of 20 mg ml^{-1} in a suitable deuterated solvent, common solvents used were CDCl$_3$, D$_2$O and d-DMSO. Spinworks v.3 was used to pick and integrate peaks.

AFM

Atomic force microscopy is an imaging technique performed by scanning a sample area with a probe. Interactions between the polymer sample and the probe tip mounted on a cantilever lead to deflection that can be measured by a laser and an array of photo-diodes. Height differences on the surfaces can be resolved on the Ångström scale[44]. Whilst the topographical images produced from contact mode AFM can be interesting, there are methods of creating phase images which can be used to understand differences in local surface properties.

Tapping mode AFM is the most common mode used to create phase images[8b, 45]. Pulsed force mode[46] has been used with some success. Force modulation mode[44] has also been reported, but provided comparatively poor resolution images.

Tapping mode AFM is performed by oscillating the cantilever near its resonant frequency. The probe repeatedly comes into contact with the surface; contact and interactions (related to mechanical and adhesive properties) restrict the amplitude of oscillation. This information is used to create a phase image alongside the topographical image[47].

Compared to TEM, sample preparation for AFM is less arduous. As there is no transmittance, a smooth surface is required but the thickness of the sample has no effect on the quality of the image. AFM was carried out on freeze fractured, bulk cast PU and solvent cast films of PUU.

Freeze fracturing was carried out by propagating a small cut in a sample frozen to liquid nitrogen temperatures. After which samples were glued to steel pucks ready for mounting on a magnetic sample holder.

Assessing the surface roughness of freeze fractured samples was achieved using scanning electron microscopy, a typical image is reported in figure 13. The surface was deemed sufficiently smooth for analysis by AFM.
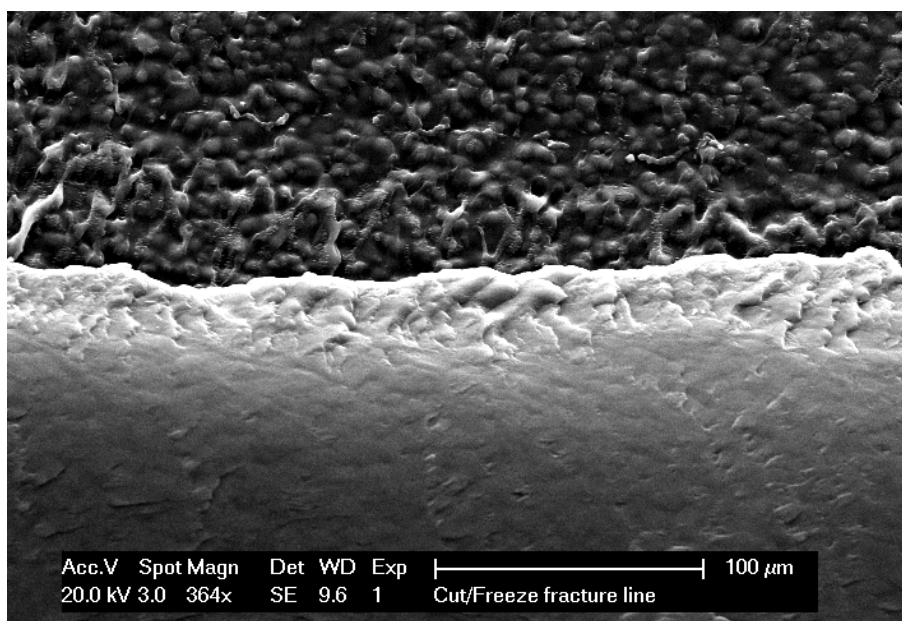
Figure 13: SEM image of the cut/freeze fracture line, the fractured portion is on the bottom.

All samples were imaged using a Veeco Dimension 3100 Atomic Force Microscope operating in tapping mode using Nanoscope v5.31. Images were acquired under ambient conditions using moderate tapping forces ($A/A_0 \approx 0.5$) and a scanning rate of 1.5-3Hz for 1μm images. The tapping force was controlled to avoid any artefacts due to excessive

29

force[48].

Topographic and phase data were recorded simultaneously and images were collected at different length scales to ensure features were representative of the bulk morphology, an example of topographical and phase data from the same sample is given in figure 14.
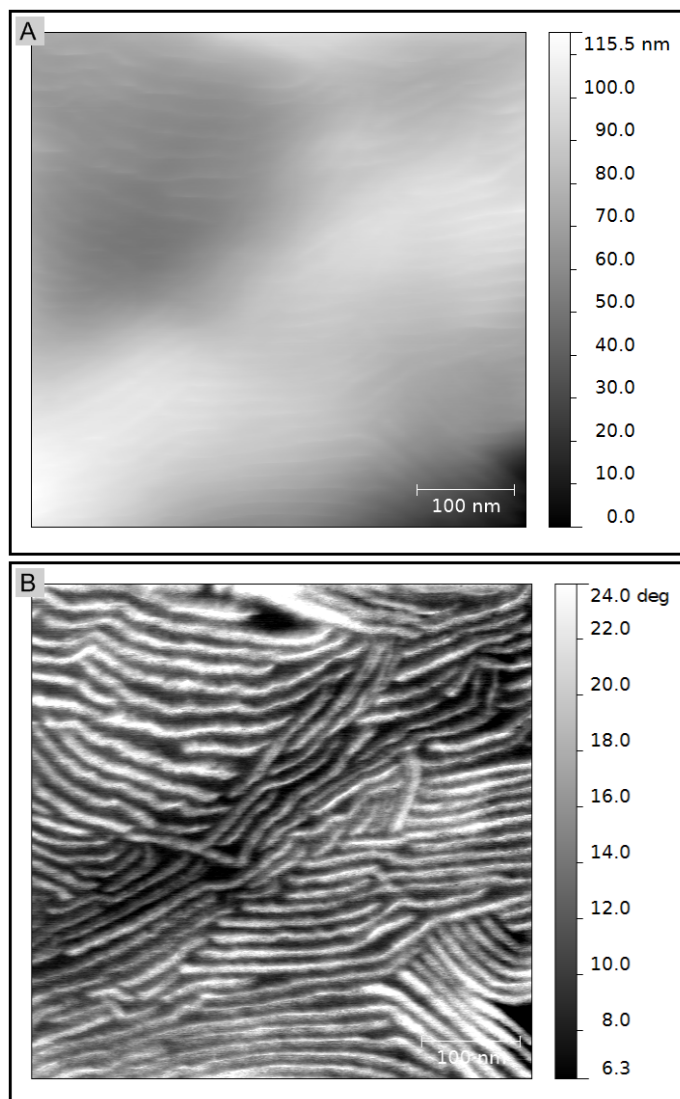
Figure 14: Example topographical (A) and phase (B) images from a 2.9kDa PTHF SS and DFDI-BD HS elastomer with a HS content of 20%.

Phase features are faintly visible in the topographical image due to the nature of tapping mode AFM. Tapping leads to slightly greater penetration in lower modulus regions, this shows up as a topographical difference. Otherwise, there are no strong features visible in topographical images.

AFM like TEM is a technique that can not be deemed representative of the bulk morphology of a sample. SAXS and DSC are much more representative due to the

amount of sample used to produce each data point, but direct visualization from microscopy techniques can provide information which cannot otherwise be revealed.

Efforts must be made to ensure the length scale extracted from an AFM image is as true as possible. As such, the power spectral density (PSD) approach was used to extract domain spacing values. An AFM image can never produce a value as quantitative as a SAXS experiment, but processing in this way at least removes any user bias from simply measuring a length scale from an image. Data was extracted from the largest image acquired (averaged over a greater area) using Gwyddion v2.25 by processing a phase image into reciprocal space (fast fourier transform) and finding the peak of the resulting data before converting back into real space.

DMTA

Dynamic mechanical thermal analysis (DMTA) is a thermoanalytical method in which a sample is subjected to an oscillating force, with displacement being measured as a function of temperature. The loss factor (tan δ (where δ is the phase angle)) is the ratio of loss modulus (E") to storage modulus (E') and a peak in this can be used to determine the Tg, which is also evident as a sharp decrease in the storage modulus. Different authors suggest different regions of the tanδ plot as the Tg indicator, either the peak centre (though the tanδ peak is often broad) or the onset of the peak (from colder temperatures) may be used[49]. In this work both the onset of the tanδ peak and the onset of the first sharp decay in storage modulus are reported. The onset of the E' decay and the onset of the tanδ peak were noted to correlate well to SS Tgs as observed in DSC experiments.

The tanδ is given by:

$$\tan \delta = \frac{E''}{E'} = \frac{E_d}{2 \pi E_e}$$

(25)

Where E" is the loss modulus, E' is the storage modulus, E_d is the energy dissipated and E_e is the energy stored.

DMTA was performed on a Metravib VA2000 Viscoanalyser in tensile mode in order to obtain the storage modulus (E') and loss factor (tan δ) of samples. Testing was

performed at a frequency of 1 Hz with an initial strain of 1% on samples cut to approximately 10 x 6 x 3 mm. The temperature was increased from -100 to 100 °C at a rate of 5 °C/min. Data was recorded and processed using Dynatest v.6.2.

DSC

Differential scanning calorimetry is a thermoanalytical technique in which the heat required to increase the temperature of a sample is measured. Samples are encapsulated in an aluminium pan and placed on a heater, an empty pan sits on a second heater and a constant heating rate is maintained for both pans. The difference in heat flow is due to the polymeric material in the pan, and changes in heat flow are due to thermal transitions.

Samples (c. 15mg) were cut from a bulk cast elastomer (or solution cast films for PUU) and enclosed in an aluminium pan. The sample was first heated to and held at 120ºC for 5 minutes to erase thermal history. Samples were then cooled to -100ºC and heated to 120ºC at a rate of 10ºC min^{-1}.

Differential scanning calorimetry was performed on a Diamond DSC (PerkinElmer) calorimeter using a power-compensation principle. The equipment consists of dual platinum-iridium furnaces with platinum resistance heaters and thermometers, which are purged with nitrogen gas at 30ml min^{-1}. Samples were placed in a 50µL aluminium pan and capped with an aluminium cover. Data was collected and analysed using Pyris v.7 software.

If no restructuring is taking place, heat flow (defined in equation 26) is constant, thermal transitions however lead to a change in the heat capacity, leading to a difference in heat flow. First order transitions have a change in heat capacity and a change in latent heat, second order transitions like glass transition temperatures however have a ΔC_p but no latent heat. Latent heat is measured by finding the area under the peak of a first order transition, Tgs are measured by either the onset or the midpoint from a Tg slope with the associated enthalpy being the offset between the straight baselines pre and post transition.

Heat flow is a measure of heat transfer per unit time:

$$Heat\,flow = q/t \qquad (26)$$

Where q is heat and t is time.

The heating rate is defined as:

$$Heating\,rate = \Delta T/t \qquad (27)$$

Where ΔT is the change in temperature. From equations 26 and 27, the heat capacity (C_p) can be calculated.

$$C_p = \frac{q}{\Delta T} \qquad (28)$$

From this equation it can be seen that the heat capacity of a transition is the energy absorbed (or given out) over the temperature range the transition is occurring.

The Fox equation[50] can be used to calculate the glass transition temperature of a mixture of polymers and is often used in polyurethane systems to asses the purity of the soft and hard segments[31].

$$\frac{1}{Tg} = \frac{W_1}{Tg_1} + \frac{W_2}{Tg_2} \qquad (29)$$

Where W_x is the the weight fraction and Tg_x is the Tg (in K) of the fraction when pure. It can be seen from the Fox equation that in a phase mixed state, glass transition temperatures will lie somewhere between the actual Tgs of the phases present. In practice Tgs are difficult to observe when material is very much phase mixed.

Hardness

Hardness was assessed using a Zwick-Roell, "A" range durometer and testing plate in accordance with ASTM D2240[51]. Testing was carried out at 21ºC and the reported hardnesses are averaged results from five measurements taken across a surface.

TGA

Thermogravimetric analysis is a technique in which a sample is heated in a controlled atmosphere with the mass being recorded as a function of temperature. It can provide useful information on the temperature stability of a material.

TGA analysis was carried out on a TA instruments TGA Q500 using advantage v.2.8 software. Samples (c.30mg) were heated in a platinum pan from 50ºC to 800ºC at 10ºC min^{-1} in a nitrogen environment.

SAXS

Introduction

Small angle X-ray scattering is a technique used to study order in material. A collimated and monochromatic beam of electrons is scattered by a sample, with the resulting scattering pattern providing data on the electron density distribution within the sample. SAXS is useful for samples containing electron density inhomogeneities in the nanometre scale[52].

Electrons resonate with the frequencies of the passing X-rays and emit coherent secondary waves (scattering centres), it is the interference between these secondary waves that scatters x-rays. The angle of diffraction is dependent on the separation between the scattering centres.

The scattering vector (q) can be calculated from equation 30.

$$q = \frac{4\pi}{\lambda} \sin \theta / 2 \qquad (30)$$

Where λ is the wavelength and θ is the scattering angle.

The invariant is used as a measure of quantifying the phase separation[53] in a sample. Care must be taken to ensure samples are normalised so the invariant is relative. The invariant is effected by volume fraction and the volume fraction of present phases as per:

$$Q \simeq \phi_H(1-\phi_H)\langle \eta_H - \eta_s \rangle^2 \tag{31}$$

Where ϕ_H is the volume fraction of the hard segment ($1-\phi_H$ is therefore the volume fraction of soft segment) and η_x is the electron density of the segments.

Method

SAXS experiments were carried out on a Bruker AXS Nanostar using a Hi-STAR 2D multi-wire detector. X-rays were generated at the Cu-α wavelength (1.54Å) and were filtered and collimated to provide a defined electron beam of known wavelength and energy. Bruker AXS v.4.1.35 software was used to collect and process frames.

A long range camera setting with a distance of 102.4cm from the sample to the detector was used with a semi-transparent beamstop mounted between the two to protect the detector from the direct beam and to allow normalisation of intensities.

Elastomers cast from bulk were cut to a thickness of around 5mm; solution cast samples were used as-cast (c. 1mm) and mounted on a steel sample holder. Samples were exposed for 4 hours, with an air background being collected for 12 hours.

The intensity was corrected for sample thickness, absorption, incident strength of the X-ray beam and duration of the experiment by normalizing data for the counts observed through the sample and semi-transparent beamstop. A background frame (also normalized) was then subtracted and the data was subject to a Lorrentz correction (Iq^2 vs. q plot). The Lorrentz correction can be applied to a system that has a morphology that is globally isotropic but locally lamellar[53b, 54].

A calculation of the domain spacing was obtained using Braggs law, where the q is taken from the first non zero-maxima not associated with the beamstop observed in Lorrentz corrected frames.

$$d = \frac{2\pi}{q} \tag{32}$$

A more detailed analysis of SAXS frames was attained by carrying out a correlation function (using CorFunc V.1.4, available from http://www.small-angle.ac.uk/small-

angle/Software.html), using the method applied by Strobl and Schneider[55].

The analysis is performed in 3 stages:

(a) Extrapolation of the experimental scattering curve to $q = 0$ and $q =$ infinity, using Guinier and Sigmoid fits respectively.

(b) Fourier transform of the extrapolated data to give the 1-D correlation function.

(c) Interpretation of the 1-D correlation function based on ideal lamellar morphology.

Prior to the correlation function, frames were corrected for thermal background[55c] to ensure the extrapolation of q to ∞ would be valid.
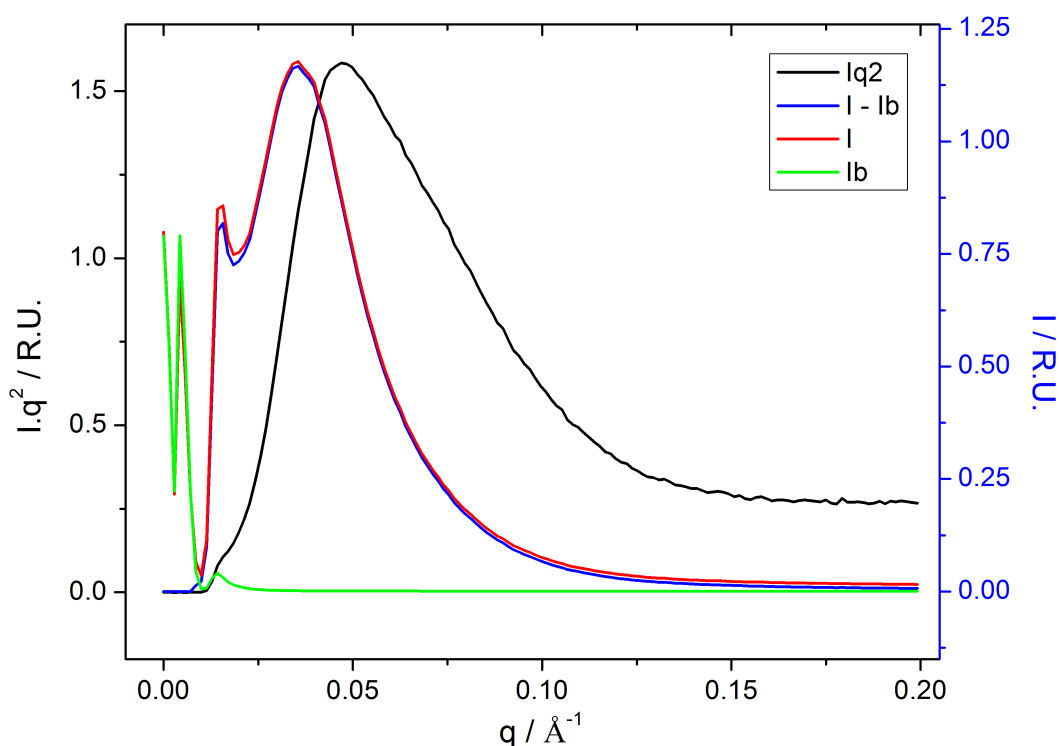
Figure 15: Example plots of intensity (background, uncorrected sample and sample with the background subtracted) on the primary (left) y axis and Lorrentz corrected intensity on the secondary (right) y axis versus q.
A small offset has been applied to make overlapping data visible.

Figure 15 shows data at different points during processing; intensities of the background, sample, the sample minus the intensity of the background and the Lorrentz corrected intensity (Iq^2) versus q are shown.

WAXS

Wide angle x-ray scattering is a scattering technique used to probe structures with

dimensions below c. 20Å, coinciding with the crystallographic morphology of materials.

Data was acquired on a Bruker D8 using a Cu-α radiation source and a 1-D detector. Samples were scanned using a 0.005º step size and 0.5 seconds exposure per step over the range 2-40º with data being averaged over three passes.

Thermal history was erased by heating samples to 120ºC in an oven before cooling slowly to liquid nitrogen temperatures, this was achieved by slowly introducing nitrogen vapour.

Samples were kept cold and ice free by applying a stream of cold nitrogen to the stage during data acquisition. Temperature was maintained below 0ºC for the acquisition but the step size had to be reduced (0.05º) to accommodate this.

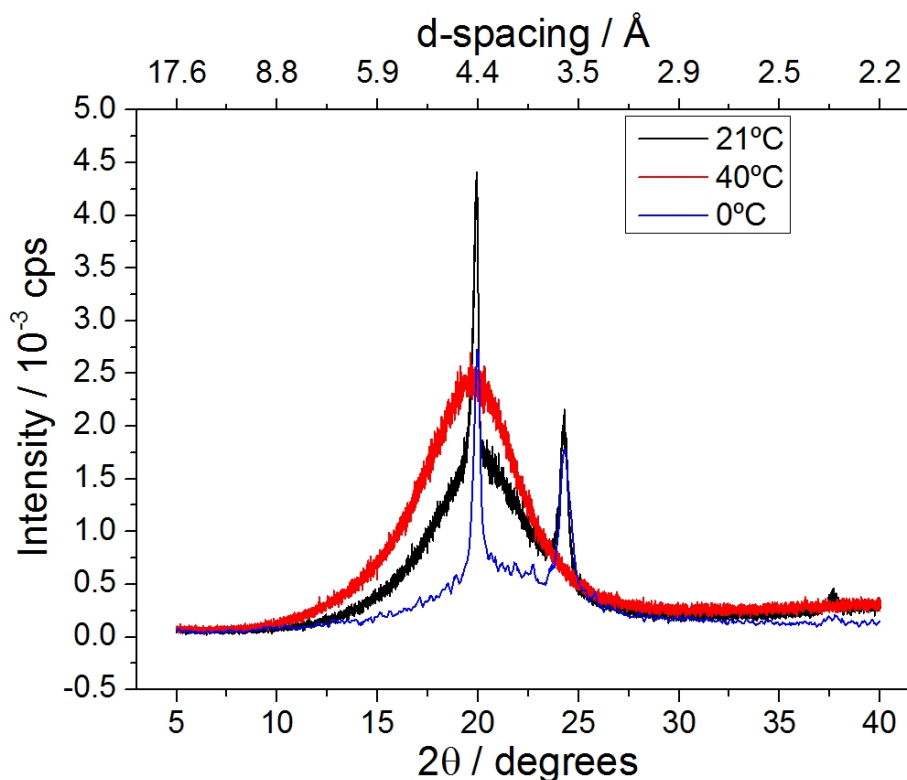*Figure 16: Example intenisty vs. 2θ plots at different temperatures.*

Figure 16 shows example WAXS frames for a 2kDa SS and a DFDI-BD HS elastomer with a HS content of 20% at different temperatures. Crystallinity was calculated by comparing the area of the crystalline regions to the total area between 12.5 and 27.5º as shown in figure 17.
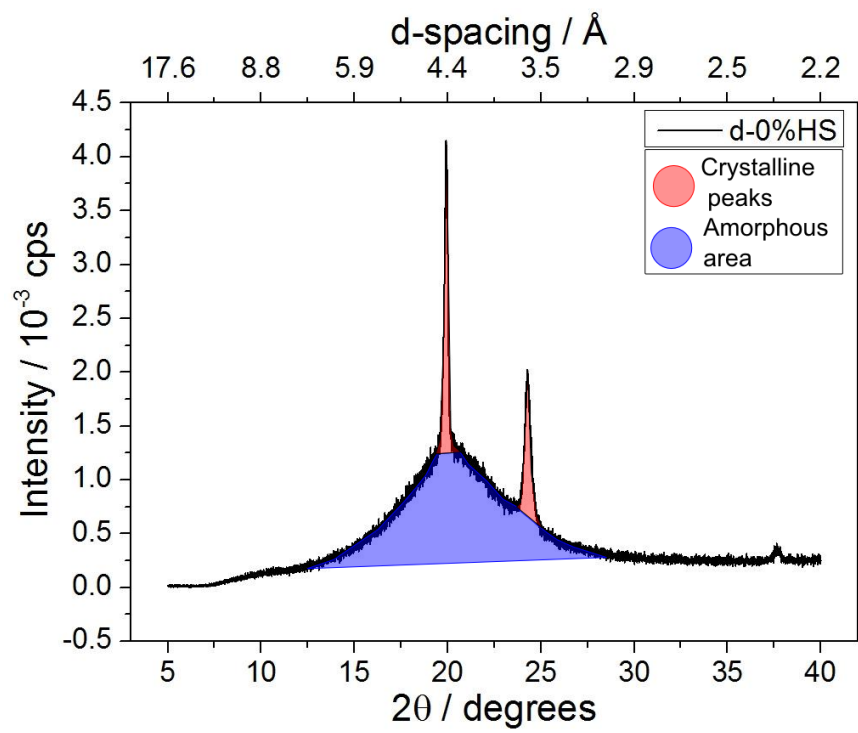
Figure 17: Plot showing the areas used in the calculation of crystallinity.

Chapter 3. Synthesis and Kinetics

Introduction

Isocyanate synthesis

Phosgenation has been the most common method of isocyanate synthesis in industry for many years[56]. Phosgene is the primary reagent used which has historically also been used as a chemical warfare reagent. It is a colourless gas with only a faint odour even at harmful levels and is highly toxic.

Other methods of forming the NCO functional group are known and are routinely used in organic synthesis. These methods are usually variations of rearrangement reactions and include the Curtius, Hofman and Lossen rearrangements. Their mechanisms are summarised in figure 18.
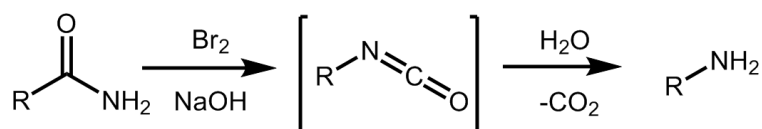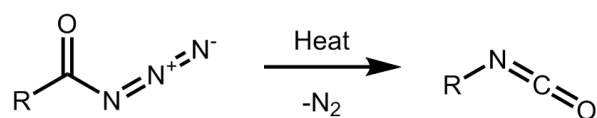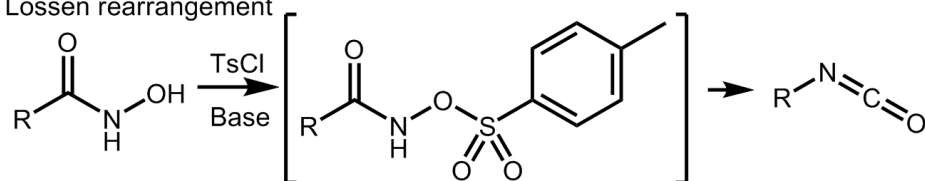
Figure 18: Mechanisms of rearrangement reactions leading to the isocyanate functional group.

In the Hofmann rearrangement the isocyanate is formed and due to the conditions immediately reacts to form the primary amine that would be the precursor in a traditional phosgenation, the isocyanate can be trapped with an appropriate nucleophile. The Curtius rearrangement is rearrangement via an acyl azide which can be prepared from carboxylic acids and other reactive carbonyl derivatives. The Lossen rearrangement makes use of a tosylate and hydroxy-acetamide to form an intermediate,

which then rearranges to form the isocyanate[57].

Phosgene is a colourless gas with a boiling point of 8.2ºC, the production and subsequent use is often carried out on the same site to minimise risks associated with transport[58].

Phosgenations are often carried out in two steps (the reactions occurring are shown in scheme 8) to reduce the urea by-product formed by the reaction of isocyanate with amine. The initial step (also known as the "cold stage") is carried out at c.40ºC, carbamoyl chlorides and hydrochloride salts are the main groups formed. The second step ("hot stage") is carried out at c.100ºC and drives the reaction towards the desired products by forcing the removal of HCl gas. The stability of the carbamoyl chloride intermediate determines how forcing the hot stage needs to be.
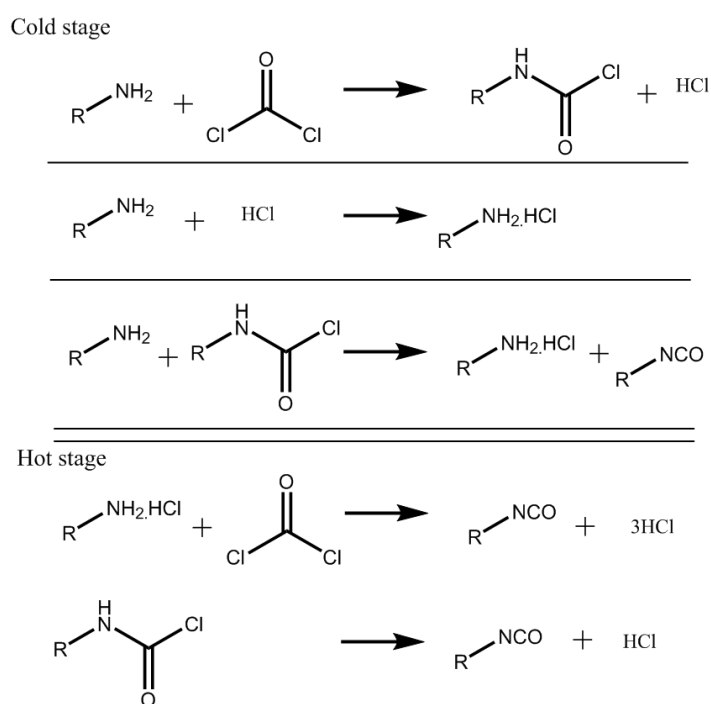
Scheme 8: The first and second stages commonly used in isocyanate formation via phosgenation.

The reaction with phosgene is often carried out in chlorinated aromatic solvents with high boiling points to allow for easier removal of excess phosgene and dissolved HCl during purification[59].

Due to the relative ease of purification in phosgenations compared to rearrangement methods, phosgene variations were developed to allow for easier and safer small scale

synthesis of isocyanates and carbonates, the structure of the phosgene based compounds used to synthesise isocyanate groups are shown in figure 19.
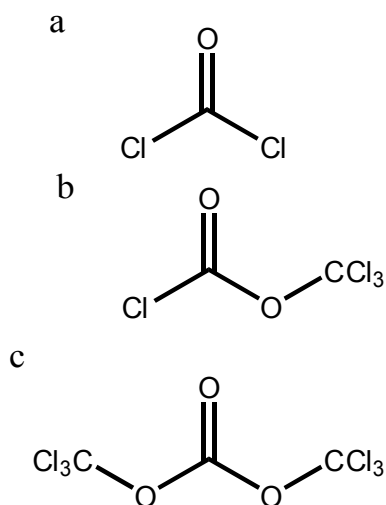
Figure 19: The structures of a. Phosgene b. Diphosgene and c. Triphosgene.

Diphosgene was originally developed as a substitute for phosgene in chemical warfare applications. It is a colourless liquid at room temperature with a boiling point of 128°C. It can react with two equivalents of amine groups.

Triphosgene is a white crystalline solid that is soluble in a wide range of solvents. It can react with three equivalents of amine groups to form isocyanates, although it is commonly used in a stoichiometric excess.

Eckert and Forster[60] recommend using using ortho-dichlorobenzene at temperatures between 130 and 180°C for the synthesis of isocyanates when using triphosgene as a replacement for phosgene. MDI synthesised from its diamine precursor was achieved with a reported 92% yield.

Charalambides and Morati[61] used ethyl acetate as the solvent for uncatalysed reactions in a four hour reflux reporting high yields in most cases (typically 70%). The base catalysed version utilised triethylamine in similar conditions but the overall conclusion was that there was little to no benefit in yields for using a catalyst and the subsequent difficulty in separating the base from the isocyanate made the uncatalysed route preferable.

MDI synthesis

The manufacture of MDI is carried out in three steps[62]. Starting with benzene, electrophilic substitution using HNO_3 and H_2SO_4 to yield nitrobenzene is carried out.

This is followed by reduction using H_2 and a nickel catalyst at 600°C to yield aniline. Aniline is then reacted with formaldehyde, followed by phosgenation to produce 2,4' and 4,4'-MDI (56%) amongst other homologs containing more aromatic rings. This mixture can be distilled to get pure MDI (used for high performance elastomers) or used crude (as a cheaper isocyanate often used in rigid foams). The synthesis of MDI is summarised in scheme 9.
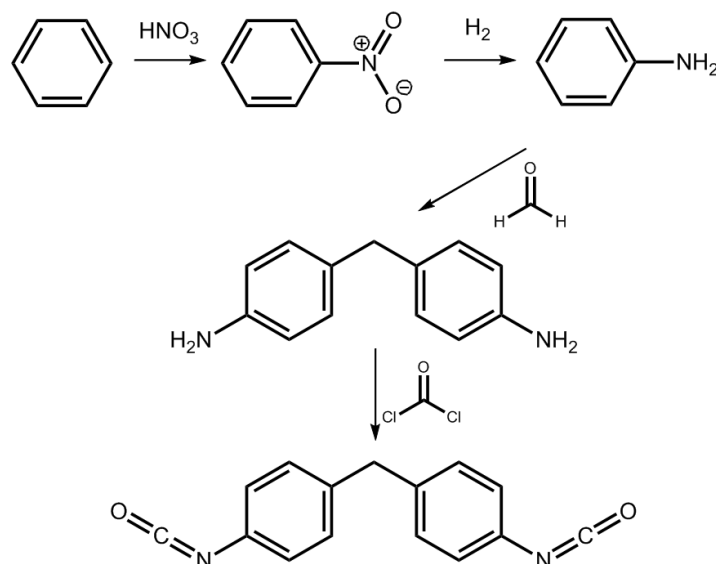
Scheme 9: Synthetic route to MDI.

DFDI synthesis

Methylenebis(2,5-furandiylmethylene)diisocyanate (DFDI) is subject of investigation in this thesis, its synthesis has previously been reported in literature[19a, 19g, 21]. The original method reported utilised phosgene in the final step to create the isocyanate moiety; Gandini used the safer triphosgene in his work[21], although a detailed description of synthetic conditions was not reported.

The synthesis of the diamine precursor of the diisocyanate was investigated by Holfinger[63], who found that yields of 29% were achievable by directly coupling the furan rings of furfurylamine without first protecting the amine (the yield of DFDA from FFA in a three step synthesis is c. 32%). The methylene bridge disubstituted diamine was easier to synthesise with reasonable yields, the same one step synthesis gave up to a 70% yield.

Reaction Kinetics

The study of isocyanate/alcohol reaction rates is older than the field of polyurethanes[64], but the industrial significance of this area grew with the use of PU. Baker and Holdsworth[13] were the first to investigate the reaction between the isocyanate and hydroxyl groups in detail.

The reactivity of the isocyanate group is of interest when considering the potential for use in polymer systems. Catalyst packages may be utilised to overcome any shortfall DFDI may display in reactivity, some reaction injection moulding polyurethane systems are catalysed to such a degree that parts may be demoulded within ten seconds of mixing. While the polyurethane industry is acquainted with catalysed polymer systems, high levels of catalyst are undesirable as common catalysts have a pungent odour (triethylamine, diazobicyclo-N,N-octane) or are toxic (dibutyltin dilaurate).

The determination of rate constants for isocyanate/hydroxyl reactions has been carried out many times with different groups utilising different methods. Calorimetric[28b, 42a, b, 65], spectroscopic[11, 21, 66] and titrimetric[19b, 67] methods have all been reported and further to these, both bulk and solution analysis can be carried out.

Bulk analysis is advantageous in that the kinetics are being assessed in an environment comparable to those that will likely be employed in industry. The negative is that the viscosity and mixing have pronounced effects on reactivity, and lab based equipment may not emulate industrial mixing effectively.

Solution analysis suffers no issues due to mixing or reactivity, but the diffuse nature of groups can make monitoring concentration more troublesome.

Titrimetric analysis has fallen out of favour due to the time that must be spent taking aliquots and carrying out titrations. While not useful for bulk analysis, titrimetric analysis allows for data points to be sampled until the solution has been consumed, and with no loss of accuracy, making slower reactions easier to follow.

Spectroscopic methods are fast and accurate. The negative is the need for an IR or UV-Vis spectrometer throughout, which is not ideal for slower reactions. This issue can be circumvented by taking aliquots from a reaction, though this leads to loss of resolution.

Calorimetric methods allow for data points to be sampled very frequently. Heat loss is

the major issue, which can be reduced by insulation and correction of the temperature curves.

Synthesis of DFDI

Experimental

The four step synthesis begins with furfural and follows a similar route to that of MDI. In the synthesis of MDI commonly employed in industry, there is no protection of the amine group. This is due to the lower reactivity of the amine directly attached to the aromatic ring and the relatively low cost of starting materials.

An outline of the synthetic route and reagents is presented in scheme 10.
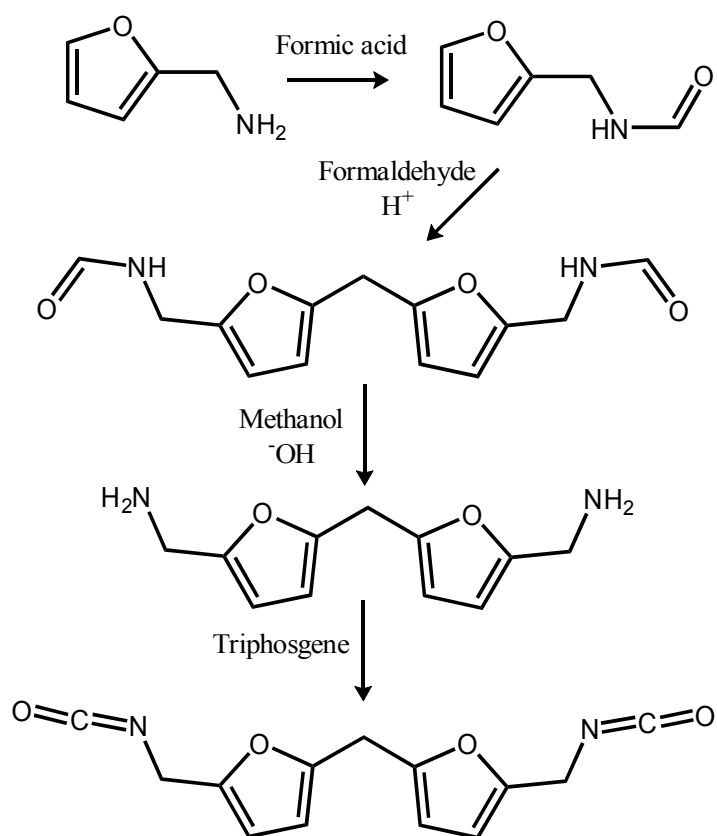
Scheme 10: Synthetic route to DFDI.

Furfurylamine is a derivative of furfural, which is readily available and is synthesised by boiling oat husks, corn cobs and other plant materials containing hemicellulose, in sulphuric acid. The method of choice for the formation of DFDI is phosgenation of DFDA as the amine precursor furfurylamine is readily available.

44

The steps can be summarised as:

1.protection of the amine,

2.fusion of the furan rings,

3.deprotection of the diamine, and

4.formation of the isocyanate group.

Yields are reported as being high for steps one and three[19a], with the fusion step being comparatively poor with only a 42% yield. A detailed account of reagent quantities and conditions used in this work follows.

Step 1:   Furfurylamide was synthesised by the protection of furfurylamine using formic acid. The reaction was driven forwards by the removal of water, which was achieved by the addition of heptane and heating above 79°C which is the temperature of the water-heptane azeotrope (in which water makes up 12.9%). The heptane was returned via the use of a dean-stark trap, with the water being drained off periodically.

Formic acid (1000ml) was added to furfurylamine (500g) under a nitrogen environment whilst maintaining the solution temperature at 10°C using an ice bath. The solution turned from colourless to yellow and then golden as addition progressed. Heptane (1500ml) was then added to the flask and the solution temperature was raised to 90°C and then refluxed until no more water was observed to separate from the condensed azeotrope. The solution became gradually darker until an oily black solution was observed after 3-4hours of heating. After separating the upper heptane layer, residual formic acid was removed by rotary evaporation. The resulting crude amide was then purified via distillation under vacuum (101°C at $2x10^{-4}$mbar) to give a colourless liquid at 91% yield. FFD was characterised by ^{1}H-NMR in CDCl$_3$.

Step 2:   Difuryldiamide was synthesised by fusing two furfurylamide molecules using formaldehyde.

FFD (455g) from step 1 was added to a round bottom flask, followed by phosphoric acid (1.8l, 10 wt%). Formaldehyde solution (150ml, standard 35wt%) was then added dropwise under nitrogen while stirring. The resulting solution was stirred for 7-12 hours and then left to settle for 4 days. Light brown crystals were observed to begin crashing out of solution soon after stirring was ceased, this continued for 48 hours. The crystals

were filtered using a sintered glass funnel and washed with portions of cold water and acetone before drying in a vacuum desiccator to give a 40% yield. The end product was characterised by ^{1}H-NMR in d-DMSO.

Step 3: Difuryldiamine was synthesised via the deprotection of difuryldiamide using sodium hydroxide and methanol.

DFDD (182g) was weighed into a 3-necked round bottomed flask and placed under a nitrogen atmosphere, methanol (250ml) was added followed by the sodium hydroxide solution (115g NaOH in 215ml H_2O). The mixture was refluxed with vigorous stirring for 6 hours, during which the initial light brown suspension turned to a dark brown solution. Methanol was removed from the mixture via rotary evaporation and the diamine was extracted from the cooled slurry by washing with cold chloroform to yield an amber oil at room temperature (crude yield = 92%).

The crude diamine was purified via distillation under vacuum (130°C at $2x10^{-4}$mbar) to yield a colourless liquid (88% yield) that slowly crystallises at room temperature to give long needles. DFDA was characterised by ^{1}H-NMR in $CDCl_3$ and stored at room temperature under ultra high vacuum.

Step 4a: To proceed to step 4b, the purified DFDA was dissolved in acetone and acidified with HCl (added dropwise to a cooled and stirred solution) to yield DFDA.HCl which precipitated out of solution. The crystals were washed with more acetone before being dried in a vacuum oven at 80ºC.

Step 4b: Carbonylation of difuryldiamine hydrochloride was achieved using triphosgene.

DFDA.HCl (20g) was weighed into a round bottom flask, toluene (300 ml) was added and the suspension was stirred under nitrogen. A solution of triphosgene (22g 1molar equivalent (three equivalents of carbonylating groups)) in toluene (200 ml) was then made up and added dropwise at room temperature. Once addition was completed temperature was raised to 60°C for 1 hour, with phosgene being returned to the flask by use of a chloroform/dry ice cold finger. The chloroform/dry ice coolant was specifically chosen to reflux phosgene and toluene while allowing HCl gas to leave the system (CCl_3/CO_2(s) = -63.5ºC, HCl bpt = -85ºC, Cl_2CO bpt = 8.3ºC, Toluene Mpt = -93ºC).

The temperature was then raised to 115°C and the nitrogen inlet was lowered below the

solution surface to aid nucleation of HCl gas. The mixture was refluxed for 5 hours before the coolant was changed to water, allowing the removal of unreacted phosgene.

All gas leaving the system was passed through a dual bubbler setup to prevent phosgene from being released. The first bubbler had a volume greater than that of the second and was empty, its role was to prevent any back pressure from sucking NaOH into the reaction mixture. The second bubbler had a sintered inlet and was filled with concentrated NaOH solution.

The reaction mixture was allowed to cool before it was filtered through a sintered funnel to give a red filtrate and a brown powdery residue. The filtrate was rotary evaporated to remove toluene leaving a red oil. The crude diisocyanate was then distilled under vacuum (120°C at 2×10^{-4} mbar) to yield a light yellow oil (yield = 45%) which was characterised by ^{1}H-NMR in CDCl^3.

Unreacted DFDA.HCl may be extracted from the brown powder residue by dissolving in hot methanol before diluting with acetone to decrease solubility. The light brown powder may then be washed with cold acetone before drying. 1H NMR confirms that the powder is DFDA.HCl.

NMR

^{1}H NMR spectra results and spectra are detailed below, proton labels are defined in figure 20. NMR results match those reported by Cawse[19a] for FFD, DFDA and DFDI. The spectra for FFA and DFDD were not reported. NMR spectra and tables summarising peak positions and attributes are presented on the following pages.
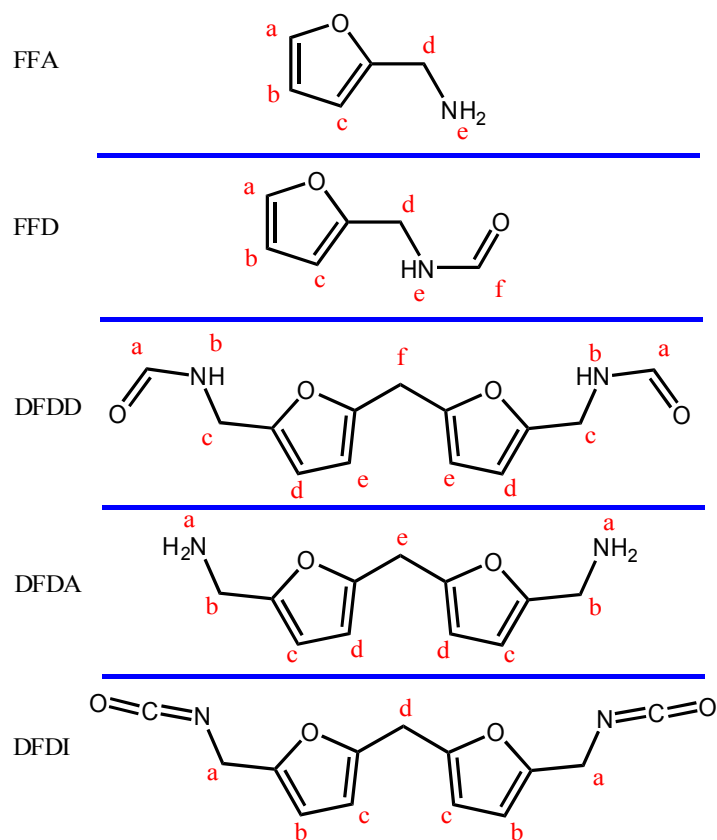
Figure 20: Proton labels for the following NMR data tables.
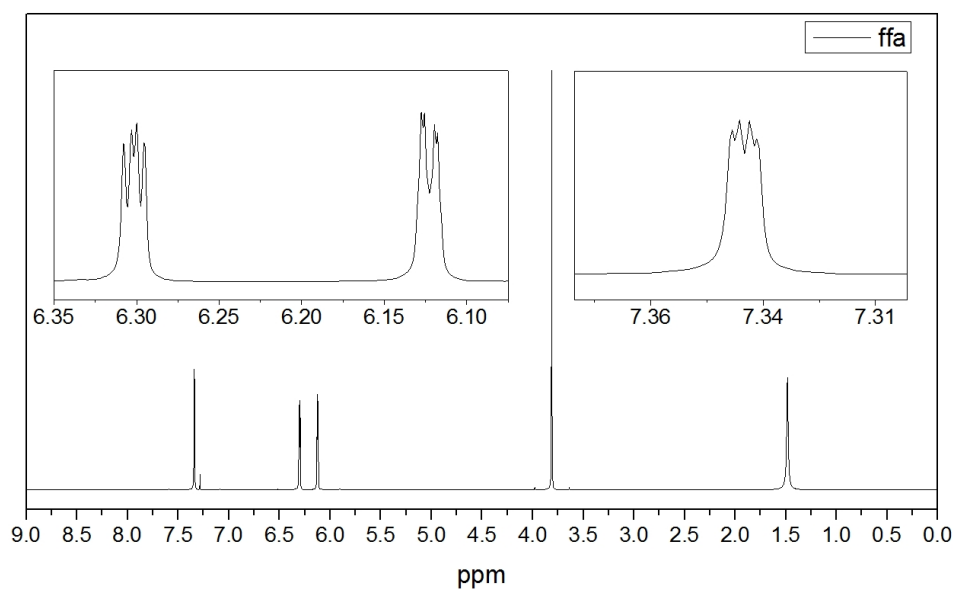
Figure 21: ¹H NMR spectrum of FFA in CDCl₃

proton label	δ	Peak attributes	J	Intensity
a	7.34	dd	0.74, 1.86	1H
b	6.30	dd	1.86, 3.20	1H
c	6.12	dd	0.74, 3.20	1H
d	3.81	s		2H
e	1.48	s, b		2H

Table 1: NMR peak positions, splitting and information for FFA.

48
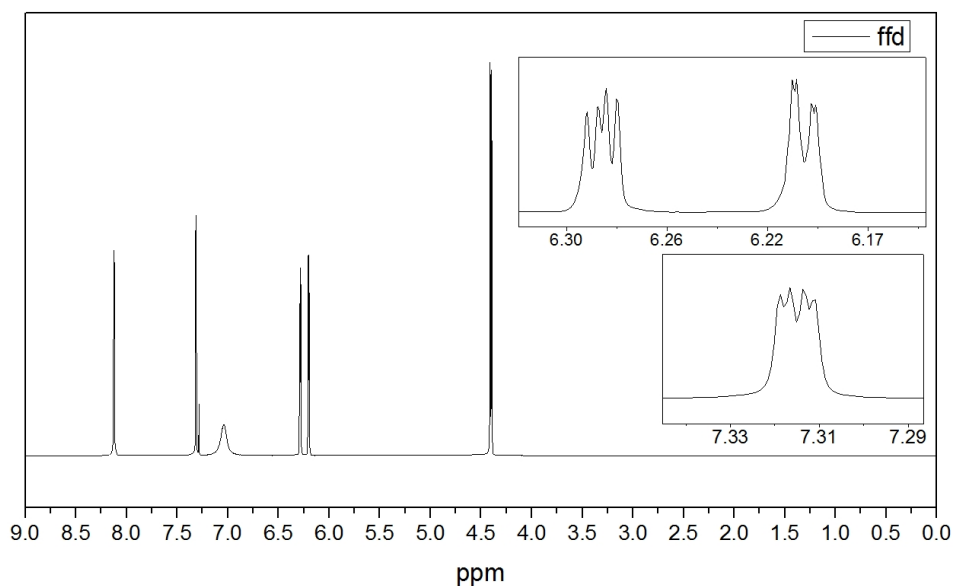
Figure 22: ¹H NMR spectrum of FFD in CDCl₃

proton label	δ	Peak attributes	J	Intensity
a	7.31	dd	0.72, 1.72	1H
b	6.28	dd	1.74, 3.20	1H
c	6.20	dd	0.72, 3.20	1H
d	4.40	d	5.76	2H
e	7.04	s, b		1H
f	8.12	s		1H

Table 2: NMR peak positions, splitting and information for FFD.
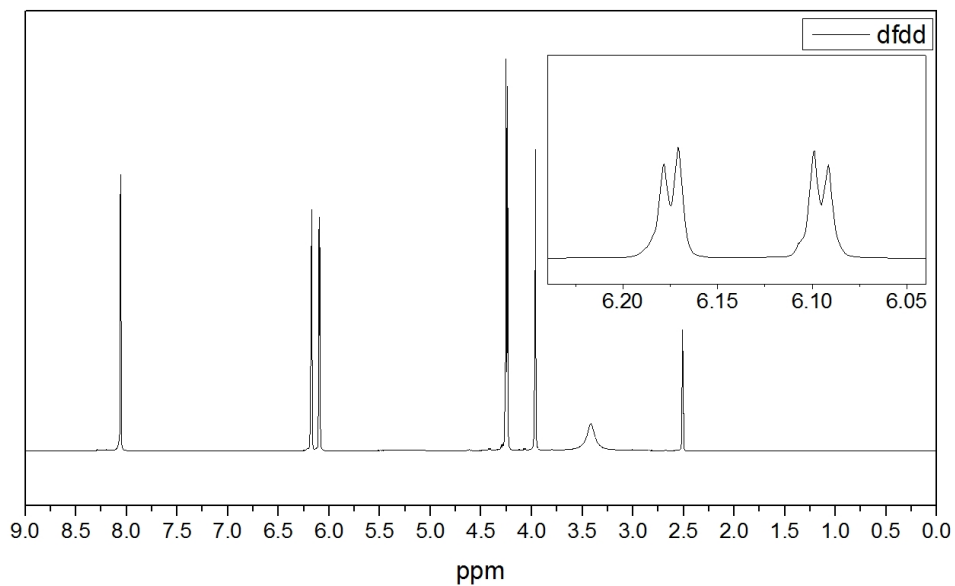
Figure 23: ¹H NMR spectrum of DFDD in d-DMSO

49

proton label	δ	Peak attributes	J	Intensity
a	8.06	s		2H
b	3.41	s, b		2H
c	4.25	d	5.69	4H
d	3.96	s		2H
e	6.18	d	3.06	2H
f	6.09	d	3.06	2H

Table 3: NMR peak positions, splitting and information for DFDD.
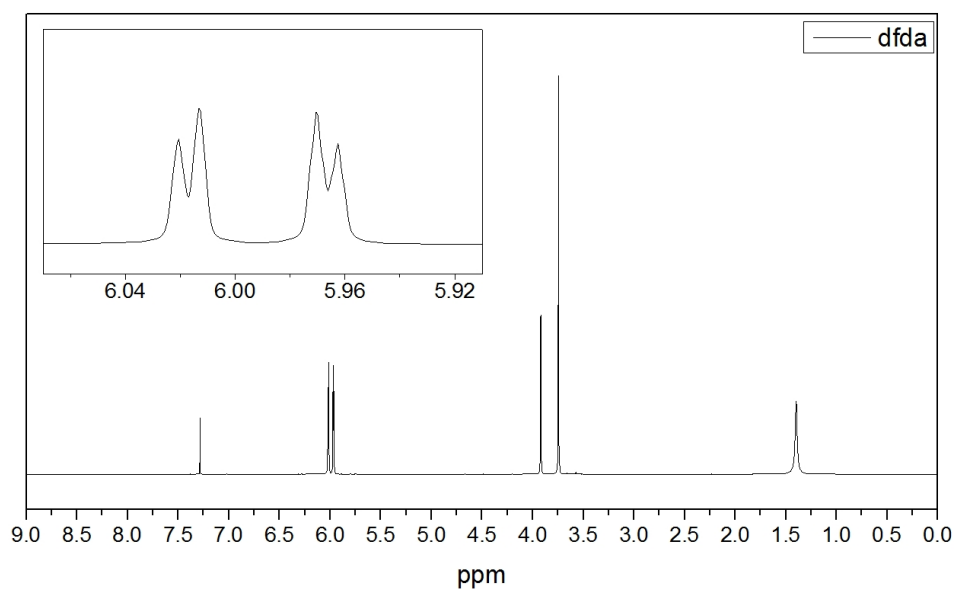
Figure 24: ^{1}H NMR spectrum of DFDA in CDCl$_3$

proton label	δ	Peak attributes	J	Intensity
a	1.39	s, b		4H
b	3.75	s		4H
c	6.02	d	3.16	2H
d	5.97	d	3.16	2H
e	3.92	s		2H

Table 4: NMR peak positions, splitting and information for DFDA.
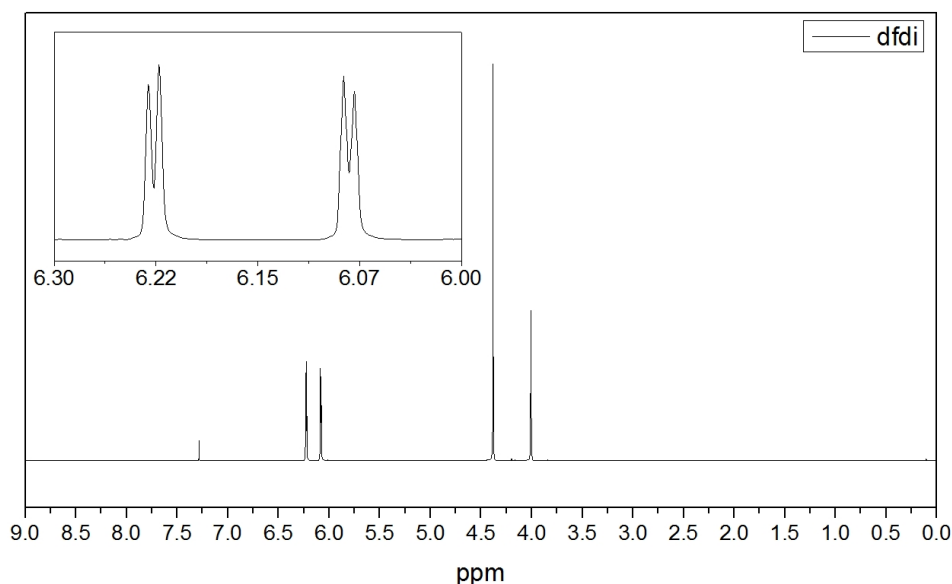
Figure 25: ¹H NMR spectrum of DFDI in CDCl₃

proton label	δ	Peak attributes	J	Intensity
a	4.38	s		4H
b	6.23	d	3.18	2H
c	6.08	d	3.18	2H
d	4.01	s		2H

Table 5: NMR peak positions, splitting and information for DFDI.

Confirmation of the nature of amine peaks can be achieved by adding a drop of D_2O to NMR samples, the proton exchange leads to a disappearance of the peak.

The spectrum of DFDI presented in figure 25 clearly shows the methyl protons adjacent to the NCO group to have shifted higher than observed in DFDA, this due to the increased electron withdrawing effect of the NCO group compared to that of the amine group. More telling is the disappearance of the protons on the amine group, previously present as a broad singlet at 1.39ppm. The bridging methylene protons remain unchanged, separated as they are by five c-c bonds from the amine/isocyanate groups.

End group analysis

End group analysis was used to determine the relative amount of NCO groups per mass of DFDI. The method used is covered in detail in the experimental section.

Fitting with expected values of a pure sample of 129.12 g mol⁻¹, the equivalent weight was found to be 128.26 ± 0.63 g mol⁻¹. Indicating purity of 99.3 ± 0.5 %.

By comparison, the purity of MDI used was found to be 99.1 ± 0.5%.

Discussion

Synthesis of amide, diamide and diamine precursors of DFDI were carried out according to published procedure[19a] with no modifications.

The synthesis of DFDI in suitable quantities was one of the major hurdles encountered in this project.

The methyl separation between the furan ring and amine causes the lone pair of electrons on the nitrogen to be more available. This leads to a stable conjugate acid (DFDA.HCl), more so than that of the analogous MDI precursor MDA. The hydrochloride salt of the amine is insoluble in all aprotic solvents leading to a heterogeneous reaction.

Heating the reaction mixture increases the solubility of the salt and bubbling nitrogen into the mixture aids nucleation of HCl gas, leading to an increased concentration of dissolved DFDA.HCl and DFDA.

Primary amines react quickly with isocyanates, but the nature of phosgenations ensures that there is always HCl present to decrease the concentration of free amine.

Utilising a base as an acid scavenger allowed slightly greater yields (50% compared to 45% with no base) and shorter reaction times. It also however led to a greater amount of unwanted by-products (due to base increasing the concentration of free amine) and the subsequent increased difficulty removing the base and by-products made the base-free method the preferred route.

Elastomers

Polyurethane elastomers synthesised from DFDI have a light red colour, darker than that of the isocyanate which appears light yellow when pure.

Viscosity rapidly builds upon addition of CE to a DFDI terminated pre-polymer, this was in agreement with the work of Cawse[19b] who reported faster gelation in DFDI based systems compared to MDI despite the k_{app} of the NCO/OH reaction of DFDI to be around a 7% that of the MDI reaction.

DFDI elastomers are harder and more rigid than analogous MDI elastomers. This was initially presumed to be due to a lower degree of phase separation. However, subsequent

results from scattering, imaging and thermoanalytical methods indicates this rigidity is due to crystallisation of the soft segment and the degree of phase separation is significantly higher in all DFDI based elastomers.

Both the increase in viscosity and the higher stiffness can be explained by two phenomena. The kinetics of phase separation are faster in DFDI systems (explained in more detail later), leading to segregated soft and hard segments and more hydrogen bonding within the HS sooner after chain extending. The oxygen heteroatom within furan rings is a potential hydrogen bond acceptor, a site not available in MDI leading to a greater degree of H-bonding in DFDI based HS.

Elastomers synthesised from both DFDI and MDI had very good physical properties, the 0%HS elastomers were synthesised in an optically clear form by applying a vacuum to the forming polymer before viscosity became too high, removing any dissolved air which would otherwise scatter visible light.

MDI based elastomers containing hard segments are translucent to white, more white as HS% increases. MDI based elastomers are known to discolour over time, first turning yellow then eventually light brown. This was not observed over the time-frame in which they were studied.

DFDI based elastomers were opaque from 20%HS, indicating trapped air in the elastomer due to the rapid rise in viscosity. DFDI based elastomers have not yet been observed to discolour (after three years) any more than that which occurs during polymerization and subsequent curing.

Kinetics

The kinetics of the hydroxyl/isocyanate reaction were investigated and comparisons made between DFDI and MDI bound NCO groups.

Kinetics were evaluated in DMF and diglyme, and with methanol and methyl-diglycol (diglyme with only one end capped with a methyl group). Figure 26 shows the structures of the solvents and monols used.

MeOH

MeOH
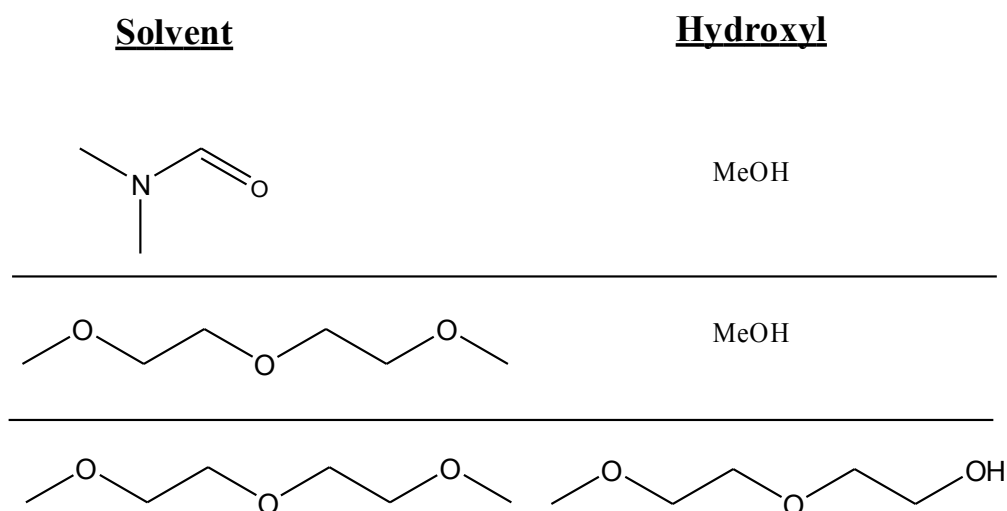
Figure 26: The systems studied to establish the k_{app} of diisocyanates.

Diglyme was used in order to simulate the environment of bulk polymerisation, analogous as it is to a polyether polyol[42b, 66d]. Methyl-diglycol was used for the same reason, it resembles a polyether backbone.

Isocyanate conversion clearly occurs at a significantly slower rate with DFDI. As seen in figure 27, 50% conversion is achieved within three minutes in the MDI system, the DFDI system requires 40 minutes to reach the same conversion.
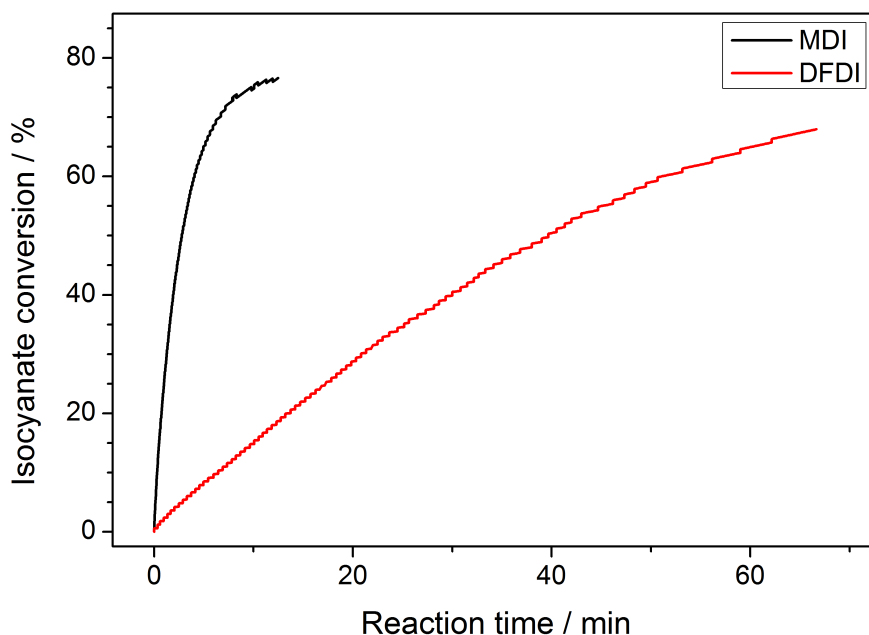
Figure 27: Example plot showing isocyanate conversion vs. reaction time.

Reported in figure 28 are second order kinetic plots of representative experiments for the three systems studied, with results summarised in table 6.

The second order rate constants are consistently smaller in DFDI systems. The apparent rate constant - k_{app} - values for MDI systems are around 14.8 times greater than the DFDI value (17.6×, 12.6× and 14.1× in DMF/MeOH, diglyme/MeOH and diglyme/methyl-diglycol systems (average of at least three runs)).

Isocyanate	Solvent	Hydroxyl	Catalyst concentration / mmol dm^{-3}	10^3 k_{app} / dm3 mol-1 s-1		
MDI	DMF	Methanol	30	8.750	±	0.017
DFDI	DMF	Methanol	30	0.496	±	0.001
MDI	Diglyme	Methanol	60	7.220	±	0.010
DFDI	Diglyme	Methanol	60	0.574	±	0.002
MDI	Diglyme	Methyl-diglycol	120	9.610	±	0.037
DFDI	Diglyme	Methyl-diglycol	120	0.681	±	0.002

Table 6: Compiled k_{app} values
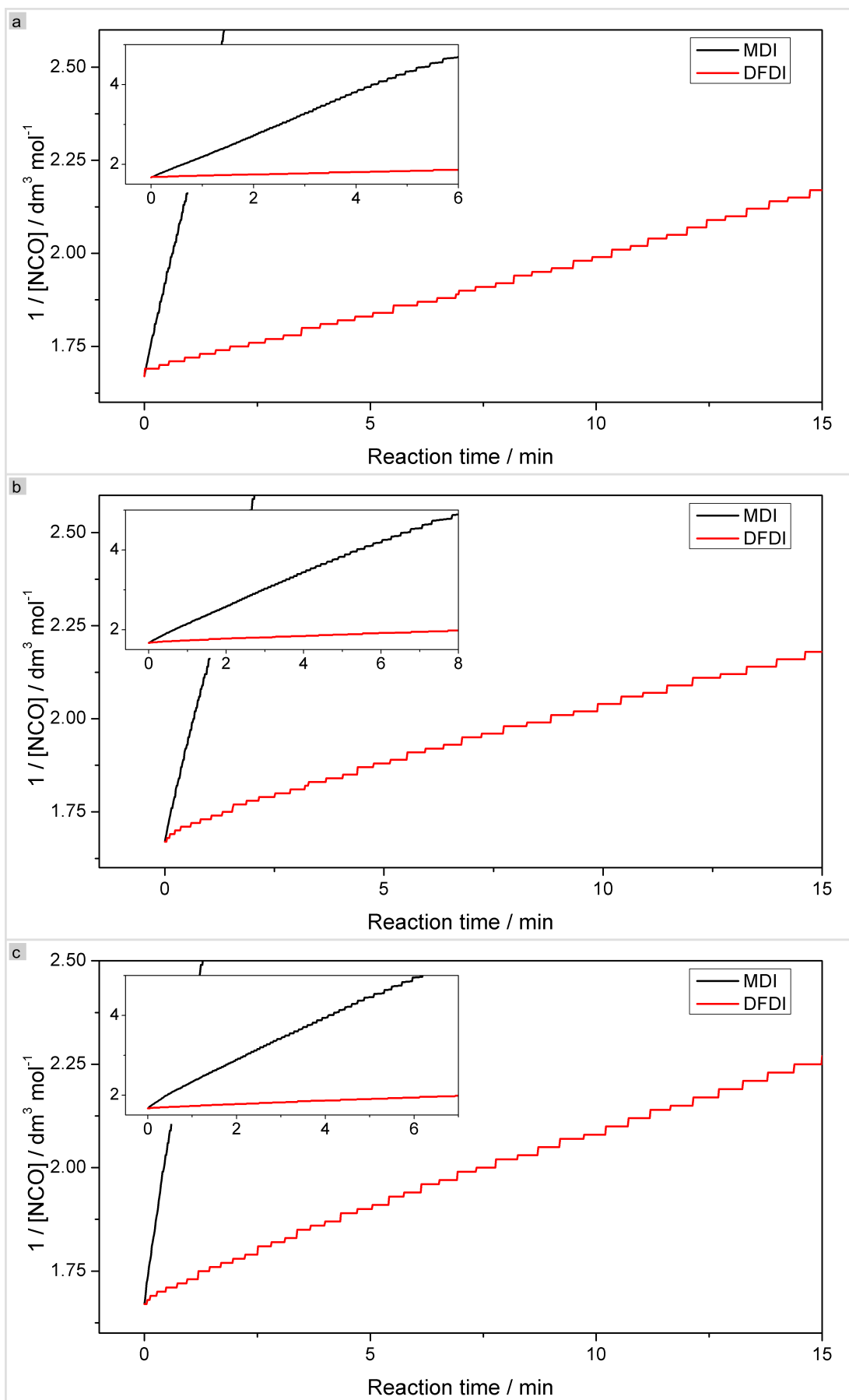
Figure 28: 2nd order plots for a. DMF-MeOH b. Diglyme-MeOH and c. Diglyme-Methyldiglycol systems found using an adiabatic temperature rise technique.

Pannone and Macosko[42a] were the first to use corrected adiabatic temperature rise profiles to follow the isocyanate conversion in polyurethane systems, since then it has been used many times by the Macosko and other groups[28b, 42b, 68].

Cawse[19b] and Boufi[21] both previously compared the reactivity of DFDI (or analogous molecules) and MDI. Cawse[19b] reacted isocyanates with 1-butanol in a toluene solution using TEA or TEDA as a catalyst. The concentration of remaining diisocyanate was determined by quenching aliquots with a solution of dibutylamine and titrating with HCl. In agreement with this work, k_{app} values in MDI systems were reported as c.14.3× those of the analogous MDI systems.

Cawse[19b] reported the apparent rate constant for the reaction between DFDI and primary alcohols is between that of aryl and alkyl isocyanates, reacting at approximately one fifteenth the rate at which MDI does. The rate constant of MDI was found to be c.192 times that of the HDI rate constant by Burkus and Eckert[23].

Boufi[21] utilised a method in which aliquots were periodically taken from a stirred solution and analysed using IR spectrometry, however the series did not use consistent conditions (varying temperature and catalyst concentration), making comparisons of k_{app} values difficult to make.

Chapter 4. Effect of hard segment content on morphology and properties

Introduction

It is generally accepted that the strength and high elasticity of polyurethanes are due to the phase separated nature, allowing the hard and soft segments to contribute both glassy and rubbery properties[69]. It is understandable then, that the relative amount of hard and soft segment present can have a marked impact on both the morphology and physical properties of PU.

The physical and chemical properties are dependent on numerous factors including soft and hard segment content, SS molecular weight, extent of crystallinity and the degree of phase separation[28b].

It is known that the hard segment weight fraction can have an effect on all properties of the resulting polymer. The SS Tg has commonly been used as a simple indicator of the degree of phase separation and most of the authors of the literature referred to in this section have assessed changes in phase separation using this method.

Li[53b] noted that while the trends in varying SS Mwt are clear and few contradictions exist, trends for varying HS% are less clear and depend on many additional factors including chemical structure of both segments, SS Mwt and sample preparation.

Schneider[8c] reported that the SS Tg had a linear relationship with the hard segment content within the range studied (30-60%) for a 2,4-TDI system, being closer to that of the pure soft segment at lower HS%. However, for 2,6-TDI there was no variance in Tg with HS%, this was attributed to ordering in the 2,6 system that is not possible for the 2,4-TDI, suggesting that the capability of ordering within the HS is enough to drive separation almost to completion without the need for the product of χN to increase.

Paiksung[37a] observed no change in SS Tg for PTHF2k and 2,4-TDI based elastomers with changing HS% for urethane or urea hard segments; for the PTHF1k variants, there were again no changes observed for the urea HS, the urethane HS elastomers displayed increased phase separation with increasing HS%.

Findings by Koberstein[70] show that for an MDI-BD and a PEO end capped PPO system, increasing the weight fraction of HS leads to more phase separation, which is backed up by SAXS data and in agreement with earlier studies on the same system[71].

Garrett[72] found phase separation to decrease beyond 22%HS for a PTHF2k system with an MDI-EDA HS, this was backed up with SAXS and AFM data. The reduced level of phase separation may be due to the greater viscosity of the urea system or a consequence of the short chain extender hindering order within the HS.

Wang[73] found phase separation to decrease with increasing HS content in an MDI-BD-PTHF system, these findings were based on Tg observations from DSC experiments.

Both Cawse[19b, 74] and Boufi[19f] have previously synthesised PU elastomers from DFDI, or DFDI like molecules (Boufi utilised the analogue with two methyl groups on the bridge as the yield for the ring fusing step is higher). Both groups reported light red, strong and rubbery elastomers with properties physical properties similar to those observed in MDI analogues.

Crystallinity

Crystallinity is often observed in the hard segment when symmetrical isocyanates are used[31]. The MDI-BD hard segment crystallises readily and its structure has been studied in detail[75].

While polyester SS can crystallise and have a complex crystallisation behaviour with elongation, SS crystallisation is less common in polyether soft segments due to the lack of any specific interactions. The driving force of soft segment crystallisation is the accumulation of weak Van der Waals interactions, as such the crystallisation is easier to disturb and not always observed.

Sonnenschein[76] published findings in which the physical properties of a PU elastomer were found to be enhanced with increased SS crystallinity. The hardness was observed to increase significantly with no effect on the tensile strength or elongation properties. The degree of SS crystallinity however was found to decrease with increasing HS content.

Results and discussion

Results presented in this chapter pertain to the varying HS% series of elastomers. All elastomers have HS based on MDI-BD or DFDI-BD and a 2kDa PTHF SS. Elastomers are either described or use the nomenclature x-y%HS where x is d or m, describing the isocyanate used (DFDI or MDI) and y is 0, 20, 40 or 60 and refers to the HS weight percent.

AFM

The morphology often reported for SPU elastomers (with non-monodisperse segment lengths) is isolated domains of hard segment at low HS% with a phase inversion occurring somewhere between 50[19b, 77] and 65%[78] HS, after which the continuous phase is HS, with isolated SS domains.

In an effort to make results comparable and relevant to potential applications, all AFM images reported in this chapter are of bulk cast elastomers.

AFM has proven to be a popular method for probing the structure of polyurethane elastomers. The ability to observe the nanoscale morphology and compare this to quantitative values such as those produced by SAXS further elucidates the complex structure.

The DFDI based elastomers at 0, 20 and 60% HS show a phase separated structure made up of stripes of a thickness between 13 and 15nm, as calculated by the PSD. The lamellae are composed of pure soft segment (PTHF) as confirmed by WAXS and DSC studies (reported later), with the space in-between being composed of amorphous PTHF and the hard segments. Tapping mode AFM images are reported in figures 29 to 32.

Figure 29: AFM phase images of 0% HS elastomers collected in tapping mode at different length scales. (DFDI left, MDI right)
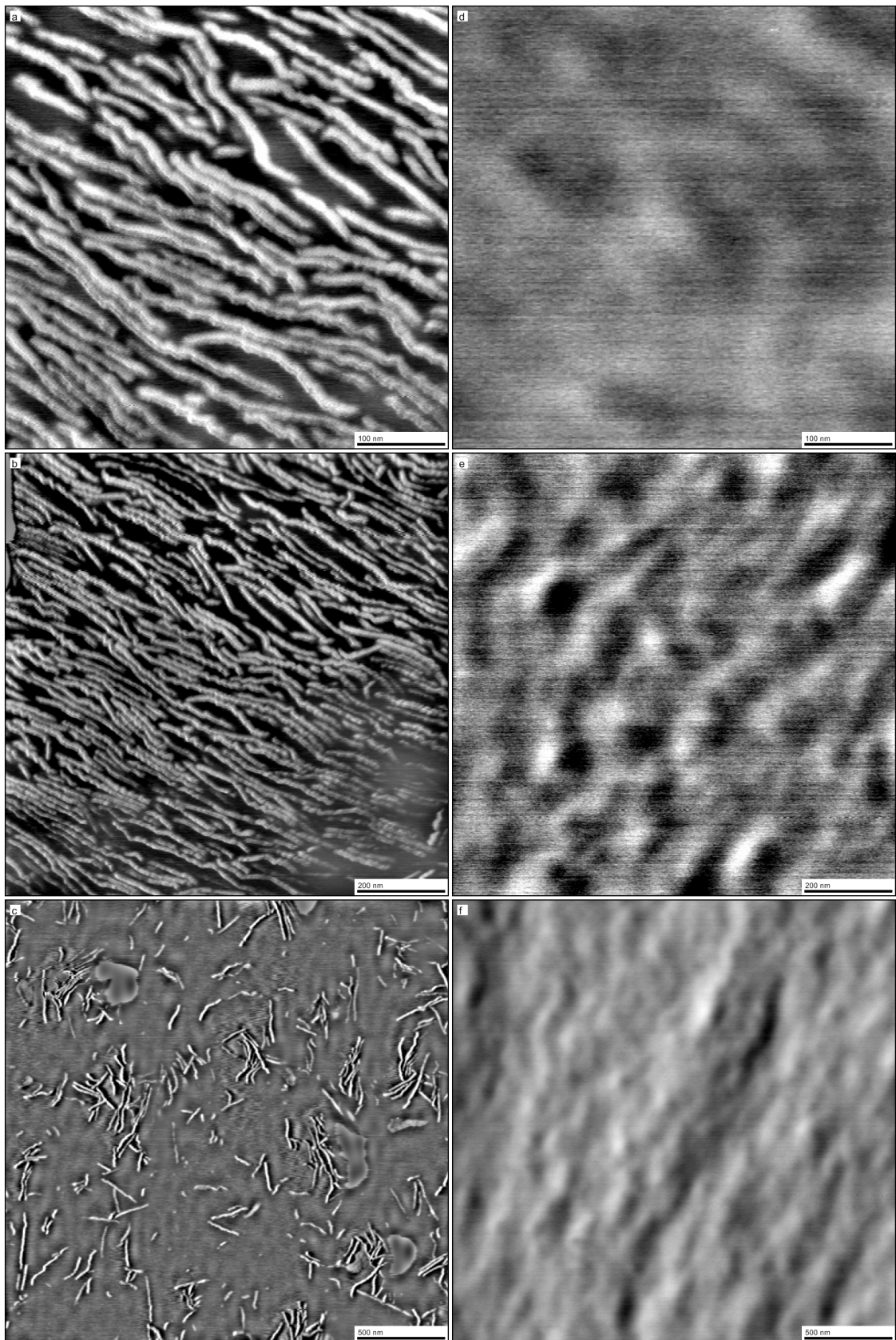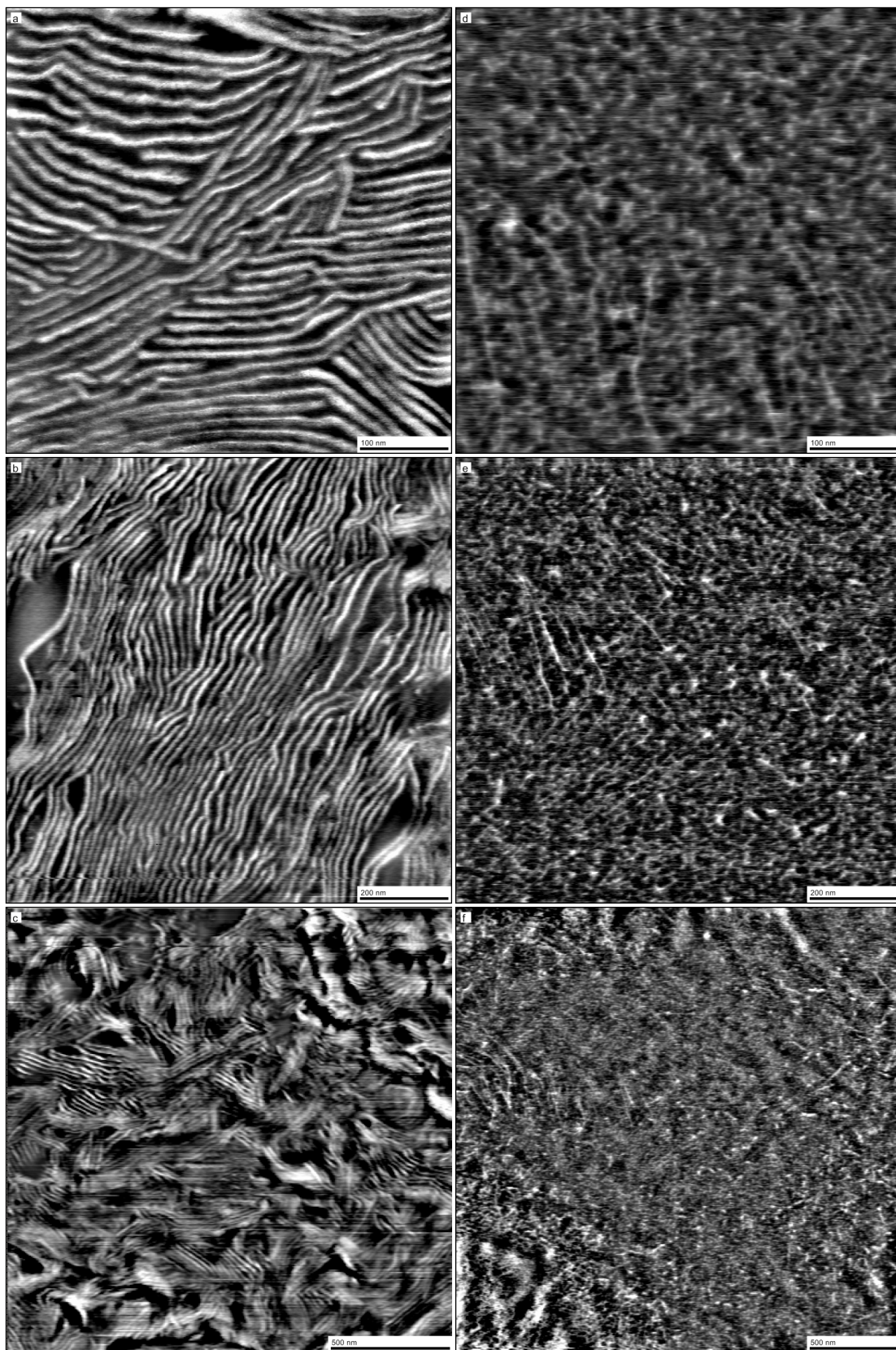
61

Figure 30: AFM phase images of 20% HS elastomers collected in tapping mode at different length scales. (DFDI left, MDI right)
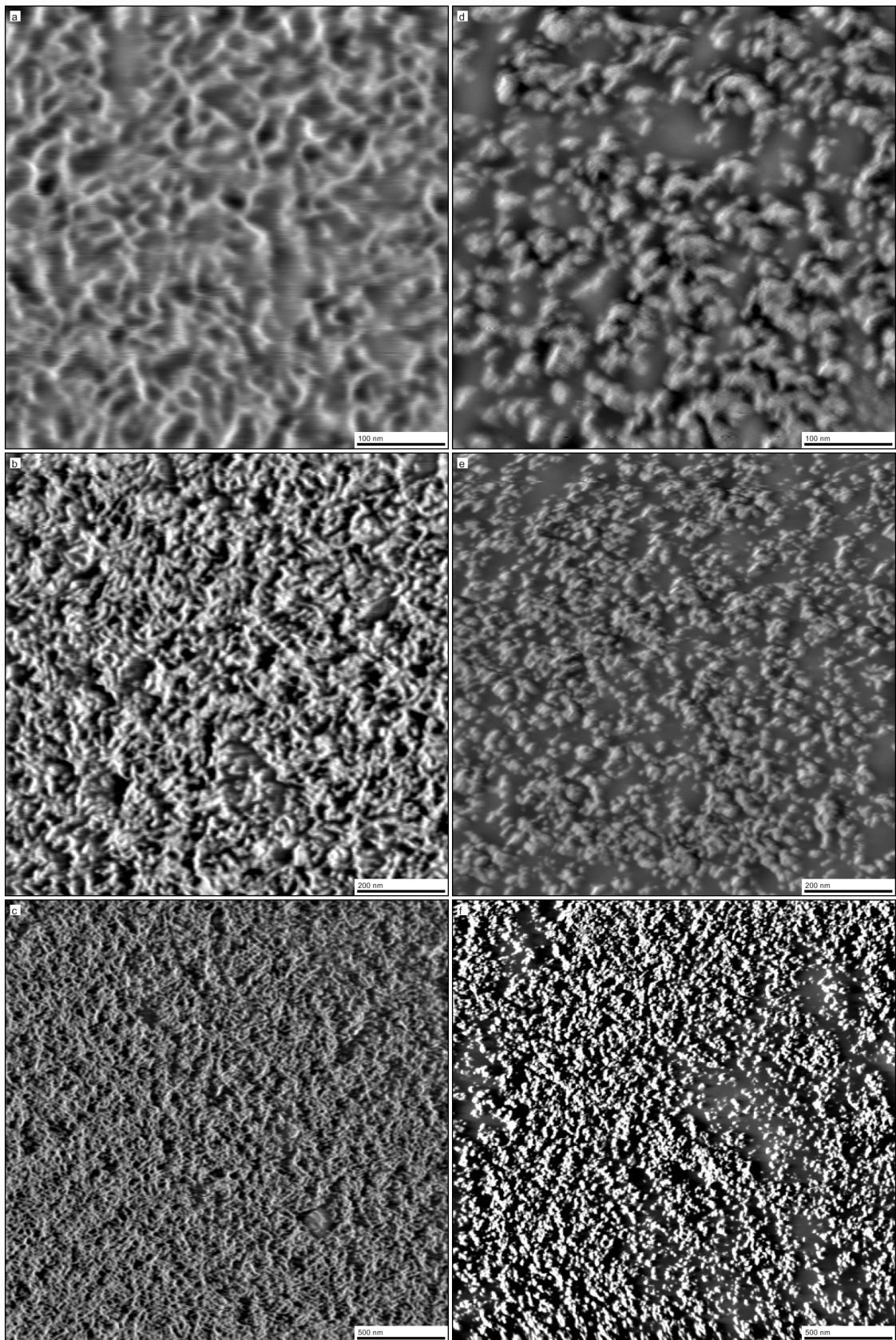
Figure 31: AFM phase images of 40% HS elastomers collected in tapping mode at different length scales. (DFDI left, MDI right)
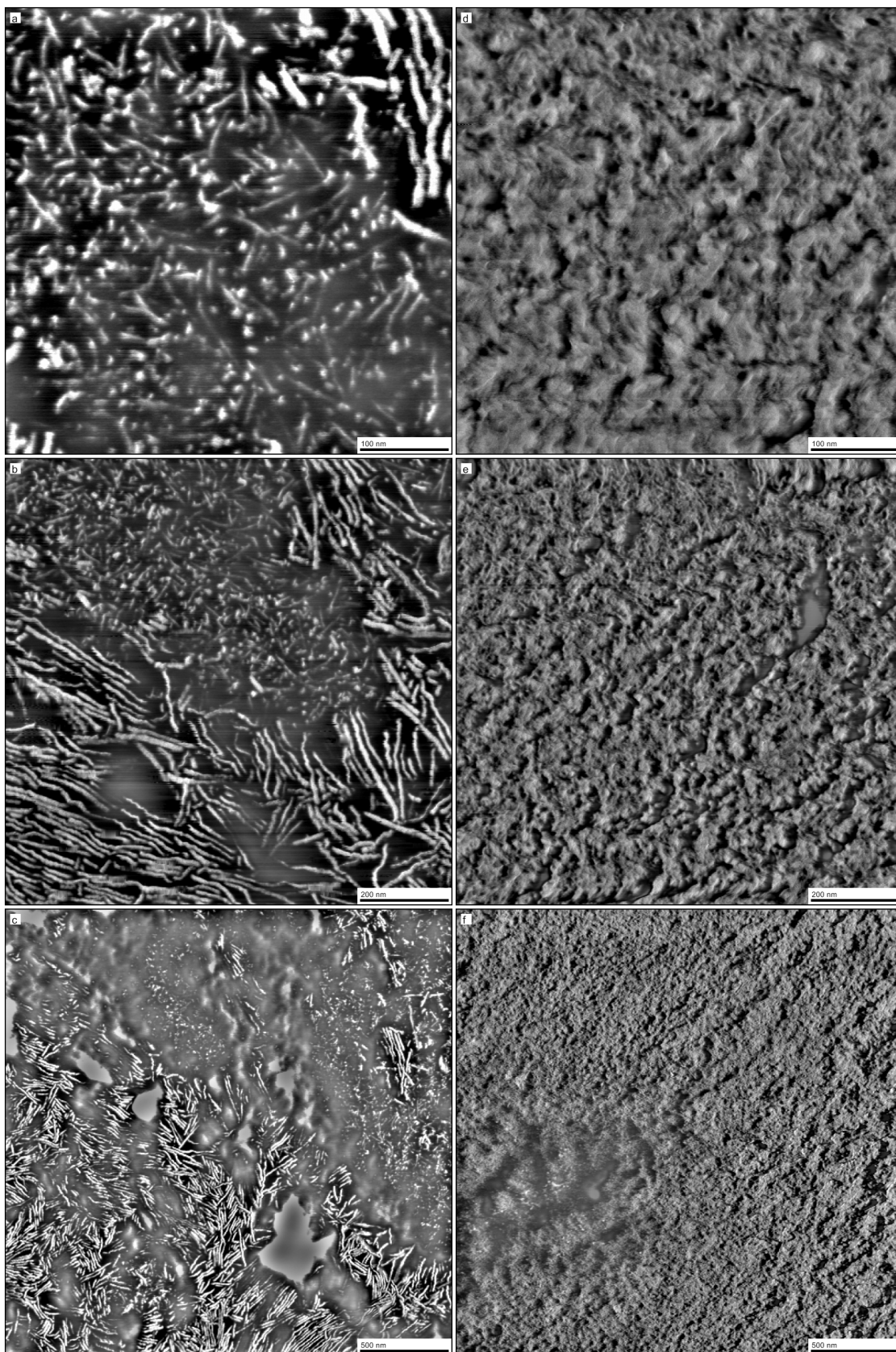
Figure 32: AFM phase images of 60% HS elastomers collected in tapping mode at different length scales. (DFDI left, MDI right)

The stripes in DFDI-0 and 20 HS% are roughly aligned over a one micrometer length scale in some images, ordering beyond this length scale was not observed. At 60% HS the stripes have very little ordering as there are two types of structure observed; a lamellae like structure similar to that observed in 0 and 20 HS% elastomers, and a phase separated structure of short rods with a thickness of around 8nm and very little alignment.

The 40% HS content DFDI based elastomer shows a phase separated structure with a length scale of 15nm. The structure appears almost cellular, composed of branched or interconnected rods. These are assumed to be soft segment as WAXS and DSC experiment show low levels of crystallinity in the soft segment.

MDI based elastomers with a HS% of 20 and above show a phase separated structure but appears to be a more commonly observed structure of regions of high and low hard segment content.

The 0% HS elastomer shows very diffuse boundaries between areas of different local modulus that can mostly be attributed to topographical effects (see theory and experimental section on AFM).

20% HS content images hint at a potential lamellae structure as faint stripes up to 100nm long can be observed in some regions. DSC and WAXS results show that while the soft segment is capable of crystallisation, at room temperature the crystalline SS regions should be mostly melted, as such only the most stable crystals would be visible to AFM at room temperature.

40% HS content images show roughly circular regions with an average diameter of 16nm. WAXS results indicate some degree of crystallinity within the hard segment, suggesting these features are crystalline hard segments.

60% HS content images show a phase separated structure similar to that of the 40%HS elastomer but with a higher degree of conglomeration, which owing to the higher amount of hard segment present seems feasible. 60% is also above the threshold noted for phase inversion to occur.

While chain flexibility is known to promote phase separation and crystallisation[53b, 79], the increased hydrogen bonding potential of DFDI relative to MDI may also contribute to the increased crystallinity observed in these samples.

The length of a single PTHF unit in the extended state is 6Å[80], the molecular weights and therefore number of repeat units can be calculated and the chain length can be derived. A 2000kDa Mwt PTHF chain would be expected to have a length of 16.5nm. The value of lamellae thickness observed (14-15nm) in 0 and 20%HS samples of DFDI elastomers suggests that the SS have crystallised in a chain extended state.

AFM investigations into the structure of solution cast polyurethanes are common[8b, 45a-e, 48, 72a, 81], but while images of solvent cast elastomers are often aesthetically pleasing, for most situations it shows an unreasonable view of the morphology to be expected in a bulk cast polymer.

Elastomers cast from solution are more likely to display a strongly phase separated state and crystallinity, as the extended time-scale and reduced viscosity allows greater mobility in the system, leading to a resulting morphology that is closer to an equilibrium state[8c, 82]. This has been observed by AFM, WAXS and DSC many times[45a-c, 45e, 48, 72a, 81, 83].

Few reports[84] of AFM images for polyurethane report bulk cast elastomers, despite this being the most common method of synthesis in industry.

No AFM studies on DFDI based elastomers were found in literature. The MDI-BD-PTHF elastomer has been studied extensively, although relatively few comparative examples were found.

The MDI-BD-PTHF2k system has been shown to produce a phase separated morphology. Images presented by McLean (see figure 33)[45d] for a 20%HS elastomer show a morphology comprised of circular domains with an 18nm diameter, similar to those of the 40%HS MDI elastomer reported in this chapter. The elastomer McLean used is Pellethane (Lubrizol), a comparatively low molecular weight polyurethane that is readily soluble in DMF and will dissolve in a THF solution over time. Sheth[8b] likewise reports a circular domain like morphology for 28%HS PTHF2k elastomers, again these were however lower molecular weight and soluble in IPA/THF. While no DSC or WAXS results were presented to confirm, it is likely the low molecular weight and solvent cast nature allowed the hard segment to crystallise in a way not observed in bulk systems until the hard segment content is higher (c.40%, see AFM images).
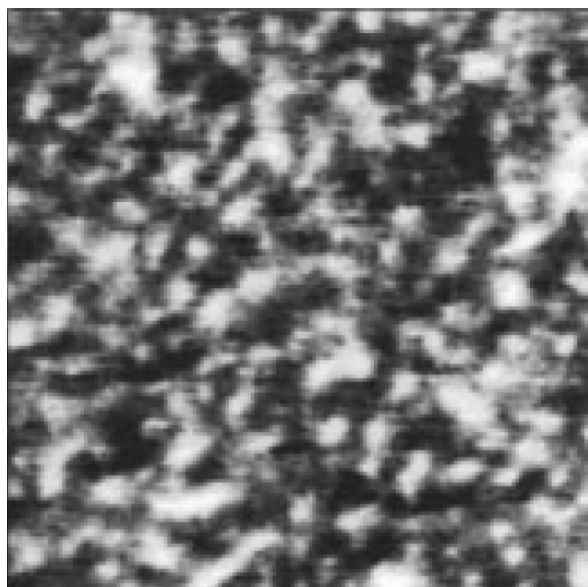
Figure 33: AFM phase image of an MDI-BD HS PU showing a similar spherical morphology to the 40%HS MDI based elastomer of this chapter, the image is 250nm^2. Reprinted (adapted) with permission from: **McLean, R. S.; Sauer, B. B., Tapping-Mode AFM Studies Using Phase Detection for Resolution of Nanophases in Segmented Polyurethanes and Other Block Copolymers. Macromolecules 1997, 30 (26), 8314-8317.** Copyright 1997 American Chemical Society.

In a bulk cast sample, Schön[84] reports images of weak rod like structures in MDI-BD-PTHF1k elastomers. 1kDa is normally considered to be below the threshold to allow SS crystallisation[85], making the rods likely to be HS, though no thermo-mechanical or scattering techniques were reported to confirm.

Unsal[81b] showed that a PTHF2k based elastomer cast from THF and with no hard segment shows a separated rod like morphology with a thickness of c. 8nm.

A solution cast MDI-EDA-PTHF2k system has been shown to have a rod/lamellae like morphology[45a, 72a, 86]. Samples at 22 and 37%HS showed a rod/lamellae morphology up to 100nm long and around 9nm thick, with a power spectral density returning 11-12nm.

Yilgor[81a] presented PUU elastomers from MDI and PTHF2k that showed rods with a 14nm width (see figure 34). The reported DMTA trace also shows a second decay at a higher temperature than the decay attributed to the SS Tg, this second decay is likely due to the melting of crystalline SS regions.
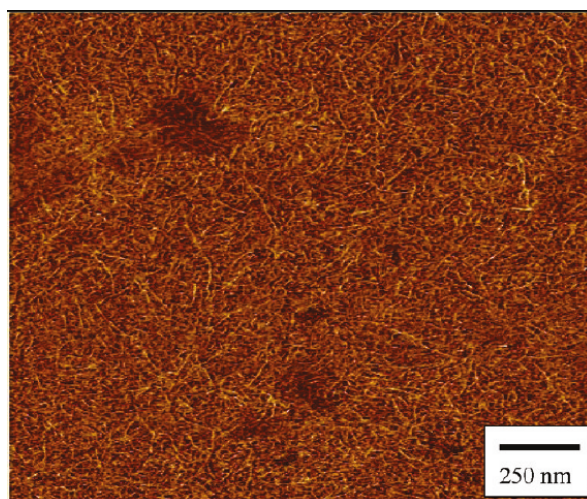
Figure 34: AFM phase image of an MDI and 2kDa Mwt PTHF based elastomer showing striped features due to crystalline SS, the image is 2μm². Reprinted (adapted) with permission from: *Yilgor, E.; Isik, M.; Yilgor, I., Novel Synthetic Approach for the Preparation of Poly(urethaneurea) Elastomers. Macromolecules **2010**, 43 (20), 8588-8593.* Copyright 2010 American Chemical Society.

Utilising a narrow or monodisperse hard segment can produce structures with a strong degree of ordering. De[45c, 81c] has shown highly regular structures in elastomers presenting curled hard segments with a width of 3nm. Krijgsman[83] presented extended rod structures with an 11nm width. Aneja[48] showed ordered structures with a rod (c. 6nm) and spherulitic morphology observed.

SAXS

Results from small angle x-ray scattering experiments show a phase separated structure is present in all elastomers with a hard segment content of 20% or higher. Lorrentz corrected intensities vs. q are presented in figures 35 and 36.

The domain spacing and relative invariants are summarised in table 7 (page 71). These values were collected by different methods, with all results presented. Domain spacing was calculated by using the Bragg equation to determine the domain spacing corresponding to the value at q_{max} and by performing a correlation function. Relative Invariants were calculated by correlation functions and integrating over the Lorrentz corrected SAXS frame over the range q= 0.015 - 0.2 .

The invariant was normalised for the lowest value (that of the PTHF-DFDI-DFDA elastomer reported later) to allow for comparisons to be made.

$$Q \simeq \underset{I}{\phi_H(1-\phi_H)} \underset{II}{\langle \eta_H - \eta_s \rangle^2}$$

(33)

The first term (I) of equation 33 shows that for two pure phases, the intensity reaches a maximum when the volume fraction is 0.5, decreasing with a higher or lower volume fraction. The peak height (being lower) for the 20%HS elastomers seems to correlate with this, but the relative invariant does not. The second term (II) accounts for differences in electron density within the sample.
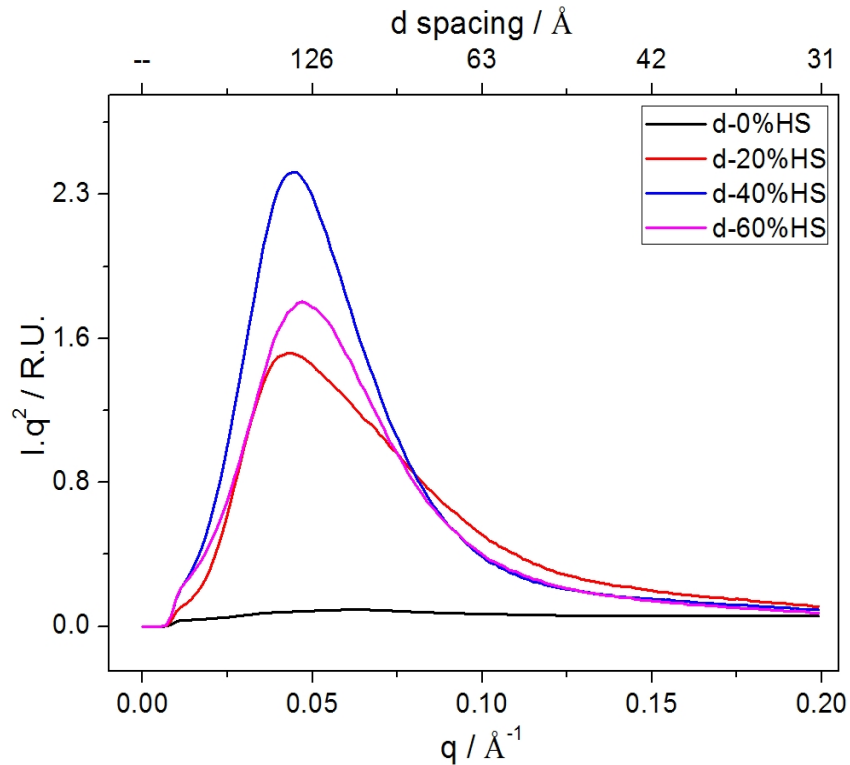
Figure 35: SAXS Lorrentz corrected intensities as a function of q for the DFDI based varying HS% series at room temperature. The upper x-axis shows the calculated domain spacing from the scattering vector, "--" is displayed for q=0 as this corresponds to an infinite domain spacing.
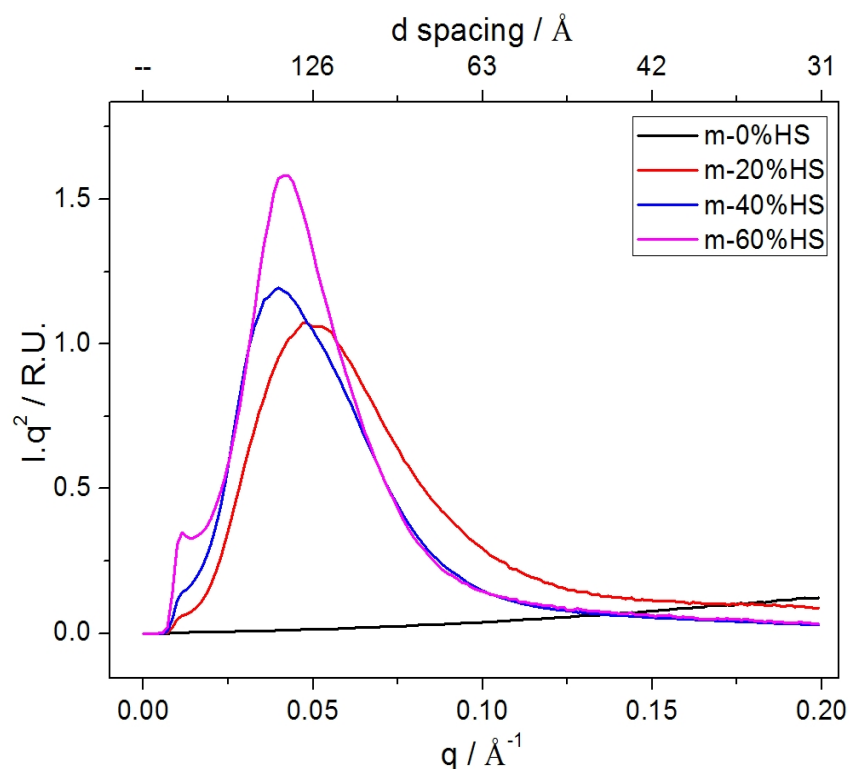
Figure 36: SAXS Lorrentz corrected intensities as a function of q for the MDI based varying HS% series at room temperature.

The 0% HS content DFDI based elastomer presents a broad peak with a very low intensity. The scattering intensity is known to be proportional to square of the difference in electron density of the two regions of interest. A lamellae structure of crystalline PTHF produces two regions; one with an electron density higher than that of amorphous PTHF due to increased density of the crystalline phase; and a second, again with slightly higher electron density of amorphous PTHF due to incorporation of DFDI units.

Using literature values of the density of the MDI-BD hard segment (1.297 g cm^{-3} [87]) and those of the amorphous and crystalline PTHF SS (0.982 g cm^{-3} [88] and 1.157 g cm^{-3} [89] respectively) as an example. Two pure phases (amorphous SS) gives rise to a value of 2.05×10^{-2} for the term $(\eta_H - \eta_S)^2$. A crystalline SS however reduces that value to 2.12×10^{-3}, almost an order of magnitude.

Calculations using the density of MDI (1.23 g cm^{-3})(calculation for elastomers not containing CE (0%HS)) result in values of 9.06×10^{-3} and 3.62×10^{-6} for amorphous and crystalline SS. The invariant for a 0%HS polymer with a pure crystalline SS would be expected to be less than 1% of the value of the amorphous SS polymer.

The relative invariants for all DFDI based elastomers 0%HS are higher than

70

corresponding values for MDI based elastomers.

The domain spacing decreases with increasing HS% for DFDI elastomers, potentially due to hard segment interfering with the growth of SS crystals. The domain spacing for MDI elastomers increases from 20 to 40%HS and then drops slightly for the 60%HS elastomer.

Isocyanate	HS%	d-spacing / nm			Relative invariant	
		Iq^2 Peak	Correlation function	AFM	Iq^2 Peak	Correlation function
DFDI	0	11 ± 2.4	7 ± 0.5	14 ± 1	1.3	1.1
DFDI	20	15 ± 0.6	15 ± 0.5	15 ± 1	10.6	9.8
DFDI	40	14 ± 0.4	14 ± 0.5	14 ± 1	12.9	10.0
DFDI	60	13 ± 0.3	13 ± 0.5	13 ± 1	10.5	9.8
MDI	0	-	-	-	-	-
MDI	20	13 ± 0.9	13 ± 0.5	14 ± 1	6.5	6.3
MDI	40	16 ± 0.5	16 ± 0.5	16 ± 1	6.0	5.2
MDI	60	15 ± 0.3	14 ± 0.5	15 ± 1	6.9	5.8

Table 7: Domain spacing (from SAXS and AFM experiments) and relative invariant (SAXS).

The correlation between AFM and SAXS values of the domain spacing is good in most cases. Other studies noting a good agreement between SAXS and values obtained through imaging methods include Neff[90] who reports comparable values for domain spacing obtained via SAXS and TEM for a flexible foam; and Garrett[45a, 72a] who noted good agreement between SAXS and AFM values for elastomers based on PTHF2k.

The discrepancy in domain spacing for the d-0%HS elastomer can be explained by the limitations of AFM. While images at smaller length scales show a mostly lamellae structure, the image at the largest length scale shows that this morphology does not extend throughout the elastomer. The difference in domain spacing is therefore due to extracting a length scale from a method that images only the local morphology, thus highlighting the need for analysis by quantitative methods such as SAXS.

Of the two groups who are known to have synthesised polyurethanes with DFDI previously, neither are known to have carried out SAXS studies. Analogous MDI systems however have been characterised and comparisons will be drawn here to help put results for DFDI elastomers into context.

Chu[53d] analysed 40%HS elastomers of the MDI-BD-PTHF type and found the domain spacing to be 17nm, which is agrees with measurements on samples presented here (16±0.5nm).

Sun[91] investigated the structure of a 13%HS solution cast elastomer (MDI-BD-PTHF) reporting 5nm diameter circular morphology. The WAXS data shows an amorphous halo at 35°C and crystalline soft segment at 18°C. The structure presented is likely due to small SS crystallites which become amorphous at slightly elevated temperatures.

Garret[72a] reported length scales between 13-16nm for a PTHF2k based elastomer with an MDI-EDA hard segment and hard segment content between 14-47%, there was no apparent correlation between the length scale and the hard segment content.

WAXS

WAXS investigations into the structure of DFDI based elastomers have not previously been reported and are presented here for the first time. WAXS frames for the segmented PU elastomers are presented in figures 37 and 38.

WAXS results show crystalline peaks associated with the SS are far more pronounced in DFDI elastomers. 0 and 20%HS content DFDI elastomers at room temperature display crystalline peaks matching those of the pure soft segment (presented in figure 39), but with a much lower intensity.

40 and 60%HS content DFDI elastomers show a broad peak at a smaller length scale than that of the amorphous SS (more obvious in the comparison to pure HS in figure 39) which matches the pattern collected for the pure hard segment. The differences are attributed to the four types of structure present, both crystalline and amorphous hard and soft segments.

0 and 20%HS content MDI elastomers at room temperature show only an amorphous peak centred at 4.4Å consistent with that observed for the DFDI 0%HS elastomer held at 40ºC (shown in figure 16). While crystallinity is observed in these samples by DSC, the SS Tm is 17ºC, and SS crystals should be mostly molten and amorphous at room temperature.

40 and 60%HS content MDI elastomers show some crystallinity which matches the profile of the WAXS frame collected for the pure HS. The high hard segment content MDI based elastomers are much closer matches to the pure hard segment profile than analogous DFDI elastomers, suggesting higher levels of HS crystallisation.
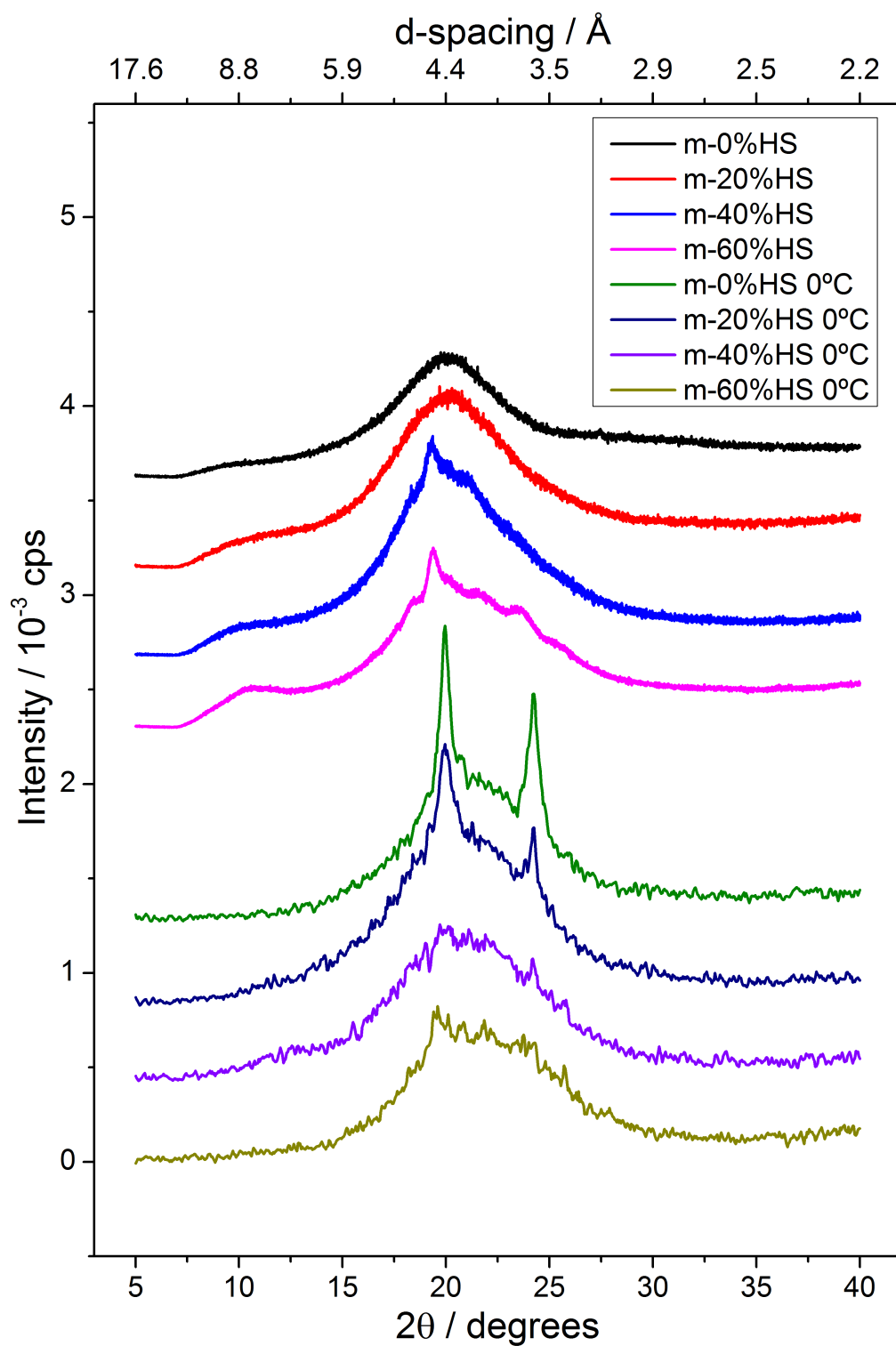
Figure 37: WAXS intensity as a function of scattering angle for MDI based HS% series at room temperature and at 0°C post erasing thermal history. Series are offset on the Y axis for clarity.
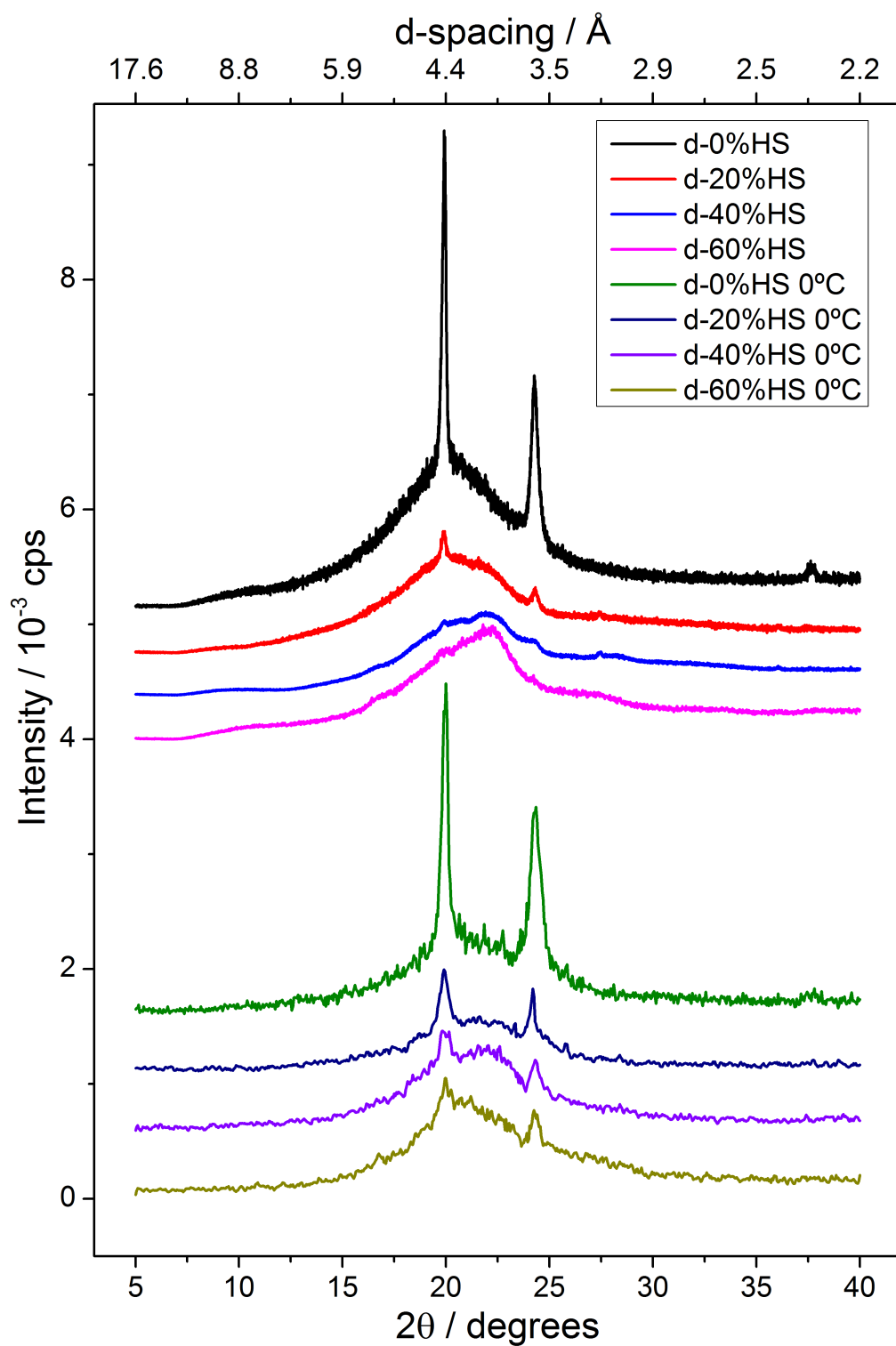
Figure 38: WAXS intensity as a function of scattering angle for DFDI based HS% series at room temperature and at 0°C post erasing thermal history. Series are offset on the Y axis for clarity.

Inconsistencies with crystallinity being observed in some samples via DSC but not via WAXS prompted the collection of WAXS frames on samples held at 0ºC post replicating the thermal history experienced in DSC experiments. Results from these experiments are presented on the lower portions of figures 37 and 38. These data sets match DSC experimental data much more closely; SS crystallinity is observed in almost all elastomers.

Upon erasing thermal history and holding at 0ºC, all DFDI based elastomers show crystalline SS peaks. The calculated crystallinity is also higher, and it is this value that is reported in table 10.

MDI elastomers at 40 and 60%HS show very weak peaks, making calculation of the SS crystallinity values difficult. The observation of weak peaks in the MDI 40%HS profile and the lack of observation of any crystallinity in the DSC trace may show a greater sensitivity in the technique, although the noise leads to greater uncertainty in predicted SS crystallinity.
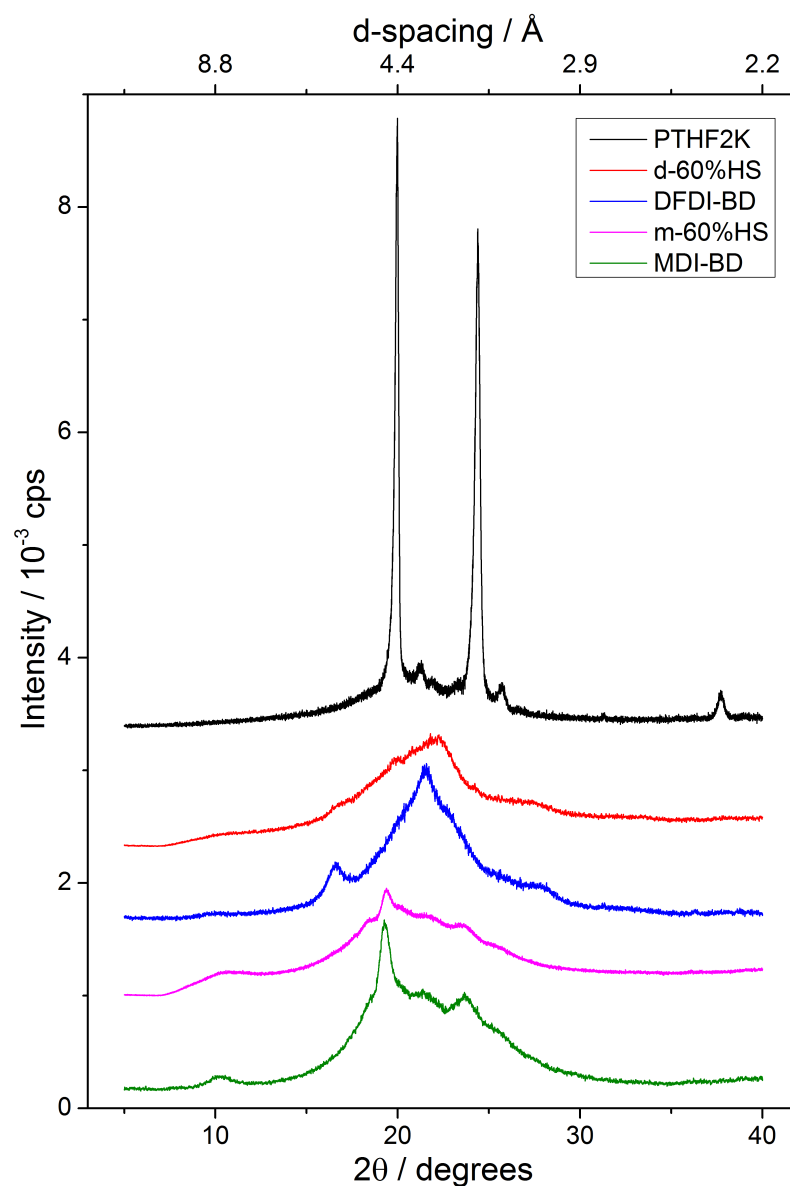
Figure 39: WAXS intensity as a function of scattering angle for pure phases used in this chapter, and the highest hard segment elastomers used for comparison. Series are offset on the Y axis for clarity.

The patterns collected for the pure SS[37a, 92] and MDI-BD based HS[53a, 75, 93] presented in this chapter match those previously reported in literature.

The PTHF SS is known to crystallise if conditions are favourable; mainly in solution cast samples or with higher molecular weight PTHF (>2kDa).

Sun[91] presented WAXS frames for a solvent cast sample of 13%HS MDI-BD-PTHF2k. The presented data shows an amorphous peak at 35ºC and crystallinity at 18ºC. No DSC data was present to corroborate the melting and crystallisation temperatures of the soft segment but the behaviour matches that observed in samples presented in this work. As expected from solution cast samples the soft segment crystallinity is more stable, noted by its continued presence at 18ºC; a property observed only in DFDI based samples in this series of bulk cast elastomers.

Garrett[72b] noted no crystallinity for MDI-ED-PTHF2k samples with HS% varying from 14-47 despite being solvent cast and relatively low HS%. No DSC data was presented, making it difficult to know if any crystalline SS was simply amorphous at the temperature that WAXS frames were collected.

Yeh[94] also reported no observed crystallinity for 12%HS MDI-EG-PTHF1.8k. This is assumed to be due to the effect of the ED/EG chain extender, noted as being too short[73, 77] to allow HS crystallisation, the amorphous nature of the HS may have disrupted any high level phase separation and therefore crystallisation in the SS.

Williams[92c] noted amorphous WAXS frames for all samples investigated in a PTHF2k-BD-HMDI series. The DSC data presented for one series shows clear crystallinity of the SS with a Tm of 14ºC. A detailed experimental outline for the WAXS analysis was absent but it seems apparent that the frame was collected at room temperature, explaining the absence of crystalline peaks.

Li[85] noted the decay in SS crystalline peaks in WAXS for PCL based elastomers with increasing HS%. This matches both series presented here and fits with the viscosity-mobility model[53b], where the increased hard segment content has restricted flexibility and therefore mobility; despite χN being higher for 40%HS compared to 20%, the purity of the SS has decreased.

DSC

All DFDI based elastomers show crystallisation of the soft segment to some degree. Crystallisation occurs almost exclusively on the cooling cycle up until a 60%HS content. This displays a greater capability for crystallisation in DFDI based elastomers, assumed to be due to the higher flexibility in the DFDI molecule compared to that of MDI. The extra methyl separation of the NCO group from the aromatic ring allows for an extra two points of rotation within the molecule. This flexibility would allow for greater mobility and more favourable packing of the SS into the growing lamellae sheet as illustrated in figure 40.
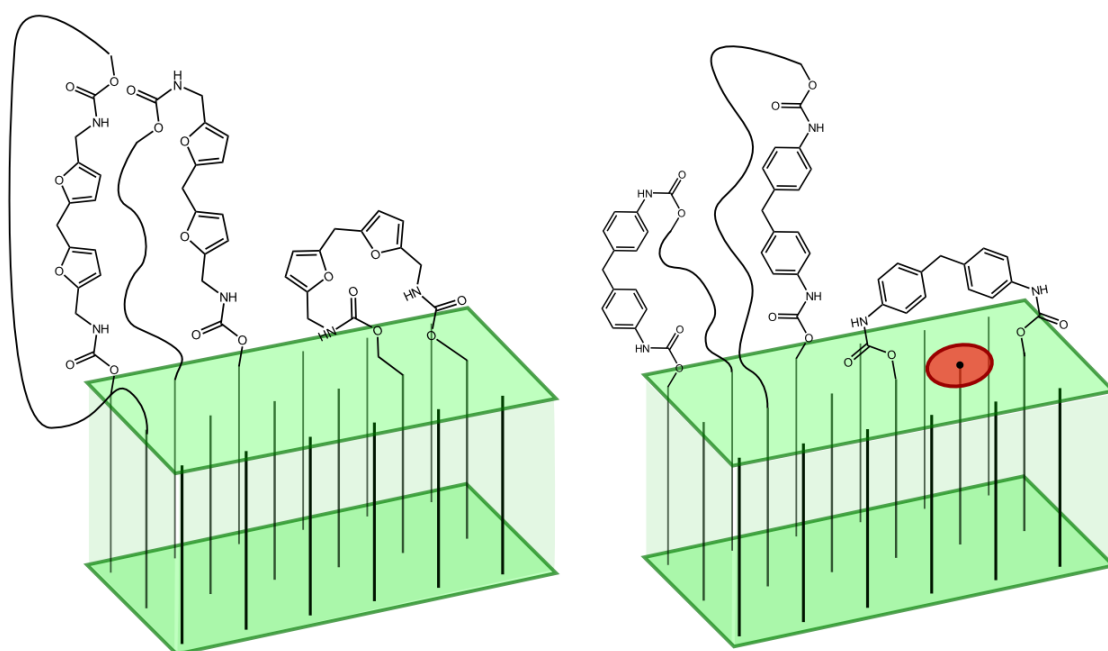
Figure 40: Rational for the difference in potential for SS crystal growth. Note with DFDI, SS can continue stacking into a lamellae sheet without contributing to the interphase; MDI units require PTHF to contribute to the interphase, thus hindering lamellae formation as they are composed of chain extended PTHF units.

The 60%HS DFDI elastomer shows crystallisation did not complete on the cooling cycle and continued on the heating cycle at the same temperature (obvious when plotted with a lesser scale).

Figure 41 shows example DSC traces for all elastomers of the HS series.
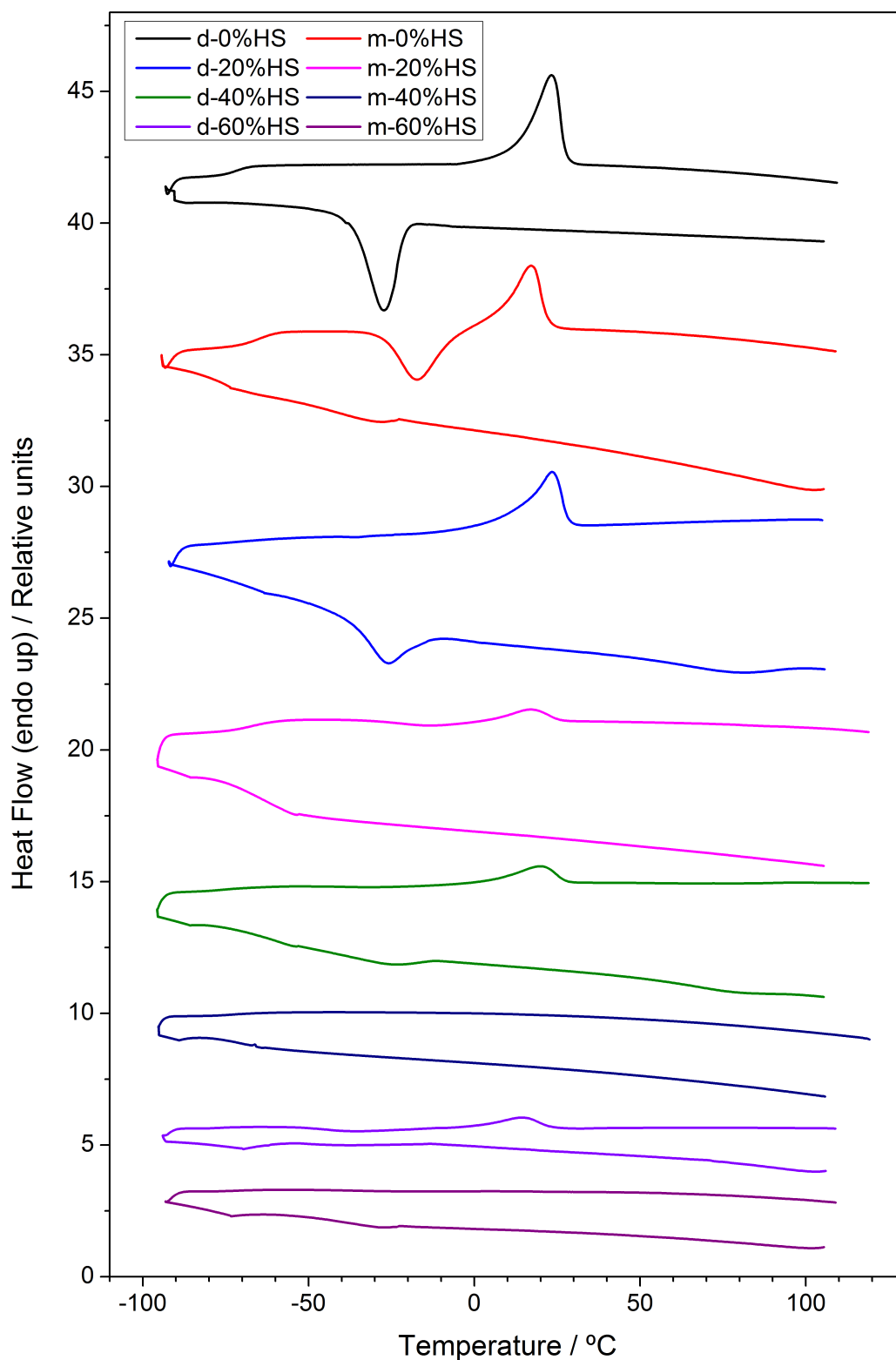
Figure 41: DSC traces for elastomer based on both isocyanates at 0, 20, 40 and 60%HS.

0 and 20%HS samples from MDI based elastomers show crystallinity, with the crystallisation occurring predominantly on the heating cycle, the 0% elastomer shows some degree of crystallisation occurs on the cooling cycle (around 13% of the total

crystallisation enthalpy).

The 60% MDI elastomer shows some degree of crystallisation occurring on the cooling cycle, a very broad and weak crystallisation is also visible on the heating phase but the melting peak is not discernible.

There is a broad range of reported Tg values for the pure PTHF soft segment ranging from as low as -96ºC[93b] but most commonly in the range of -83 to -86ºC [95].

As expected, glass transitions are of a lower enthalpy in DFDI elastomers when compared to MDI elastomers. The crystallisation occurring on the cooling phase reduces the amount of amorphous SS, the portion that would contribute to the glass transition.

Glass transition temperatures are 4-6ºC lower in all DFDI elastomers when compared to MDI versions, and are in the range of -70 to -77ºC. This shows a good degree of phase separation and is consistent with the lower values of Tg reported in PTHF based PU elastomers in literature.

A drop of 5ºC in the Tg is observed in both series between 20 and 40%HS, explained by the greater product of the term χN aiding phase separation.

Crystallisation of the SS displays a greater degree of undercooling when occurring on the cooling cycle and predominantly in DFDI elastomers. Crystallisation occurs at c. -30ºC in DFDI samples, the only MDI sample (0%HS) that displayed crystallisation upon cooling also crystallised around this temperature.

In DFDI samples where crystallisation occurs on both cooling and heating, crystallisation continues at a similar temperature upon heating. The 0%HS MDI elastomer however only continued crystallisation upon warming to -15ºC.

The degree of crystallisation was calculated for all samples that display melting peaks by comparing the enthalpy for the transition to that of a purely crystalline sample (167 J.g^{-1})[96]. The degree of crystallinity was further normalised to represent the degree of crystallinity for the SS and not the polymer as a whole, to quantitatively compare the degree of crystallinity within the soft segment.

Before normalisation, the degree of crystallisation for DFDI-40%HS was higher than that of DFDI-60%HS. Post normalisation, the crystallinity in DFDI-60%HS is

marginally higher. This fits better with AFM phase images as the DFDI-60% sample showed more lamealle like features.

Transition temperatures are reported in tables 8 and 9 along with associated enthalpies.

HS%	Experiment phase	Tg_{ss} / °C	ΔH / $J g^{-1}$°C-1	$Tcrys_{ss}$ / °C	ΔH / $J g^{-1}$	$Tmelt_{ss}$ / °C	ΔH / $J g^{-1}$
0	Cool cycle			-30	-3.70		
	Heat cycle	-66	0.44	-17	-25.07	17	26.23
20	Cool cycle						
	Heat cycle	-67	0.33	-13	-4.01	17	5.55
40	Cool cycle						
	Heat cycle	-72	0.16				
60	Cool cycle						
	Heat cycle	-71	0.08				

Table 8: Temperatures and associated enthalpies of transitions observed in DSC traces for MDI based HS% series. The error on all quoted temperatures is ±1℃.

HS%	Experiment phase	Tg_{ss} / °C	ΔH / $J g^{-1}$°C-1	$Tcrys_{ss}$ / °C	ΔH / $J g^{-1}$	$Tmelt_{ss}$ / °C	ΔH / $J g^{-1}$
0	Cool cycle			-27	-43.09		
	Heat cycle	-70	0.10			23	36.73
20	Cool cycle			-26	-26.35		
	Heat cycle	-71	0.06			24	28.00
40	Cool cycle			-27	-6.33		
	Heat cycle	-76	0.07	-30	-2.62	18	9.90
60	Cool cycle			-37	-1.60		
	Heat cycle	-77	0.05	-36	-3.91	14	6.77

Table 9: Temperatures and associated enthalpies of transitions observed in DSC traces for DFDI based HS% series. The error on all quoted temperatures is ±1℃.

Table 10 compares crystallinity as calculated by DSC and WAXS techniques. These values follow the same trends but can differ by large margins. The DSC values are viewed with more credence in this work as the the background fitting of WAXS frames is poor due to the low overall degree of crystallinity and the presence of HS peaks.

Isocyanate	HS%	% Crystallinity WAXS	% Crystallinity DSC	Difference
DFDI	0	32.6	24.7	7.8
DFDI	20	16.2	23.5	7.3
DFDI	40	15.4	11.1	4.3
DFDI	60	9.0	11.4	2.4
MDI	0	21.0	17.6	3.4
MDI	20	13.3	4.7	8.7
MDI	40	0.0	0.0	0.0
MDI	60	0.0	0.0	0.0

Table 10: Values of crystallinity (normalised) as calculated from WAXS and DSC data, and the difference between these values.

Tsuchiya[80] carried out a thorough investigation into the melting behaviour of PTHF at

different molecular weights. The melting behaviour of PTHF2k matches that observed in this work, with a main melting peak occurring at 29ºC and a shoulder at 26ºC.

Martin[93b] reports the MDI-BD Tg to be 80ºC for a pure sample, close to the value presented by Cawse[74], of between 84-89ºC for quench cooled samples. Cawse also reported a value of 28ºC for the DFDI-BD HS, again for a quench cooled sample.

Wang[73] found SS Tgs for the MDI-BD-PTHF2k elastomer to be -67ºC and -66ºC for 22 and 38%HS respectively. The value for the 22%HS matches that of the 20%HS in this work, the value for the 38%HS however is significantly higher than the SS Tg of the 40%HS elastomer in this work. Wang's method utilised no cycle erasing thermal history and the samples contained a 5% excess of isocyanate. This is a common method of assuring cured elastomers are formed, it does however especially at higher HS%, increase the amount of free isocyanate (known to be soluble in the SS) in the system. This is the likely cause of the increased SS Tg; if the 60%HS elastomer from this work was synthesised with a 5% excess of isocyanate, it would be expected to increase the SS Tg further still.

The melting endotherm was reported as 5.7 Jg^{-1} for the 22%HS system, consistent with the m20 elastomer and indicating SS crystallinity in the order of 5%.

Both groups who previously made elastomers based on DFDI (or their analogues) reported results of DSC experiments[19b, 19f].

Boufi[19f] synthesised DFDI-BD-PTHF2k elastomers with HS% ranging from 14-45. The DSC data is presented in table 11.

Isocyanate	HS%	Tg / ºC	Tcrys^{SS} / ºC	Tm^{SS} / ºC
DFDI	14	-65	#	#
DFDI	25	-61	-11	20
DFDI	33	-57	-7	18
DFDI	40	-62	*	18
DFDI	45	-70	*	21
MDI	23	-65	*	5

Table 11: DSC data from Boufi[19f].

 # - DSC trace not reported and this value was not mentioned.

* - Not mentioned and too broad to be determined from the presented DSC trace.

It can be seen from this data that as the Tgs do not correlate perfectly with those observed in this study. The only HS% that is shared exactly is the 40%HS elastomer

which deviates by 14ºC for the SS Tg.

This could be a consequence of the difference in pre-polymer method utilised (the chain extending method is essentially identical). Boufi end-capped pre-polymers for two hours at 50ºC; owing to the reduced reactivity of DFDI compared to MDI, it was decided to allow a longer time to allow for all PTHF molecules to be end capped (c. 4h at 80ºC, see experimental for details). If the end-capping is not complete, there is less control over the hard segment segment length. A more polydisperse hard segment would increase phase mixing and therefore the SS Tg (the HS Tg would be suppressed).

The SS crystallisation and melting temperatures were not reported, but values were extracted from presented DSC traces when possible. The Tcrys values were much higher than observed in this work, but the full DSC methodology was not reported and with only two values (extracted manually), there is insufficient data to draw a solid conclusion. The Tm values are around the same as observed in the polymers presented here for DFDI based elastomers, with a matching value for the 40%HS elastomer. The MDI elastomer at 23%HS appeared to present a SS Tm at 5ºC but again, without more data it is difficult to make a fair comparison.

Cawse[19b] used a 1kDa PTHF SS which would not be expected to display crystallinity, this elastomer matches more closely the structure of the series investigated in the next chapter and a more detailed analysis is present there. The Tg (for the HS% elastomers studied; 0, 10 and 50%HS) appears independent of the HS%, but is consistently lower than in analogous MDI elastomers.

Hu[97] synthesised a series of solvent cast elastomers with varying chain extenders, SS molecular weight and HS%. The MDI-PTHF based elastomers showed crystallinity when the PTHF Mwt was ≥2kDa. The crystallinity was also observed to decrease with increasing HS% in agreement with the series' presented in this work.

Williams[92c] observed the SS Tg of a solvent cast 37%HS PTHF2k based elastomer to be -78ºC, understandably lower than observed in bulk cast variants in this work.

Unsal[81b] noted crystallisation (-11ºC) on the cooling curve and subsequent melting (25ºC) on the heating cycle for a solvent cast PTHF2k system. The enthalpies of transitions were not reported but the Tm value is quite high indicating a pure SS phase and the Tg appears very weak in comparison, again indicating a high degree of

crystallinity. The solvent cast nature and lack of hard segment accounts for the degree of crystallisation.

Paiksung[37a] found that while the value of Tg changed over the HS% range for PTHF2k based PU and PUU, no trend was noted. They did however have a very limited HS% range (only between 17-35%).

DMTA

DMTA data shows peaks in the tanδ and decays in storage modulus for all samples (figures 42 to 45). All samples known to have crystalline segments (from DSC and WAXS) show broad tanδ peaks due to overlapping peaks of glass and melting transitions. Tanδ traces of higher hard segment content elastomers are further broadened due to the contribution of the HS glass transition.

The storage modulus starts higher in DFDI elastomers, an effect of the increased hydrogen bonding potential afforded by the heteroatom on the diisocyanate and the stiffness of the crystalline soft segment, effectively increasing the HS content at low temperatures. The modulus decays to a lesser degree with increasing HS%, a consequence of more glassy material retaining stiffness.

At 20 and 40%HS, the modulus in DFDI elastomers remains higher than MDI versions throughout the range investigated. MDI elastomers at 40 and 60%HS retain modulus at temperatures between 25 and 50ºC, due to crystalline HS as opposed to separated but amorphous HS in DFDI elastomers.

The storage modulus of the 0%HS MDI based elastomer decays to only c. 6MPa at 100ºC despite there being no separated HS or crystalline SS to maintain structure, this would indicate a cross-linked polymer; the DFDI based 0%HS elastomer was synthesised using the same batch of PTHF however suggesting cross-links are not from the SS but the isocyanate, and are therefore assumed to be allophanate linkages.

Glass transition temperatures were found by two methods, the onset of the tanδ peak and the onset of the first significant decay in the storage modulus. Both of these are reported alongside Tg values from DSC with differences for both methods in table 12.

The difference between Tg values reported by DSC and DMTA methods is generally agreed to be around 10ºC[73, 98], this difference is often understood to be due to the effect

of the greater thermal gradient in DMTA experiments, an effect of the greater sample size and slower heat transfer of air as opposed to the aluminium pans used in DSC.

Figure 42: Storage modulus (E') and mechanical damping (tanδ) as a function of temperature for 0%HS elastomers from both diisocyanates.

Figure 43: Storage modulus (E') and mechanical damping (tanδ) as a function of temperature for 20%HS elastomers from both diisocyanates.

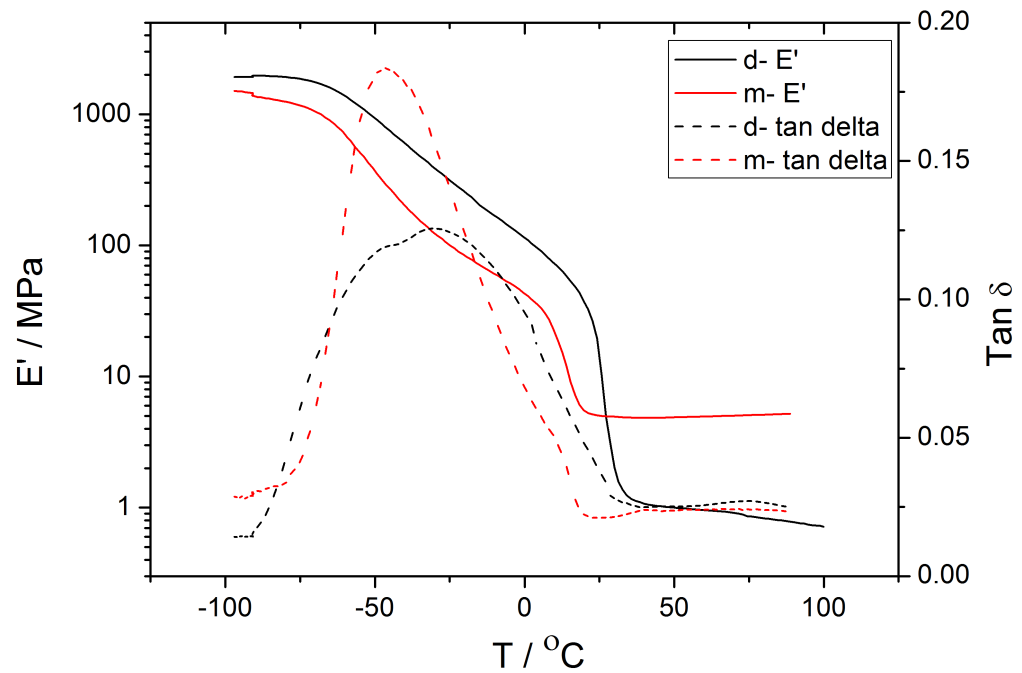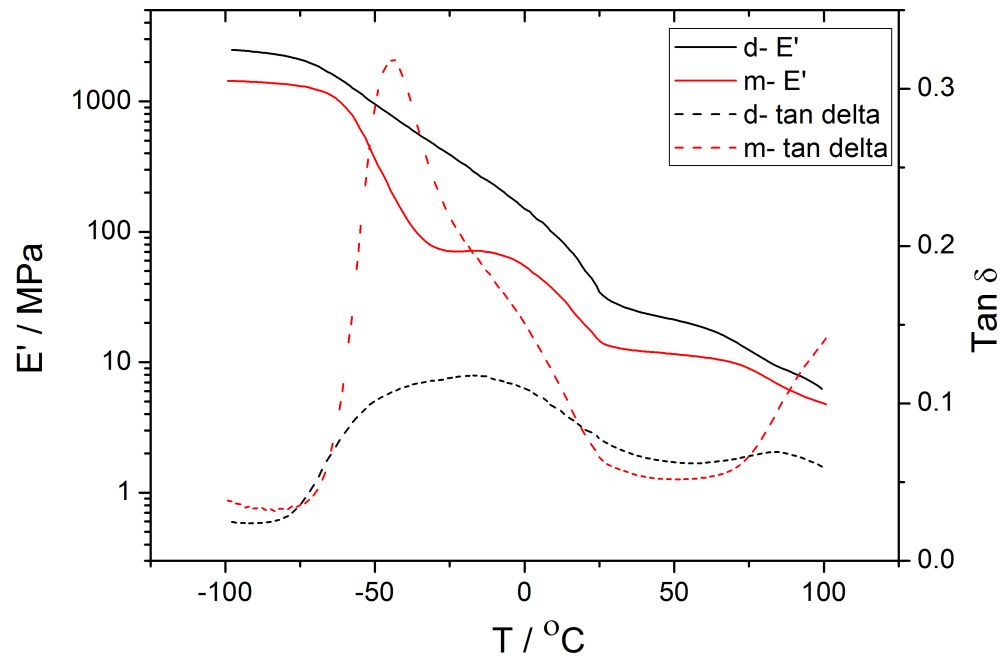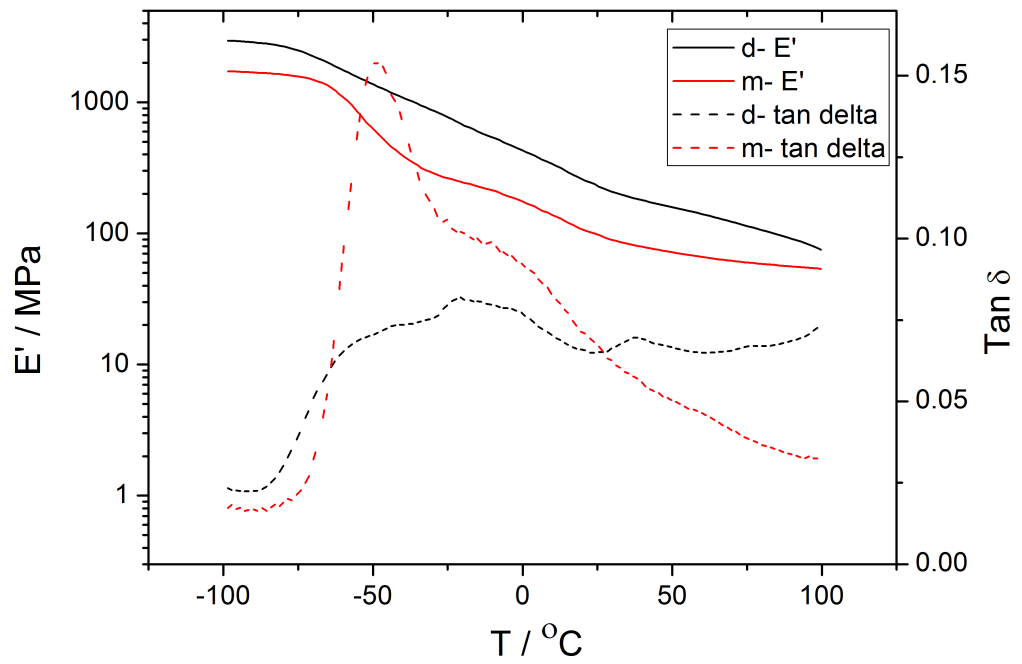*Figure 44: Storage modulus (E') and mechanical damping (tanδ) as a function of temperature for 40%HS elastomers from both diisocyanates.*

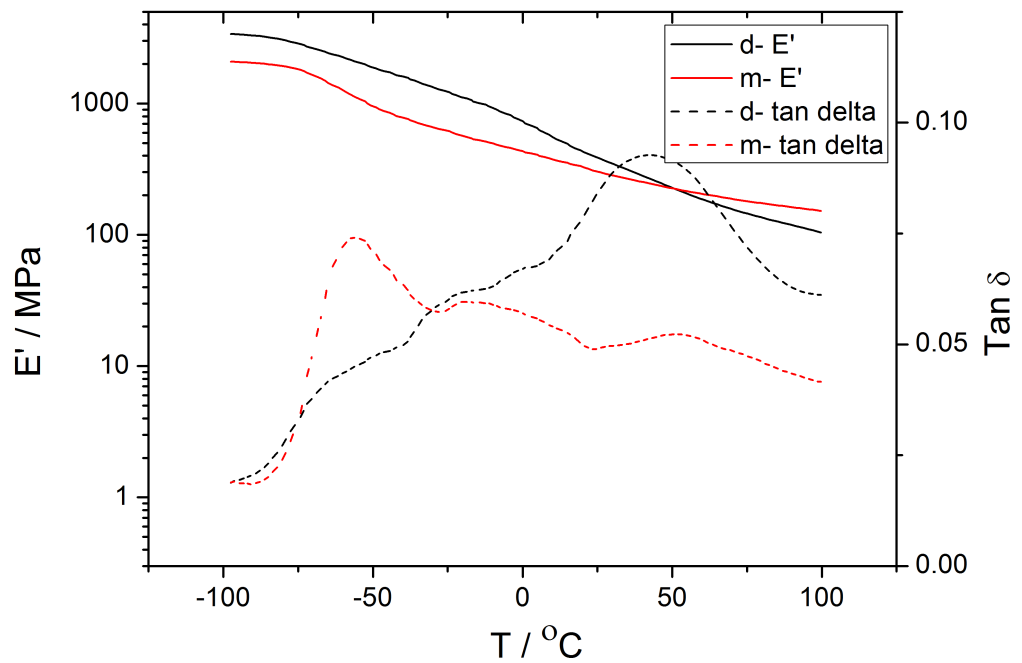*Figure 45: Storage modulus (E') and mechanical damping (tanδ) as a function of temperature for 60%HS elastomers from both diisocyanates.*

Isocyanate	HS%	DSC	DMTA			
		Tg / °C	Tg (tanδ onset) / °C	Δ (to DSC) / °C	Tg (E' decay) / °C	Δ (to DSC) / °C
DFDI	0	-70	-77	7	-71	1
DFDI	20	-71	-79	8	-71	0
DFDI	40	-76	-84	8	-77	1
DFDI	60	-77	-84	7	-82	5
MDI	0	-66	-64	2	-56	10
MDI	20	-67	-68	1	-62	5
MDI	40	-72	-74	2	-70	2
MDI	60	-71	-81	10	-72	1

Table 12: Glass transition temperatures calculated from DSC and DMTA (two methods) experiments for the HS% series. The error on temperatures from DSC measurements is ±1℃ while the error on DMTA measurements is ±2℃.

The modulus decay is known to be slower at higher HS%, and the tanδ broader[98]. The decay in modulus at higher HS% is indeed slower in this series, the tanδ however is affected by the crystallinity in the SS and diffuse boundaries and is somewhat broad in all traces. As noted by Sonnenchein[76], increased crystallinity leads to more gradual decays in modulus, and as a consequence, broader tanδ peaks.

Both groups who previously synthesised DFDI based elastomers carried out DMTA tests.

Cawse[19b, 74] reported DMTA data for a PTHF1k based elastomer with a BD chain extender, traces have a very similar shape in both MDI and DFDI variants. For the 10%HS elastomer the decay in modulus occurs 10℃ colder in the DFDI version, indicating greater phase separation and in agreement with DSC data from the same paper and data in this chapter. The 50%HS elastomers are again very similar, the DFDI version presents a flatter rubbery plateau than the 40%HS elastomer studied in this chapter. This would be expected from a 1kDa SS, as there is no crystallinity and consequent broadening of the tanδ peak or modulus decay.

Boufi's[19f] 25%HS (no other DMTA traces or values were presented) 2kDa PTHF polymer presents a more gradual decay in modulus for the DFDI based elastomer than the analogous MDI version also reported. The first decay in the modulus occurs 15℃ warmer in the DFDI version, with the modulus dropping further, from slightly above 1000MPa to 3.2MPa by 50℃ for DFDI, and to 10MPa for MDI. This would indicate a higher Tg and more diffuse boundaries in the DFDI version. Whilst diffuse boundaries fits with the data presented in this chapter, the higher Tg does not; as discussed earlier, the end-capping method utilised by Boufi is the likely cause of the higher degree of phase mixing.

Wang's[73] series of polymers with varying HS% and structure presented DMTA curves for 22 and 38%HS MDI-BD-PTHF2k elastomers. The curves match their closest counterpart (20 and 40%HS) of those reported in this work but with slightly greater decays in modulus over the range tested in Wang's data.

Williams[92c] presented a DMTA curve for a 37%HS PTHF2k elastomer utilising a HMDI-BD hard segment. The curve is similar to the MDI 40%HS trace reported in this work in many aspects. The decay in modulus is more severe which can be explained by lack of interactions within the hard segment; HMDI has no aromaticity and therefore no π stacking interactions, the e⁻ withdrawing experienced by the proton on the nitrogen is also reduced, making the proton a weaker hydrogen bond donor.

Hardness

Shore A hardness (figure 46) was observed to increase in the MDI series with a roughly linear relationship. The DFDI series tends to increase across the series with a notable dip at 60 %HS. This can be explained by the degree of SS crystallisation across the series.

SS crystallisation in the MDI series decreases with increasing HS% but DSC data suggests all SS should be amorphous at room temperature, the linear increase across the series is therefore due to the hard segment.

WAXS results for the DFDI series indicate a notable decrease in SS crystallinity from 0 to 20%HS, this coincides with a plateau in hardness. The crystallinity is consistent from 20 to 40%HS and drops in the 60%HS elastomer, the SS in the 60%HS elastomer is also notable for having a lower melting temperature. The decrease in crystallinity and purity again coincides with a decrease in hardness. As with the increased modulus at colder temperatures observed in DMTA, the crystalline SS is acting as effective HS.
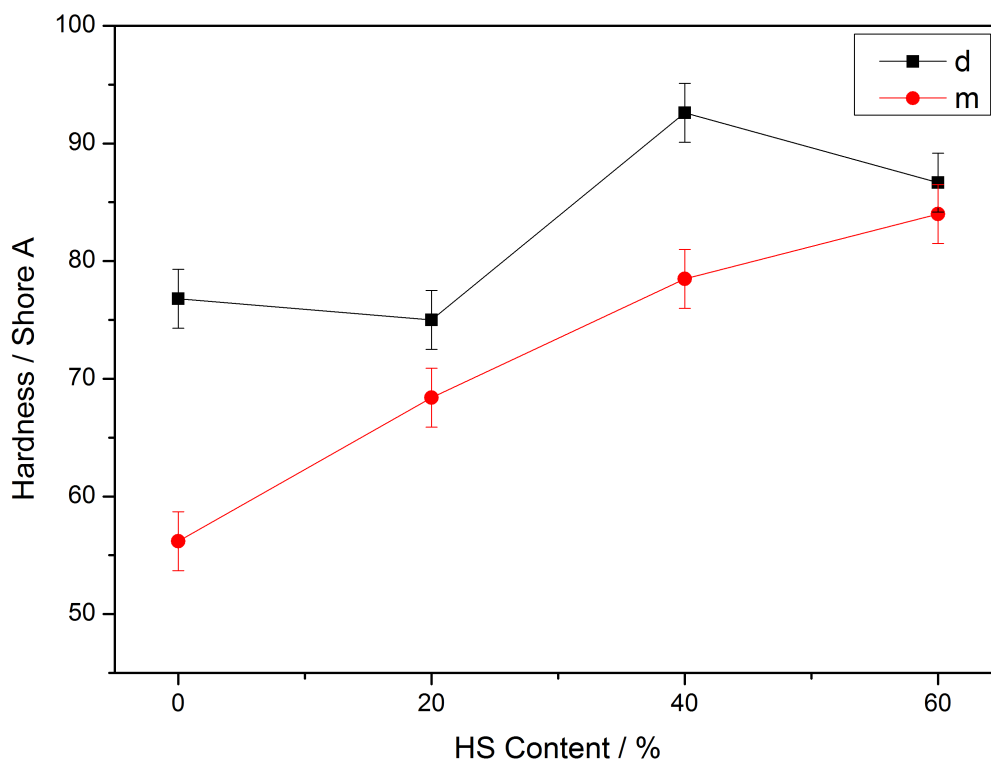
Figure 46: Shore A hardness of elastomers in the HS series.

TGA

The TGA results for the pure hard and soft segments investigated are reported in figure 47. The degradation of PTHF goes to near completion (mass loss is greater than 99%) by 425ºC.

The pure hard segments follow similar trends, with onset occurring almost immediately with a low rate of mass loss and a more pronounced mass loss beginning at around 266ºC and 280ºC for MDI-BD and DFDI-BD respectively. The eventual mass loss is much lower for the DFDI hard segment, ending at 72% whereas the MDI hard segment has lost 97% of its mass by 800ºC. Furthermore both MDI and DFDI hard segments slow dramatically at around 365ºC, and 88% and 53% mass loss for MDI and DFDI respectively.

The mass loss at 800ºC is lower in DFDI samples; it is known that furanic urethanes have a tendency to char at higher temperatures[20-21], with the formation of a char layer protecting against mass loss. This correlates with observed results as mass loss decreases with increasing HS% (and therefore increasing furanic content) for DFDI samples.

TGA results are reported in figures 48 and 49 (for DFDI and MDI based elastomers respectively) with onset and mass loss values reported in table 13 and for the pure phases in figure 14. Both series follow similar trends, with the onset of mass loss occurring sooner at higher HS%, and a stepwise drop in mass at higher HS%. The onset of mass loss occurs at cooler temperatures in DFDI based samples at 277-340ºC compared to 349-308ºC.

Figure 47: Sample weight as a function of temperature from TGA experiments for pure phases used.

Figure 48: Sample weight as a function of temperature from TGA experiments for DFDI based HS% series.

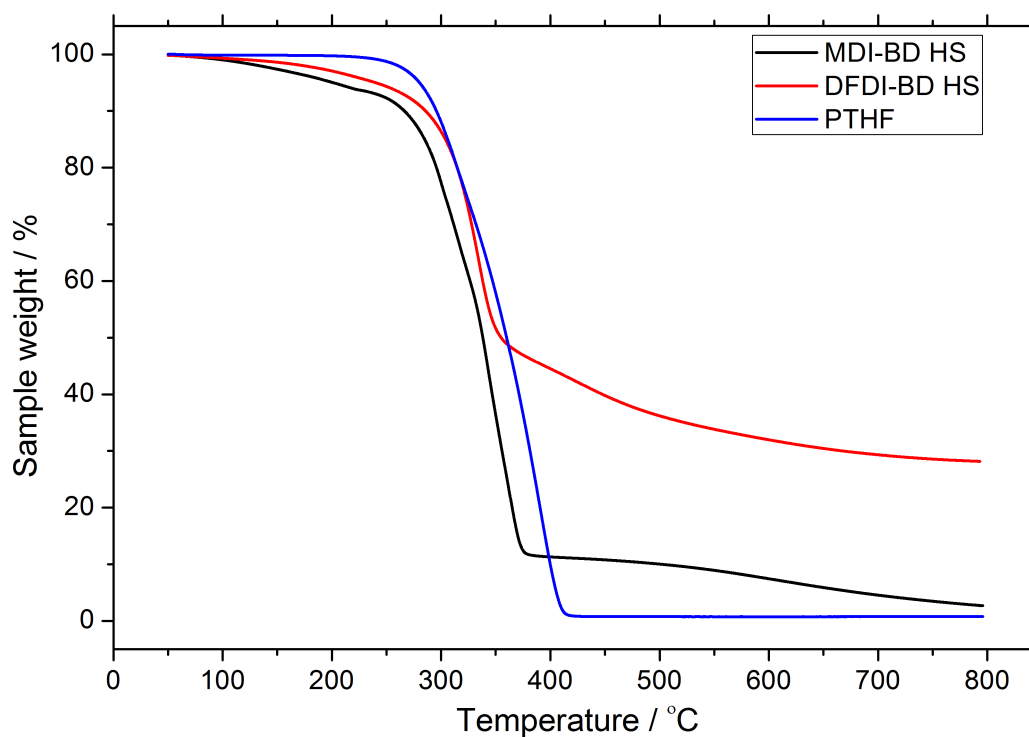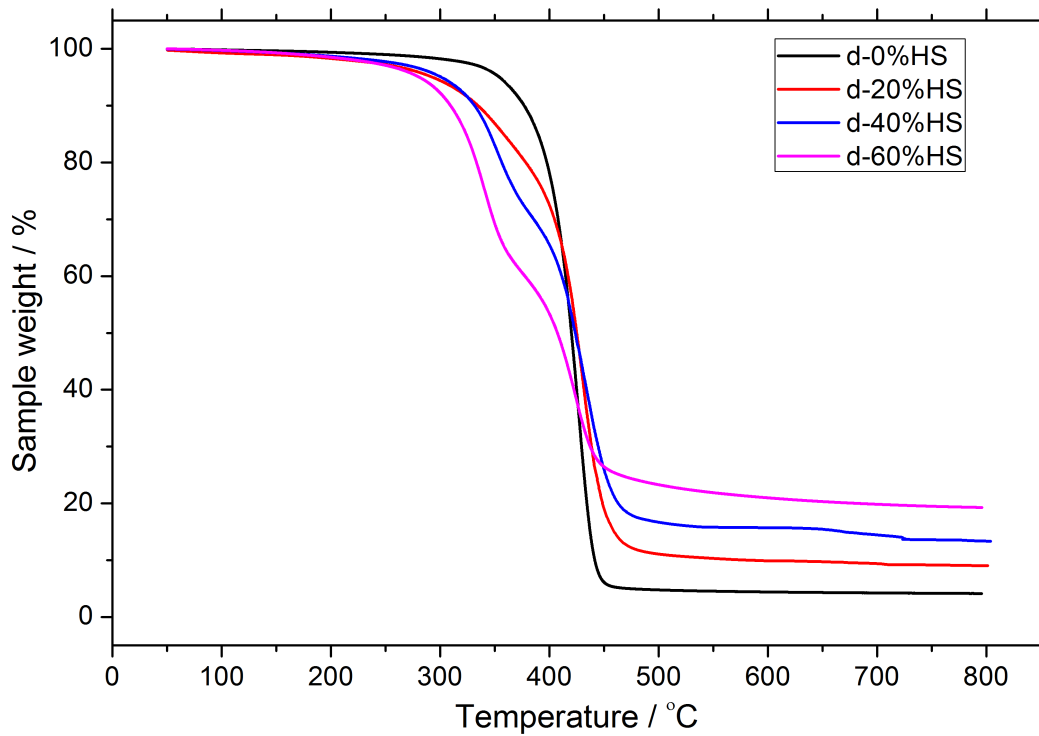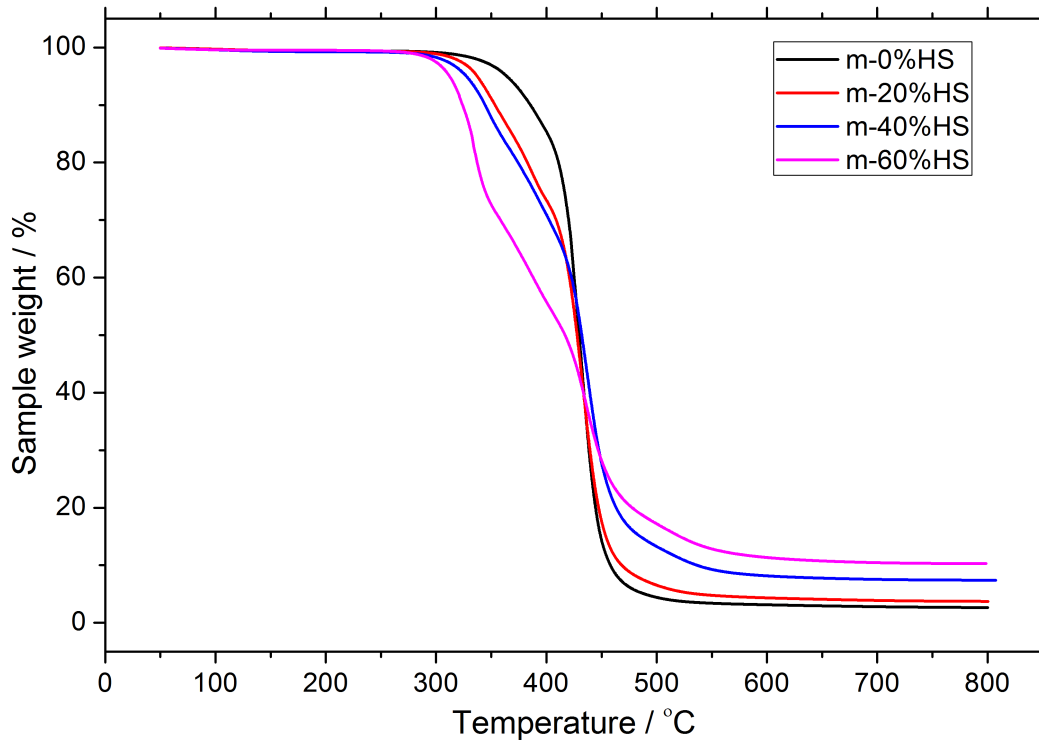*Figure 49: Sample weight as a function of temperature from TGA experiments for MDI based HS% series.*

92

Isocyanate	HS%	Onset of mass loss / °C	Mass loss at 800ºC / %
DFDI	0	342	95.9
DFDI	20	304	91.0
DFDI	40	304	86.7
DFDI	60	277	80.7
MDI	0	349	97.4
MDI	20	325	96.3
MDI	40	318	92.6
MDI	60	308	89.7

Table 13: Weight loss % and onset of mass loss for varying HS% of DFDI and MDI based elastomers. The error on temperatures is ±2ºC.

Pure phase	Onset of mass loss / °C	Mass loss at 800ºC / %
PTHF	247	99.3
MDI-BD	266*	97.0
DFDI-BD	280*	72.0

*Table 14: Weight loss % and onset of mass loss for pure phases. The error on temperatures is ±2ºC. *Mass loss evident at a slow rate immediately, temperature reported is that of the more severe mass loss.*

Boufi[21] carried out TGA experiments on a series of furanic, aromatic and aliphatic polyurethanes. None matched the structure of polymers reported in this work but general trends can be seen. The all aliphatic PU experienced >90% mass loss by 460ºC, in this work the pure SS was found to completely degrade by 425ºC.

A purely aromatic polymer was not studied, but furanic, furanic-aromatic and furanic aliphatic polymers were studied which leads to the following conclusions;

- The onset of mass loss occurs sooner (20-50ºC) when furanic groups are present.
- Aromatic groups help maintain mass at higher temperatures.
- Furanic groups are even more effective at preventing degradation.

These observations match results found in this work.

Rueda-Larraz[98] studied HDI-BD based elastomers (purely aliphatic) and noted earlier mass loss onset for higher HS% and a stepwise nature of mass loss for the pure HS. These characteristics are also found in the results presented in this chapter. The stepwise mass loss in hard segments is visible in high hard segment content elastomers and is presumed to be due to the thermolytic breaking of urethane groups and subsequent evaporation of small molecules (the urethane bond is reversible above 140-160ºC).

Chapter 5. Effect of soft segment molecular weight on morphology and properties

Introduction

The length of the soft segment has a strong influence on the morphology observed. Unlike with the relative proportions of hard and soft segments, varying the soft segment length generally has a more predictable effect.

Increasing the segment length also increases the degree of phase separation[37a, 99], the interdomain spacing and if the SS is capable of crystallisation, the degree of crystallinity.

Li et. al.[85] reported greater phase separation with increasing SS Mwt for PCL based elastomers based on the trends in Tg. They noted that crystallinity within the SS is possible from c. 2kDa Mwt, and reaches a maximum for low HS% at c. 4kDa.

Martin[93a] utilised SAXS and DSC to show increased SS Mwt leads to greater phase separation and greater domain spacing.

Chu[53d] found the relaxation time of one and two thousand Da Mwt PTHF based polyurethanes to be 1000 and 64 seconds respectively, suggesting that interactions between the hard segment and therefore the mobility of the system are the controlling factors. As such, the kinetics of phase separation in higher Mwt SS PU should should be faster, allowing the system to get closer to equilibrium before the system vitrifies.

Previous investigations into DFDI based PU[19b, 19f] showed a greater degree of phase separation in DFDI compared to MDI, as confirmed by DSC and DMTA. Fitting with the Chu's "viscosity-mobility" theory[53b], the increased flexibility in DFDI allows for greater mobility and therefore faster phase separation; more flexible segments are known to favour crystallisation[79].

Sonnenschein[76] found that an increase in hardness could be achieved with no adverse effects towards tensile and elongation properties by increasing the degree of crystallinity within the SS.

Results

Results presented in this chapter pertain to the varying SS series of elastomers. All elastomers have a HS based on DFDI-BD or MDI-BD and a hard segment content of 20 wt%. Elastomers are either described or use the nomenclature x-yk, where x is d or m, describing the isocyanate used (DFDI or MDI) and y is 1, 2 or 2.9 and refers to the SS molecular weight in kDa.

AFM

Phases images for elastomers containing 1kDa SS (figure 50) do not show any long range ordering, although a phase separated nature is observed. The AFM images for the both the MDI and DFDI based 1kDa SS elastomers show an average domain spacing of 11nm. The MDI based elastomer appears to be made up of small rods, this is likely to be crystalline HS as the WAXS frame for the elastomer shows a weak peak coincident with the pure HS WAXS frame (see the weak at c. 19º in figure 56 coinciding with the peak in MDI-BD pure HS of figure 58).

The 2kDa SS elastomers both show lamellae nature to some degree (figure 51), though far more clearly in the DFDI elastomer. The stripes are 15nm thick in the DFDI elastomer, while the images for MDI based elastomers only show hints of a lamellae structure. This is due to the SS being mostly molten at room temperature (as shown by DSC results), the PSD returns 14nm.

When a 2.9kDa SS is used both elastomers clearly show a lamellae structure (figure 52). The structure in the DFDI elastomer looks similar to that of the 2kDa SS elastomer. The MDI elastomer shows a much clearer structure that was not observed with SS Mwt lower than 2.9kDa, there are however prominent voids visible at both length scales presented, it is thought that these are amorphous regions. PSD calculated domain spacings return 18 and 15nm for DFDI and MDI elastomers respectively.

Figure 50: AFM phase images of 1KDa SS (20% HS) elastomers collected in tapping mode at different length scales. (DFDI left, MDI right)
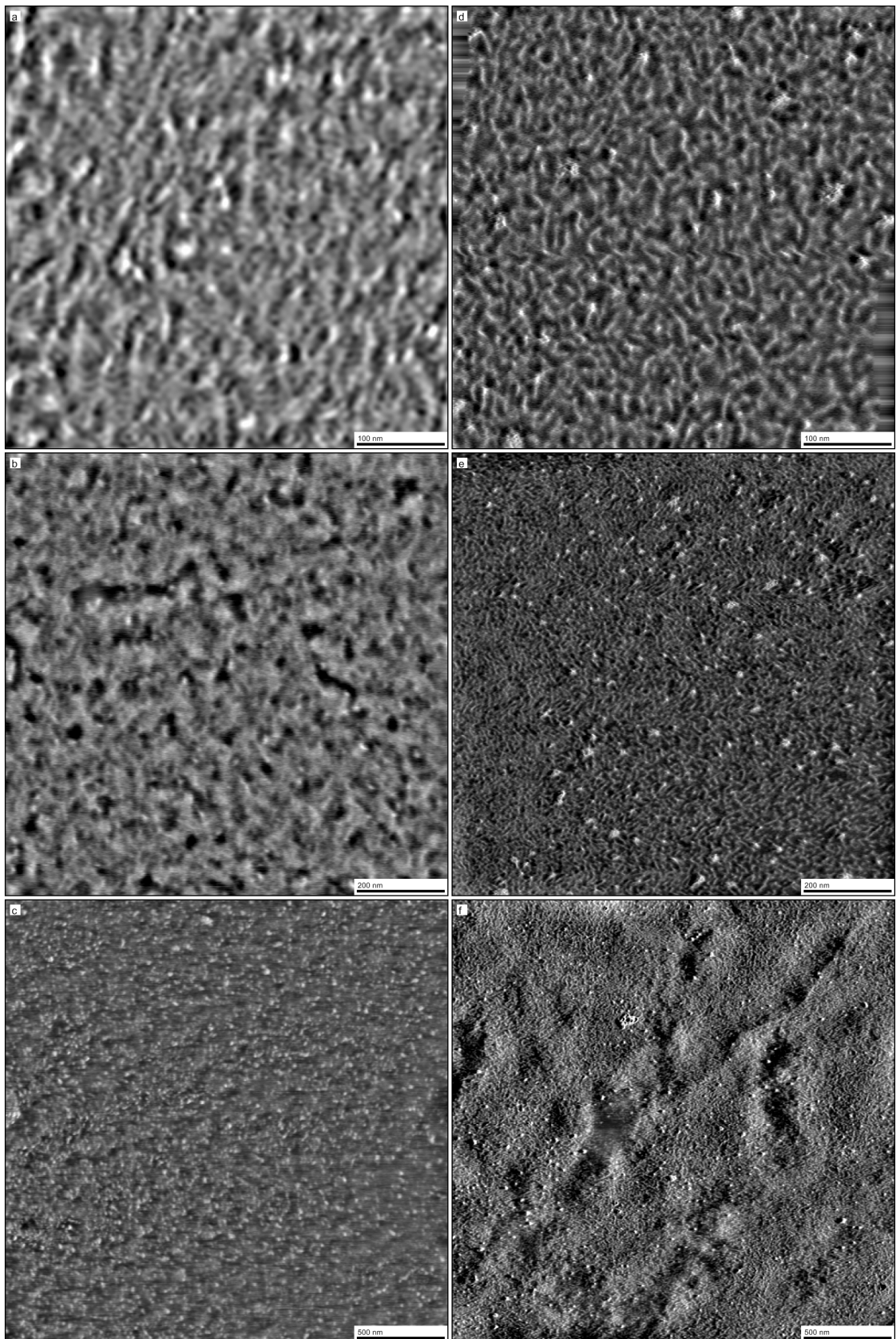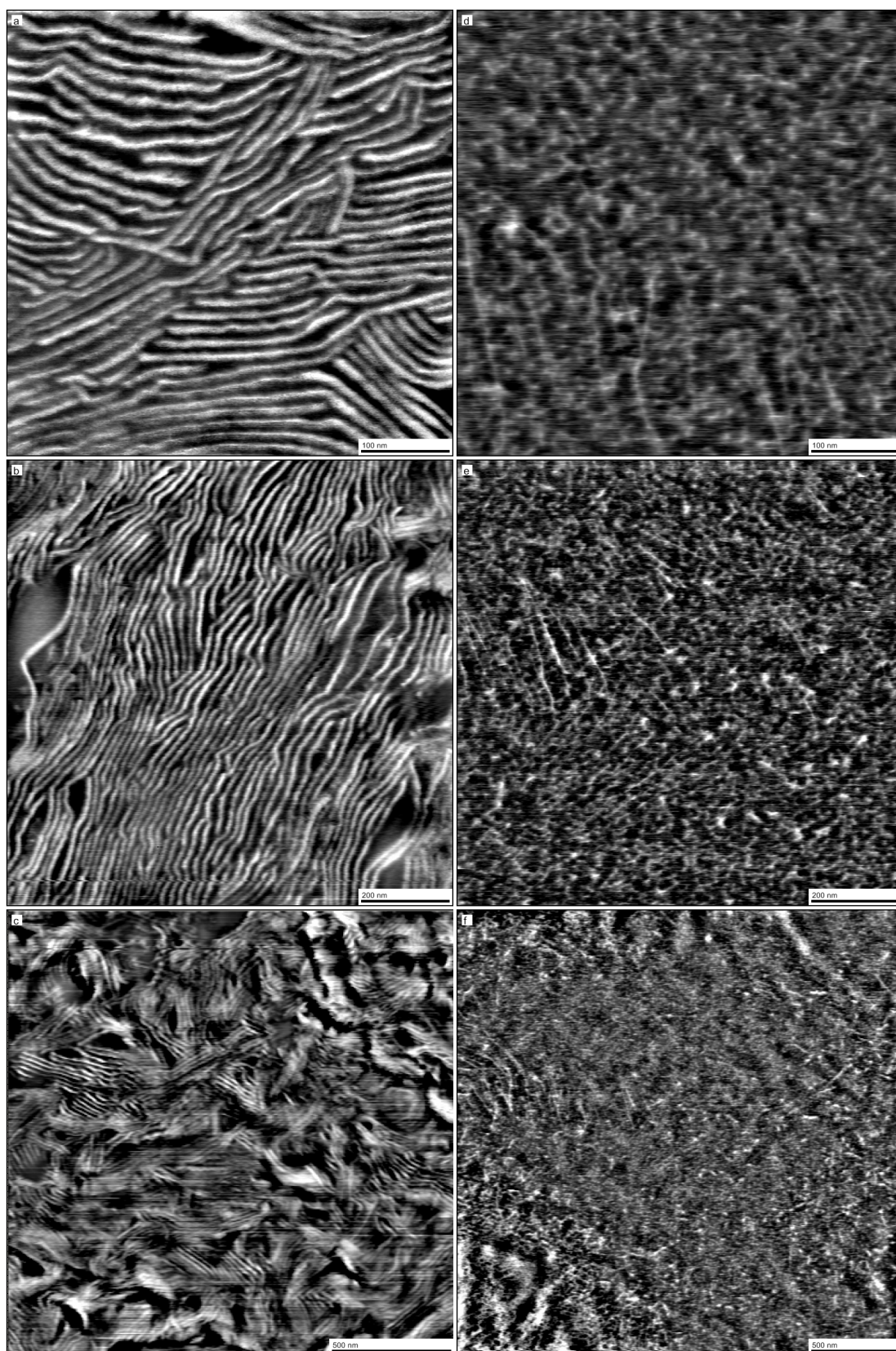
Figure 51: AFM phase images of 2KDa SS (20% HS) elastomers collected in tapping mode at different length scales. (DFDI left, MDI right)
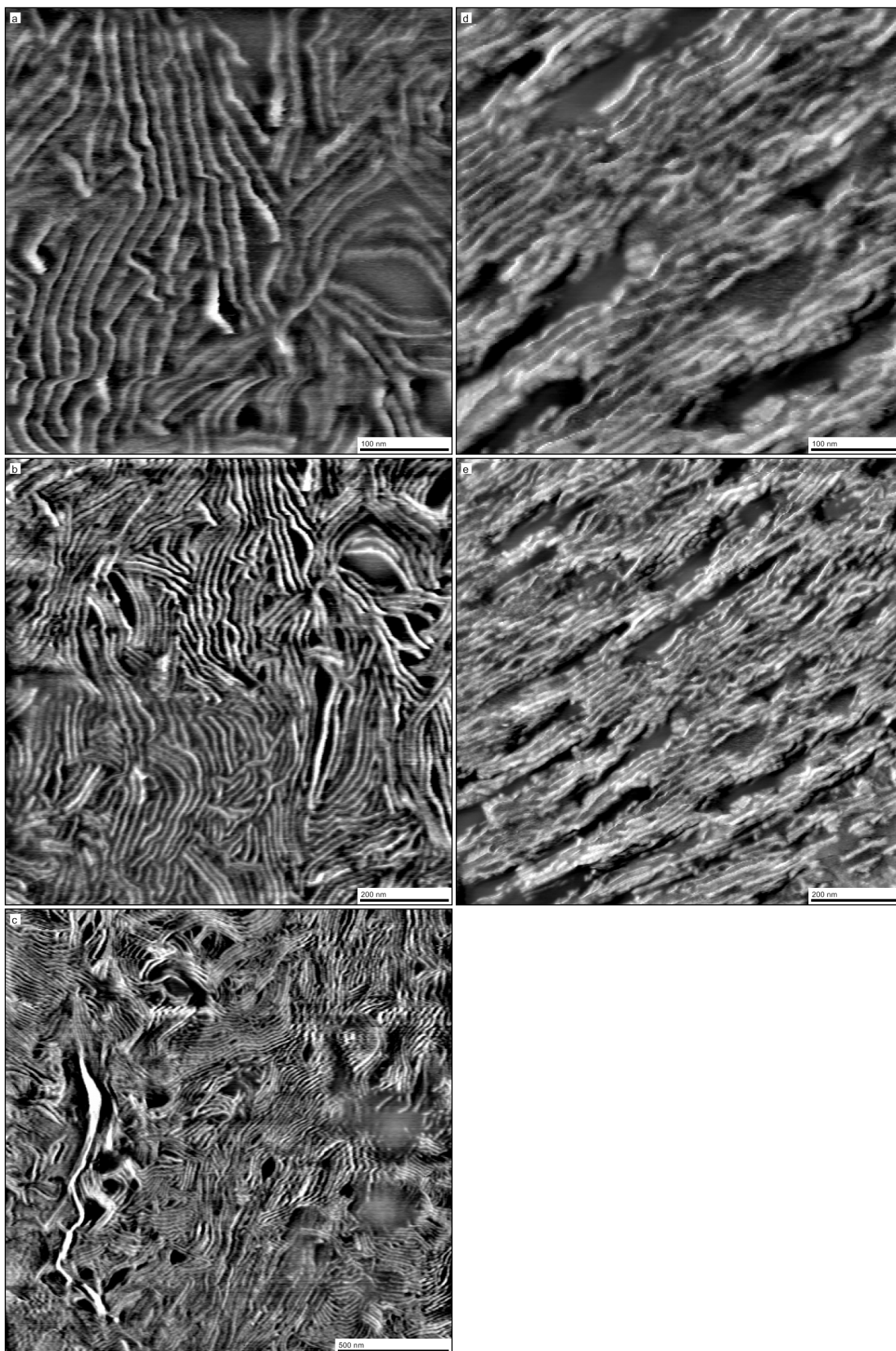
Figure 52: AFM phase images of 2.9KDa SS (20% HS) elastomers collected in tapping mode at different length scales. (DFDI left, MDI right). An image for the MDI based elastomer at the largest length scale was not acquired.

The trends in domain spacing values are clear and the same for both series, increasing the SS Mwt leads to an increase in domain spacing. Values are reported in table 15 (p103) alongside values calculated from SAXS experiments.

The thickness of a lamellae crystal is mostly determined by kinetic factors and is known to be independent of molecular weight. Entangled chains, that is to say, chains with a greater relaxation time take longer to arrange into crystals[33]. It is known that polyurethane with shorter soft segments have longer relaxation times[53d], as such it is expected that the kinetics of crystal growth are faster with increasing SS Mwt, leading to thicker lamellae.

Schön[84] presented AFM phase images of rods in an MDI-BD-PTHF1k bulk cast system with a 30%HS content. Rods were between 15 and 25nm thick and up to 140nm long, these values were not reported but measured from the images presented. The width is inconsistent with domains observed in the m-1k images of this chapter, the length of observed rods suggests a higher degree of HS crystallinity (due to higher HS content), which explains the increase in domain size.

Yilgor[81a] used 1 and 2kDa PTHF systems with a TDI-water hard segment. 10nm thick lamellae were visible in 2kDa elastomers with only a faint lamellae structure observable in 1k systems. The observed structures are likely hard domains with phase separation being possible due to the solvent cast preparation.

Christenson[86] observed short (8-10nm thick) rods in an MDI-BD-PTHF1k system, consistent with images of the same system reported in this chapter (see figure 53). A second 2kDa SS system utilising a urea hard segment showed 10-15nm thick lamellae, although the difference in hard segment makes comparison difficult as urea hard segments are known to increase phase separation[37a].
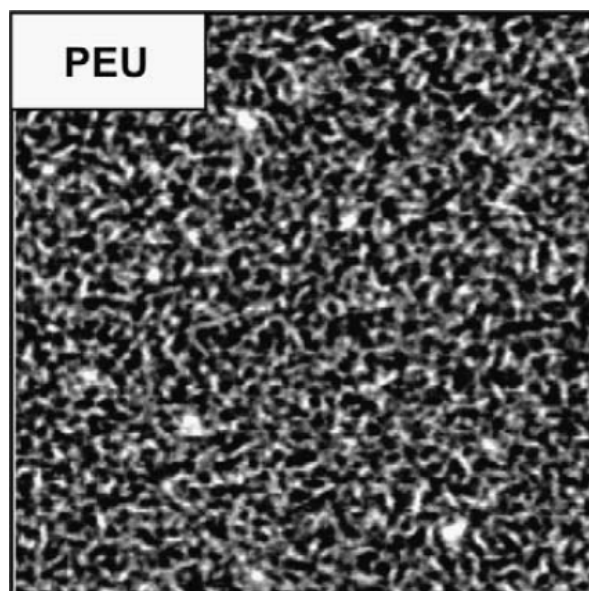
Figure 53: AFM phase image of an MDI-BD HS PU with a 1kDa Mwt PTHF SS showing a similar short rod structure to the 1kDa Mwt SS MDI based elastomer of this chapter, the image is 850nm². Reprinted (adapted) with permission from: *Christenson, E. M.; Anderson, J. M.; Hiltner, A.; Baer, E., Relationship between nanoscale deformation processes and elastic behavior of polyurethane elastomers. Polymer 2005, 46 (25), 11744-11754.* Copyright 2005, with permission from Elsevier.

Das[100] studied elastomers synthesised from the same soft segments employed in this chapter, although modified to be amine terminated. The hard segments were made up of different short symmetrical diisocyanates and all images showed some lamellae/rod structure. Images showed shorter less ordered rods with a width of 8-12nm in 1kDa SS Mwt elastomers, while 2kDa elastomers had cleaner looking 12nm thick lamellae that extended up to 250nm. While the elastomers utilise different hard segments, similar trends are observed in images reported in this chapter.

Garrett[45a, 72a] presented images of urea HS elastomers with 2kDa PTHF SS. Images showed 5-10nm thick rods up to 100nm long which were reported to be HS, though no WAXS or DSC data was presented to confirm.

Other studies have shown lamellae structures in 1kDa SS based elastomers, although driven by crystallisation of monodisperse hard segments[48, 83].

SAXS

All SAXS frames show clear peaks in the Lorentz corrected intensity (figures 54 and 55). Trends are clear and remain the same for both isocyanates studied. The peak shifts to lower q values (larger domain spacing), at a higher intensity and with an increasingly

narrow distribution with increasing SS Mwt.

The DFDI based elastomer with a 1kDa SS has a very broad peak, indicating polydisperse domain sizes. The DFDI-BD HS does not crystallise as readily as the MDI-BD HS, clearly shown by the crystalline HS rods observed in the MDI 1kDa SS elastomers.

While the peak height hints that the degree of phase separation is increasing with increasing SS Mwt, the invariant contradicts this. The invariant shows that the degree of phase separation varies very little throughout the series. This may be due to the electron density difference between phases from the 1kDa SS system where HS have crystallised, to the higher Mwt SS systems where phase separation may have increased viscosity more rapidly and hindered pure HS crystallites from forming.

A pure HS with an amorphous SS has the greatest variance in electron density which, as shown in equation 34, increases the intensity of scattering. A two phase system comprised of pure SS and HS dissolved in an amorphous SS has a lower electron density variance.

$$Q \simeq \phi_H (1 - \phi_H) \langle \eta_H - \eta_s \rangle^2$$

(34)

The invariant is noticeably higher in all DFDI based elastomers when compared to MDI variants, even for the broad peak observed in the 1kDa SS elastomer. Showing that despite the more clear rod structures observed in the 1kDa SS MDI elastomer, the DFDI elastomer also has a high degree of phase separation.

Domain spacing values were calculated by the 1D correlation function and using Braggs law ($2\pi/q$) for the first maxima not associated with the beamstop. Invariants were calculated by correlation functions and integrating over the Lorrentz corrected SAXS frame over the range q= 0.015 - 0.2 . The invariant was normalised for the lowest value (that of the PTHF-DFDI-DFDA elastomer reported later) to allow for comparisons to be made. All values are reported in table 15.

The correlation between domain spacing from AFM and SAXS is generally good, although not as close as in the HS series' of chapter 4. The m-2.9k elastomer shows the greatest variance, potentially due to the voids present on AFM phase images.

The trend observed in this data of higher Mwt SS leading to larger (peaks at lower q) structures with narrow size distributions is common in literature and follows predicted values of domain spacing based on the difference in block length[35]. Domain spacing would be expected to be in the ratios of 1:1.4:1.7 for SS molecular weights of 1:2:2.9 kDa as domain spacing changes with the square root of block length. A domain spacing of 11.0nm for a 1000 Mwt SS based elastomer would lead to predicted domain spacings of 15.6 and 18.7 for 2000 and 2900 Mwt soft segments respectively. In rough agreement with domain spacing values reported in table 15 (page 103).
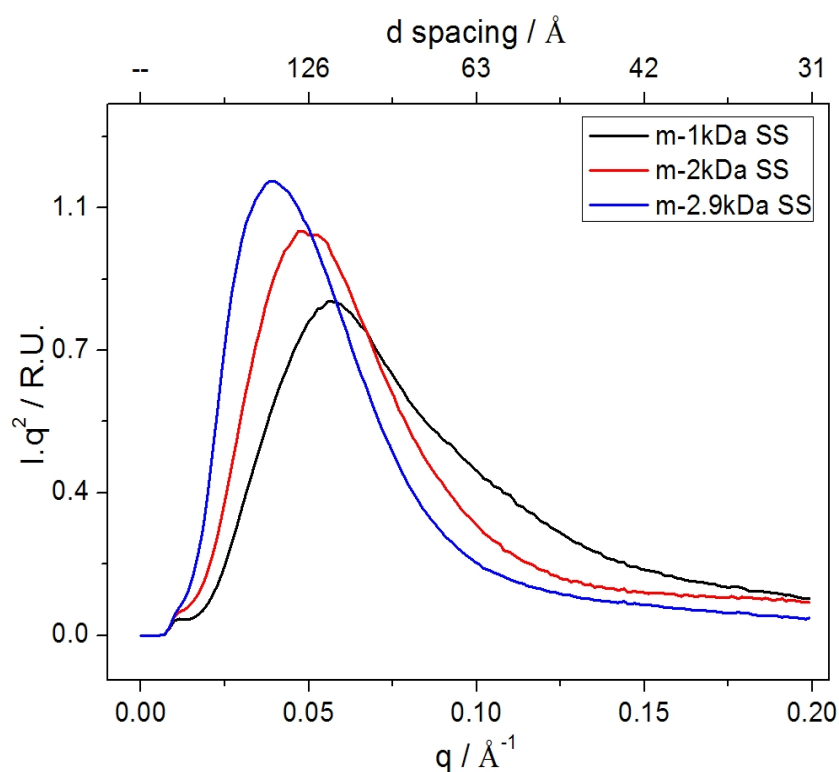
Figure 54: SAXS Lorrentz corrected intensities as a function of q for the MDI based varying SS Mwt series.
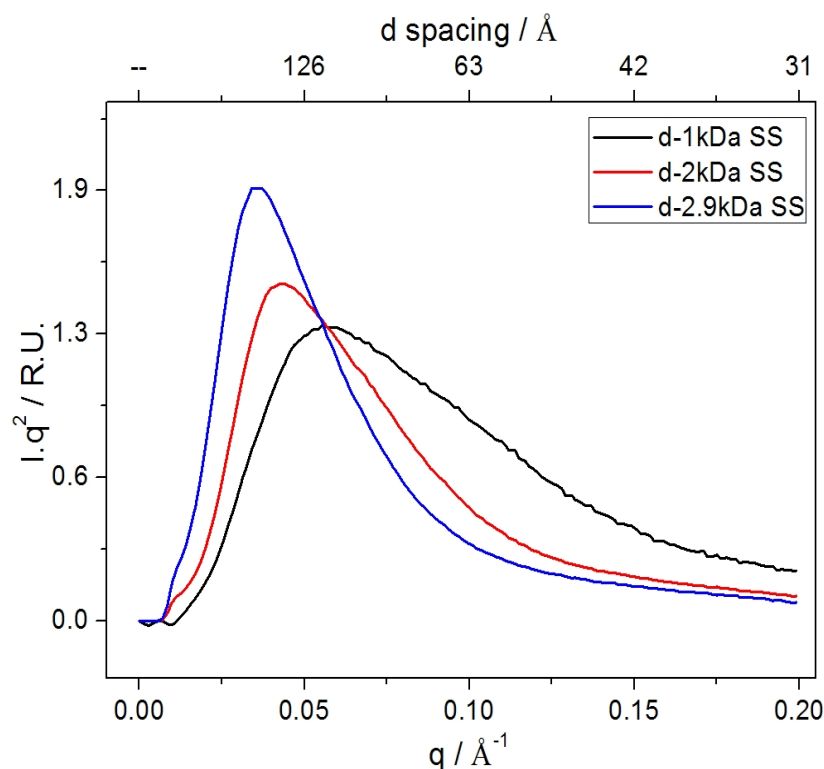
Figure 55: SAXS Lorrentz corrected intensities as a function of q for the DFDI based varying SS Mwt series.

Isocyanate	SS Mwt	d-spacing / nm			Relative invariant	
		Iq² Peak	Correlation function	AFM	Iq² Peak	Correlation function
DFDI	1k	11 ± 0.7	12 ± 0.5	11 ± 1	10.7	10.3
DFDI	2k	15 ± 0.6	15 ± 0.5	15 ± 1	10.6	9.8
DFDI	2.9k	18 ± 0.7	18 ± 0.5	18 ± 1	11.0	9.1
MDI	1k	11 ± 0.4	11 ± 0.5	11 ± 1	6.9	6.1
MDI	2k	13 ± 0.9	13 ± 0.5	14 ± 1	6.5	6.3
MDI	2.9k	16 ± 0.6	17 ± 0.5	15 ± 1	6.8	5.8

Table 15: Domain spacing (from SAXS and AFM experiments) and relative invariant (SAXS) for the SS Mwt series.

Martin[93a] used varying SS Mwt PHMO (polyhexamethylene oxide) systems and noted peaks shifted to lower q values and appeared both more intense and more narrow with greater SS Mwt. Velankar[99c] noted the same trends in a PCL based elastomer system.

Das[100] found SAXS peaks to be broader and less intense in 1kDa PTHF based PU compared to 2kDa systems. The domain spacing increased by 2nm for the 2k PTHF system, consistent with this work.

Unsal[81b] founds SAXS peaks to be larger and narrower in PTHF2k systems when compared to 1k.

WAXS

No MDI based elastomers show SS crystallinity at room temperature; upon erasing thermal history and maintaining a 0ºC temperature, crystalline peaks are clear in 2 and 2.9kDa SS elastomers. The relative intensity in both elastomers is similar, indicating a comparable degree of SS crystallinity (this is contradicted by DSC data). WAXS frames are reported in figures 56 and 57.

The 1kDaSS elastomer presents a shoulder at 19.3º, coincident with the peak in the MDI-BD HS (figure 58), clearly displaying some degree of HS crystallinity, although the peak is too weak to make a quantitative calculation.

DFDI based elastomers show SS crystallinity for 2 and 2.9kDa SS elastomers even at room temperature (DSC results reported later show the SS crystals melt at higher temperatures in these elastomers). The relative intensity of the SS crystal peaks increases from 2 to 2.9kDa SS in both room temperature and 0ºC experiments, showing the degree of crystallinity increases with increasing SS Mwt.

The patterns collected for the pure SS[37a, 92] and MDI based HS[53a, 75, 93] presented in this chapter match those previously reported in literature.
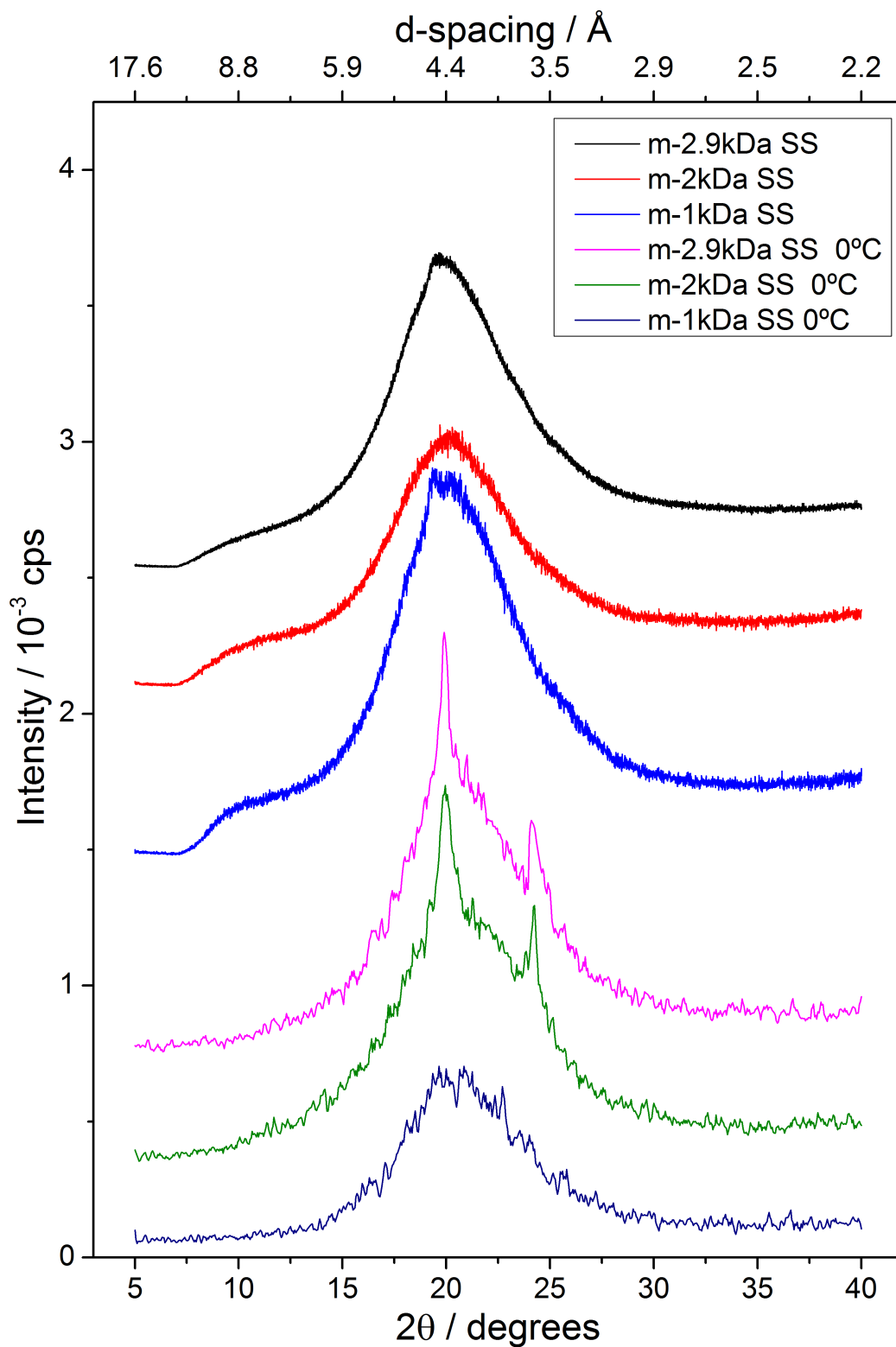
Figure 56: WAXS intensity as a function of scattering angle for MDI based SS Mwt series at room temperature and 0°C. Datasets are offset on the Y axis for clarity.
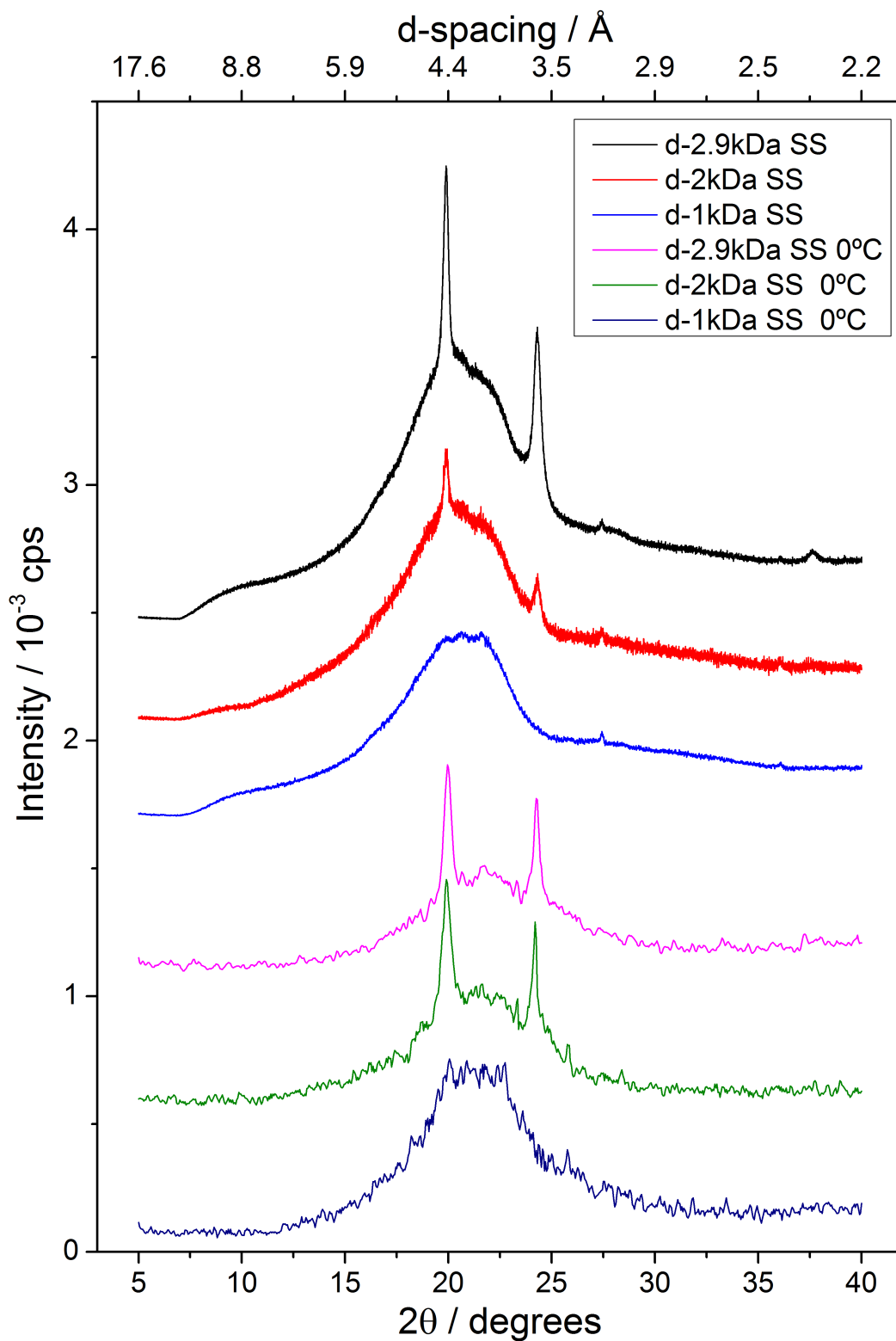
Figure 57: WAXS intensity as a function of scattering angle for DFDI based SS Mwt series at room temperature and 0ºC. Datasets are offset on the Y axis for clarity.
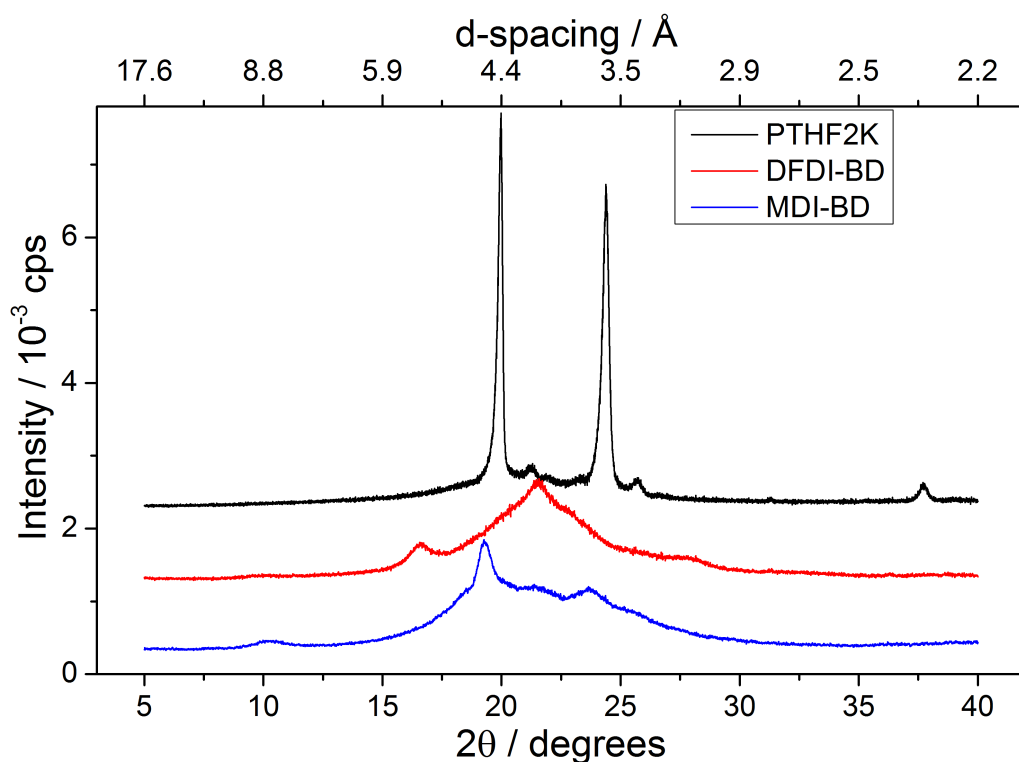
Figure 58: WAXS intensity as a function of scattering angle for pure phases utilised in this chapter. Datasets are offset on the Y axis for clarity.

Martin[93a] found the crystalline nature of SS WAXS peaks to become more pronounced with increasing SS Mwt in a PHMO system. This is consistent with the series reported here.

Sun[91] noted crystallinity in a 13%HS solvent cast MDI-BD-PTHF2k elastomer when held at 18ºC, the WAXS frame then showed the polymer was amorphous at 30ºC. The low HS% and solvent casting account for higher SS Tm than MDI elastomers of this work.

Authors reporting no crystallinity observed in WAXS frames of PTHF SS based SPU include; Martin[93b], who reported that the WAXS frame of an MDI-BD-PTHF1k 45%HS elastomer is amorphous. Garrett[72b], who reported no crystallinity was observed in an MDI-ED-PTHF2k elastomer, although the temperature was not given and no DSC experiments were reported.

Williams[92c] presented amorphous WAXS frames for a 2kDa PTHF system despite DSC results clearly showing SS crystallinity, the experimental section however states that WAXS frames were collected at room temperature, explaining the absence of peaks associated with crystallinity.

Paiksung[37a] reported WAXS frames showing no crystalinity in a TDI-ED-PTHF1k system, the lack of HS crystallinity is likely due to the short chain extender and non-linear diisocyanate.

DSC

Figure 59 shows the DSC traces for the SS Mwt series foe both MDI and DFDI based elastomers, tables 12 and 13 summarise the temperatures of transitions and the associated enthalpies of those transitions for SPU elastomers with varying SS Mwt.

Tgs are clear in the traces for all elastomers (not as clear when plotted on the scale used here), with a noticeable high value recorded for both 1kDaSS elastomers. This is due to a higher degree of phase mixing and can be accounted for using the Fox equation.

$$\frac{1}{Tg} = \frac{W_1}{Tg_1} + \frac{W_2}{Tg_2} \tag{35}$$

The weight fraction of HS in the phase presenting the SS Tg is predicted to be 0.43 and 0.36 in MDI and DFDI based elastomers respectively (using values of HS Tg reported by Cawse[74]), which is higher than the proportion of HS in the elastomer, suggesting there is a second more pure SS rich phase.

The enthalpy associated with the glass transition decreases as the degree of crystallinity increases, this trend is far less noticeable in MDI elastomers as the bulk of the SS crystallisation is occurring on the heat cycle, after the SS Tg presents.

This preference for crystallisation upon heating is consistent with that observed for the HS% series' discussed in the previous chapter and displays a greater capability for SS crystallisation for DFDI elastomers.

The MDI-2.9k elastomer shows crystallisation partly occurs on the cooling cycle, evidence that the molecular weight is sufficiently high to overcome the mobility restriction of the inflexible MDI unit.
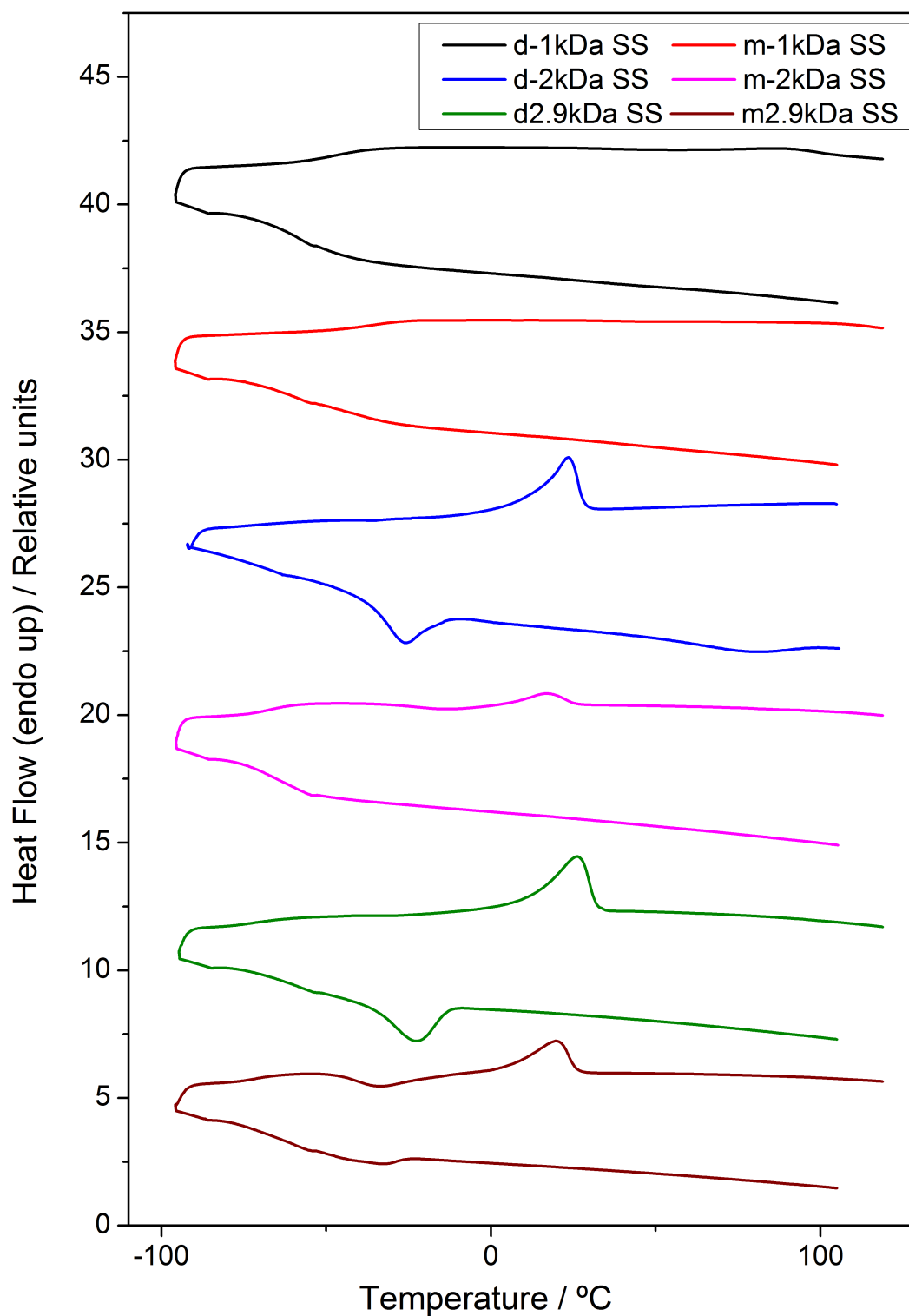
Figure 59: DSC traces for elastomer derived from both diisocyanates and utilising the different soft segment molecular weights.

The trends in SS Tg are similar in both series. The SS Tg decreases with increasing SS Mwt, though this is less noticeable for the DFDI series between 2 and 2.9kDa SS; the Tg, SS Tm and calculated degree of crystallinity show the degree of phase separation is similar in both of these elastomers, in agreement with the SAXS invariant.

SS Mwt	Experiment phase	Tcrys$_{SS}$ / °C	ΔH / J g^{-1}	Tmelt$_{SS}$ / °C	ΔH / J g^{-1}
1	Cool cycle	-1	-70.64		
	Heat cycle			26	74.28
2	Cool cycle	7	-95.05		
	Heat cycle			28	98.91
2.9	Cool cycle	6	-95.68		
	Heat cycle			29	107.46

Table 16: Crystallisation and melting temperatures and enthalpies for pure polyols utilised in this series. The error on given temperatures is ±1°C.

The melting behaviour displayed in the DSC traces for pure SS used match those reported previously by Tsuchiva[80]. There are two noticeable melting transitions that occur close together, these are further apart and more noticeable in lower Mwt PTHF. Melting and crystallisation temperatures are reported in table 16 (the DSC traces are presented in figure 60).

Figure 60: DSC traces for the different Mwt PTHF soft segments used.

SS Mwt	Experiment phase	Tg_{ss} / °C	ΔH / J g^{-1}°C-1	$Tcrys_{ss}$ / °C	ΔH / J g^{-1}	$Tmelt_{ss}$ / °C	ΔH / J g^{-1}
1k	Cool cycle						
	Heat cycle	-36	0.34				
2k	Cool cycle						
	Heat cycle	-67	0.33	-13	-4.01	17	5.55
2.9k	Cool cycle			-33	-9.11		
	Heat cycle	-72	0.27	-34	-9.20	19	17.33

Table 17: Temperatures and associated enthalpies of transitions observed in DSC traces for MDI based SS Mwt series. The error on given temperatures is ±1°C.

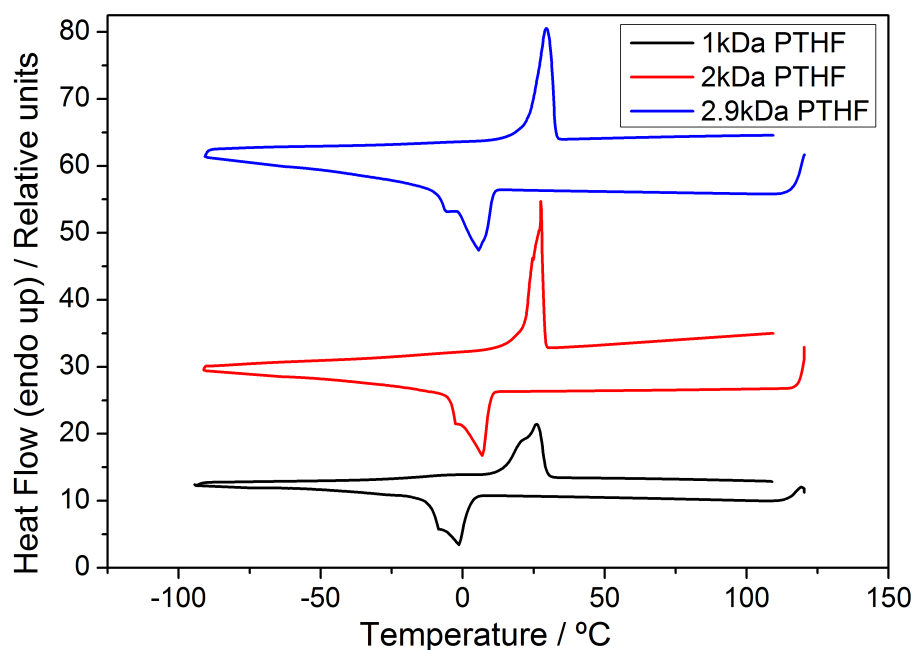| SS Mwt	Experiment phase	Tg_{ss} / °C	ΔH / J g^{-1}°C-1	$Tcrys_{ss}$ / °C	ΔH / J g^{-1}	$Tmelt_{ss}$ / °C	ΔH / J g^{-1}
1k	Cool cycle						
	Heat cycle	-49	0.50				
2k	Cool cycle			-26	-26.35		
	Heat cycle	-71	0.06			24	28.00
2.9k	Cool cycle			-23	-28.02		
	Heat cycle	-72	0.11			26	29.43

Table 18: Temperatures and associated enthalpies of transitions observed in DSC traces for DFDI based SS Mwt series. The error on given temperatures is ±1°C.

The %crystallinity calculated from DSC and WAXS studies (presented in table 19) shows a greater than expected variance, but the trends are in agreement; the degree of crystallinity in the SS increases with increasing SS Mwt. The crystallinity in MDI elastomers is low when compared to DFDI counterparts, and even in the 2.9kDa SS elastomer is lower than the 2k DFDI elastomer.

Isocyanate	SS Mwt	% Crystallinity		Difference
		WAXS	DSC	
DFDI	1k	0.0	0.0	0.0
DFDI	2k	16.2	23.5	7.3
DFDI	2.9k	19.6	24.0	4.4
MDI	1k	0.0	0.0	0.0
MDI	2k	13.3	4.7	8.7
MDI	2.9k	11.1	14.1	3.0

Table 19: Comparison of crystallinity as calculated from WAXS and DSC data.

The degree of crystallinity throughout the series' matches that observed in the images acquired by tapping mode AFM most closely. DFDI elastomers at 2 and 2.9kDa SS showed similar structures and as such the degree of crystallinity changes by very little. In the MDI series, clear lamellae are only observed from 2.9kDa SS, and there is a three-fold increase in crystallinity as calculated from DSC data.

In a study of PCL based PU, Li[85] found that crystallinity of the SS was possible from

2kDa, with a sharp increase in the degree of crystallinity from 2kDa to 4kDa after which no further crystallisation was observed (max at c.40% crys). Likewise, Das[100] presented DSC traces for 1 and 2kDa amine functionalised PTHF based PUr. Only the 2kDa SS elastomer displayed crystallisation.

The SS Tg is known to decrease with increasing Mwt; Zdrahala[99a] used a PPO-PEO SS with varying Mwt and Martin[93a] used a PHMO based system. Both noted that the Tg was found to decrease with increasing Mwt.

Tg values are consistent with those previously reported in literature. The Tg of the m-1k system (-36ºC) matches the literature value of MDI-BD-PTHF1k elastomers at -39ºC presented by Martin et. al.[93b]. Wang[73] reports the Tg of the MDI-BD-PTHF2k system (at 22%HS) to be -67ºC, identical to the value presented here.

Cawse et. al.[19b, 74] reported that DFDI based elastomers present consistently lower Tg values for the SS, matching precisely the trends in all series reported here. They cast elastomers of DFDI/MDI-BD-PTHF1k at 10 and 50%HS from bulk. As expected, no crystallinity was observed within the SS. The Tg values were -50 and -33ºC for DFDI and MDI based elastomers at 10%HS (respectively), which agrees well with results from 20%HS elastomers presented earlier (-49ºC and -36ºC).

In a TDI-BD-PTHF1k system, Schneider[8c] found the SS Tg to be -35ºC, matching the Tg in analogous MDI systems. Unsal[81b] reported DSC traces showing weak and broad melting and crystallisation in a PTHF1k elastomer (solvent cast and 0%HS), with Tcrys and Tm at -30ºC and -20ºC. The lack of HS explains the otherwise unexpected crystallinity within the SS.

Paiksung[37a] found the Tg of a PTHF SS to be -40ºC and -60ºC for 1 and 2kDa based TDI-BD systems, this agrees well with results in this chapter. Urea hard segment versions had lower Tg values, especially at lower SS Mwt, suggesting phase separation was driven by the greater value of χ and not hindered by the reduction in mobility caused by hydrogen bonding between hard segments.

Hu[97] synthesised a series of PUU's with different chain extenders and PTHF SS of 1, 2 and 2.9kDa Mwt. Trends were identical to the series' presented here; with increasing SS Mwt the Tg decreases and the associated ΔH is lower, also the SS Tm increases and has a greater associated enthalpy.

DMTA

All traces present significant decays in modulus and peaks in tanδ (reported in figures 61 to 63). The 1kDa SS elastomers show similar shape peaks for tanδ and the same trends in modulus decay. The tanδ peaks are noticeably narrow when compared to higher Mwt traces, evidence that as stated in the previous chapter (and matching previous reports[76]), it is the crystallinity in the SS that broadens the observed transitions.

The MDI based elastomer with a 2kDa Mwt SS retains a somewhat narrow tanδ, which fits with the low values of SS crystallinity calculated from DSC data. The modulus follows the same trends, with a noticeable rubbery plateau from 25-75ºC.

The 2.9kDa SS elastomers both present very broad tanδ peaks, fitting with the higher degrees of SS crystallinity observed. The MDI elastomer has a distinct rubbery plateau from 25-100ºC, comparatively the DFDI elastomer displays a plateau from 25-75ºC and is much less pronounced. The 2.9kDa SS DFDI elastomer presents further broadening of the tanδ trace due to contribution of the HS Tg. This is not observed in any other sample and is likely due to the high degree of phase separation in this elastomer due to the greater χN contribution of the high Mwt SS, greater hydrogen bond potential and flexibility of the diisocyanate.
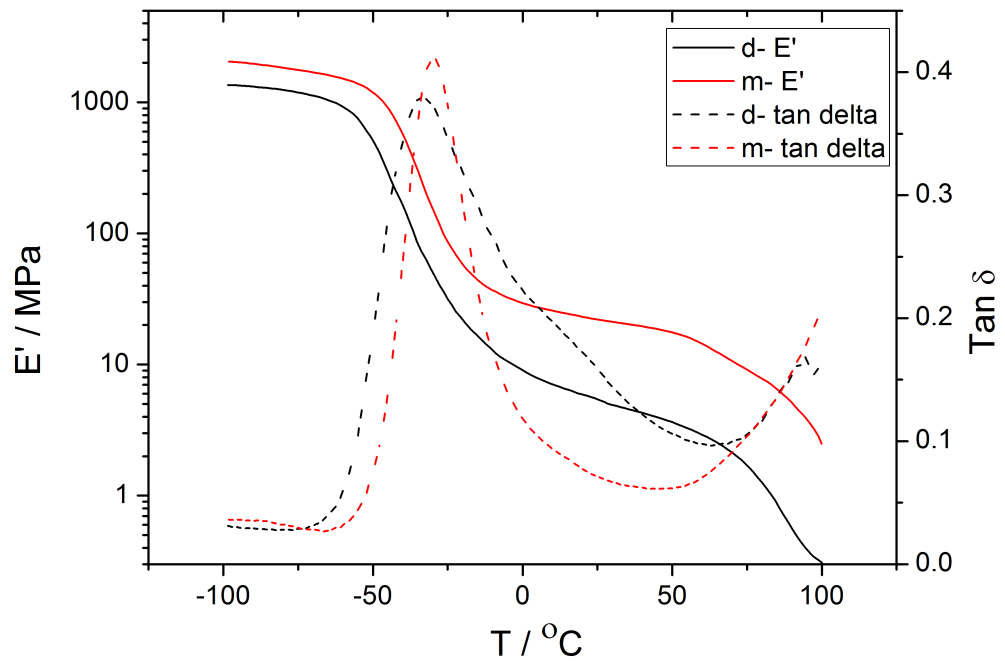
Figure 61: Storage modulus (E') and mechanical damping (tanδ) as a function of temperature for 1KDa Mwt SS elastomers from both diisocyanates.
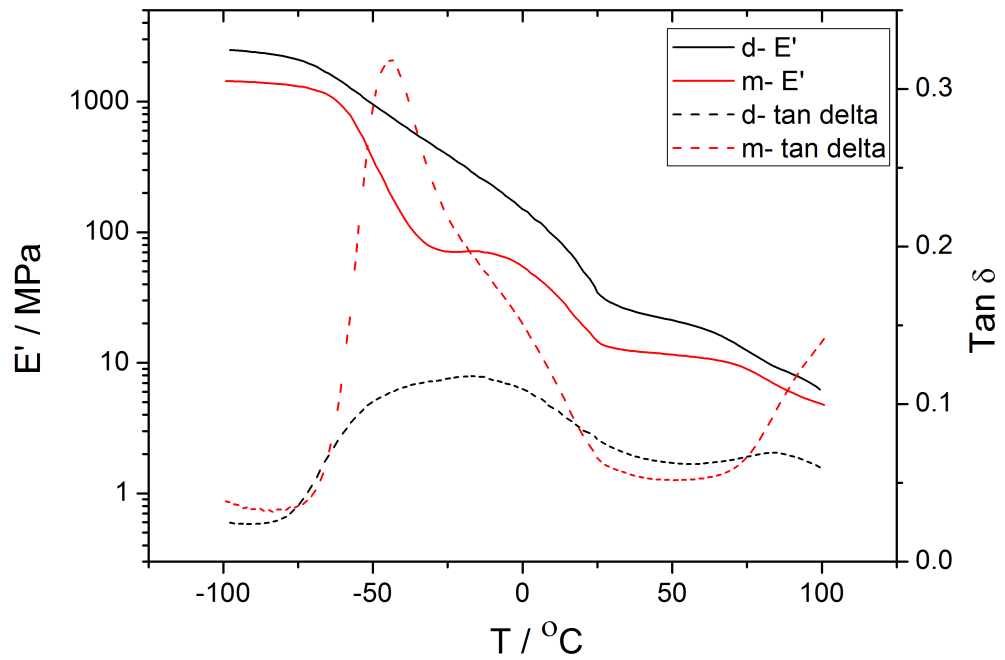
Figure 62: Storage modulus (E') and mechanical damping (tanδ) as a function of temperature for 2KDa Mwt SS elastomers from both diisocyanates.
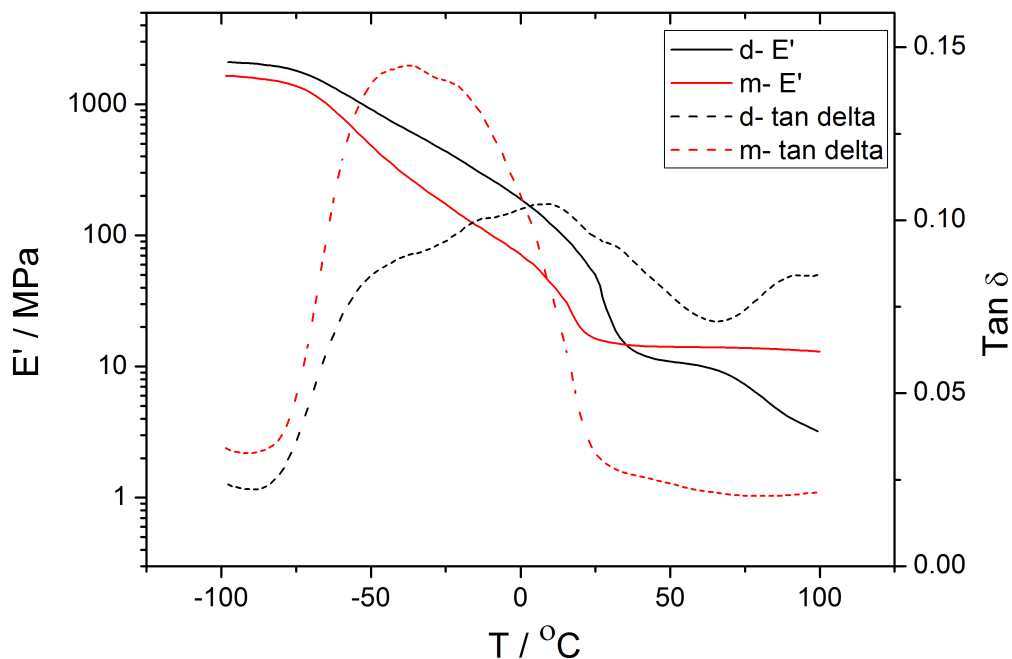
Figure 63: Storage modulus (E') and mechanical damping (tanδ) as a function of temperature for 2.9KDa Mwt SS elastomers from both diisocyanates.

The 1kDa SS MDI based elastomer is the only elastomer that shows greater modulus than the DFDI variant throughout the testing range. It is also the only elastomer to show clear signs of HS crystallinity in the AFM phase image, which account for the increase in modulus.

Compiled Tgs found from the decay in modulus and the onset of the tanδ are reported in table 20.

Isocyanate	SS Mwt	DSC	DMTA			
		Tg / °C	Tg (tanδ onset) / °C	Δ (to DSC) / °C	Tg (E' decay) / °C	Δ (to DSC) / °C
DFDI	1k	-49	-59	10	-54	5
DFDI	2k	-71	-79	8	-71	0
DFDI	2.9k	-72	-80	8	-74	2
MDI	1k	-36	-52	16	-46	10
MDI	2k	-67	-68	1	-62	5
MDI	2.9k	-72	-79	7	-70	2

Table 20: Glass transition temperatures calculated from DSC and DMTA (two methods) experiments for MDI based SS Mwt series. The error on temperatures from DSC measurements is ±1°C while the error on DMTA measurements is ±2°C.

Tg values found by all methods are generally close, with the notable exceptions of the 1kDa SS elastomers. These elastomers have a broad distribution of domain sizes (see earlier scattering data), which accounts for the discrepancy in values.

Previous studies on the same or similar systems have presented DMTA data that is consistent with data presented here. Christenson[86] presented the DMTA trace of a solvent cast MDI-BD-PTHF1k elastomer which matches closely the m1k elastomer in this chapter. The tanδ peak onset occurs at c. -55ºC (-52ºC in this work) and the decay in storage modulus begins at -43ºC (-46ºC). Pukanszky[101] analysed a 50%HS MDI-BD-PTHF1k elastomer and reported DMTA traces following the same trends as the m1k system in this chapter. The modulus was higher throughout, as expected with a significantly greater HS%.Wang[73] reported the DMTA trace of an MDI-BD-PTHF2k (22%HS) system, which matches the trace of the m2k elastomer in this work, the decay in modulus began at -60ºC (-62ºC in this work). Cawse[19b, 74] presented the DMTA traces for the DFDI-BD-PTHF1k polymers with 10 and 50%HS. Storage modulus for the 10%HS elastomer was noticed to decay from -58ºC (-54ºC the 20%HS version in this work).

Other authors have noted similar trends in different systems; Boufi[19f] found the decay on modulus to occur warmer in DFDI based elastomers, but as discussed in the previous chapter, it is expected that the pre-polymer preparation method contributed to this anomaly. Yilgor[81a] noted that the decay in storage modulus occurs around 20ºC cooler in a 2kDa PTHF SS PU compared to the analogous 1kDa version. Das[100] presented DMTA curves for 1 and 2kDa Mwt PTHF based versions of elastomers. The tanδ peaks were noticeably broader in 2k versions in agreement with this series. Martin[93a] used PHMO based elastomers with varying SS Mwt. The decay in storage modulus was lower and the decay more gradual with increasing SS Mwt, the tanδ peak became more broad and occurred at a cooler temperature. Precisely matching trends in this series.

Hardness

Hardness within the DFDI (figure 64) series decreases from one to two kDa Mwt SS. While there is a significant increase in SS crystallinity from 1 to 2kDa Mwt SS, the contributing factor is the molecular weight between hard segments.
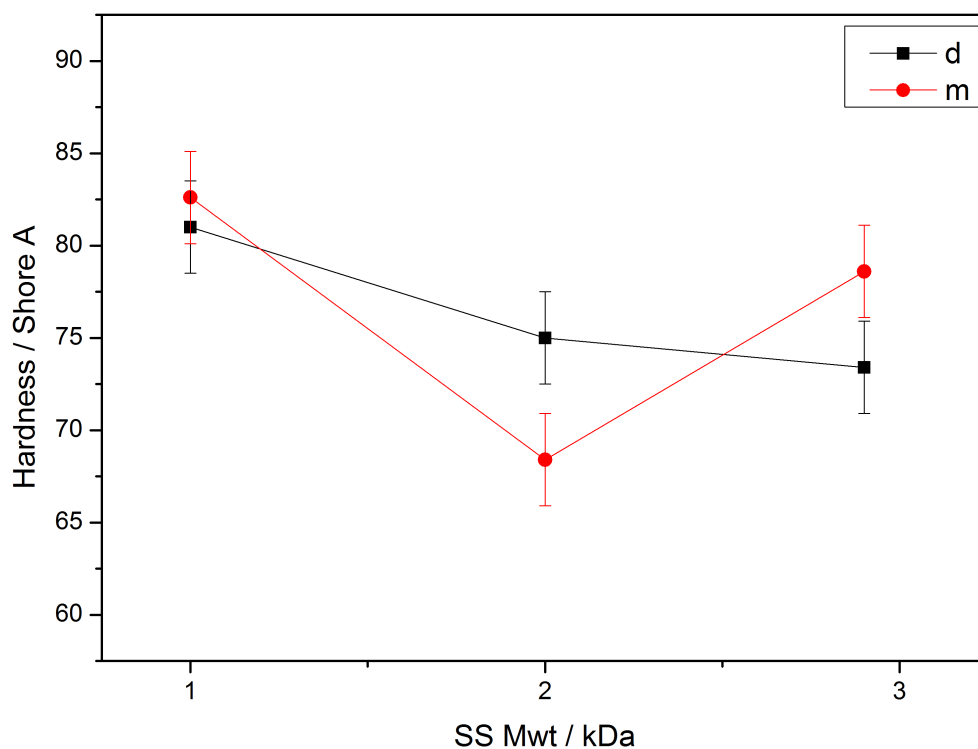
Figure 64: Shore A hardness for the SS series elastomers at room temperature.

The results in the MDI series shows a sharp decrease in hardness from 1 to 2kDa Mwt SS, with a significant increase from 2 to 2.9. The decrease agrees with the data from the DFDI series, the Mwt between hard segments is a significant factor in hardness, the greater decrease is due to the loss of HS crystallinity. The increase in hardness from 2 to 2.9 kDa Mwt SS is due to the increase in SS crystallinity at room temperature.

TGA

TGA results are presented in figures 65 and 66 for the elastomers and figure 67 for the pure phases (results are summarised in tables 21 and 22). There is little change throughout the series, fitting with earlier results showing differences in mass loss and onset were dependent on the relative quantities of groups present. This series presents data from elastomers in which the proportion of aromatic, furanic and aliphatic components changes very little throughout the series.
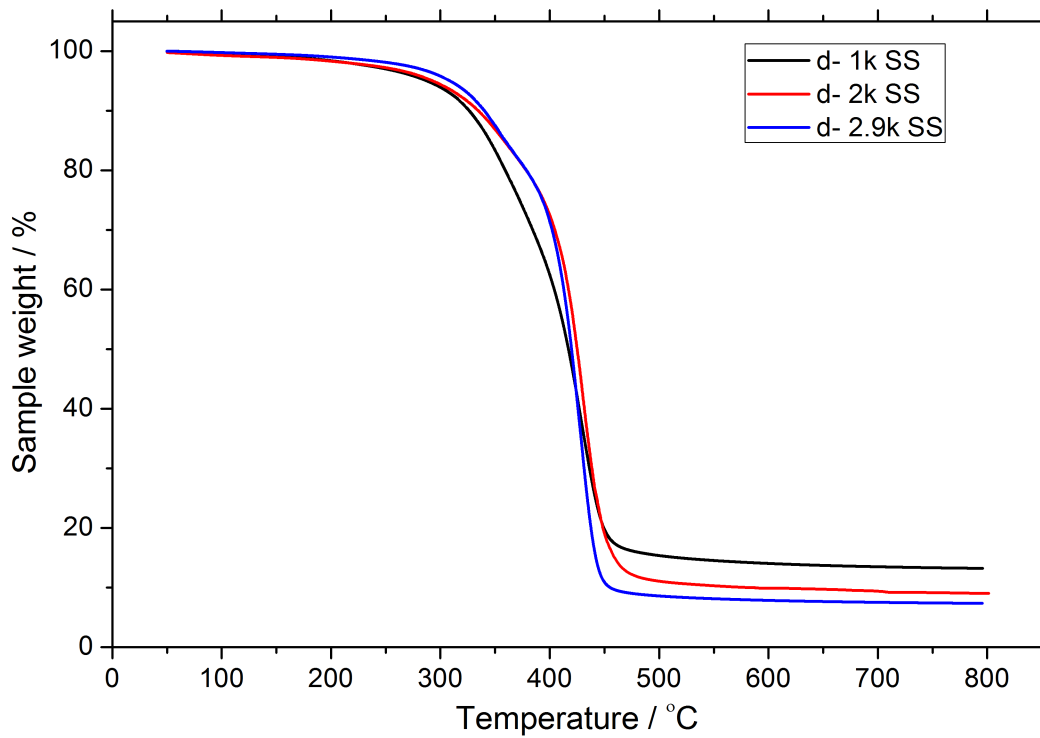
Figure 65: Sample weight as a function of temperature from TGA experiments for DFDI based SS Mwt series.
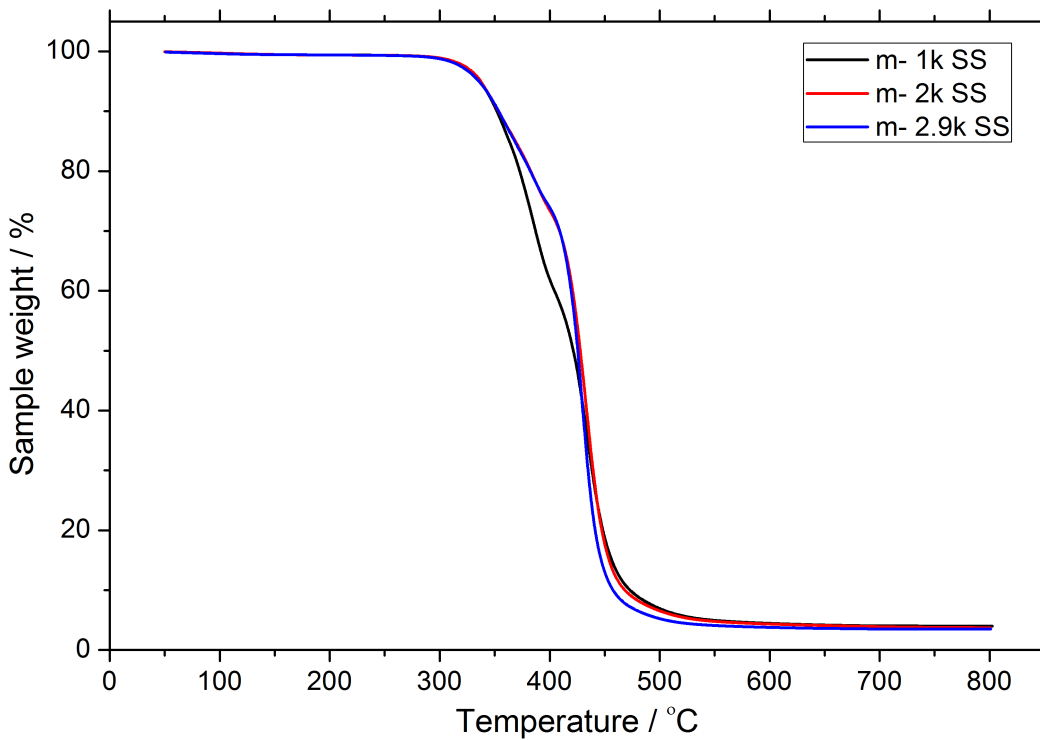
Figure 66: Sample weight as a function of temperature from TGA experiments for MDI based SS Mwt series.
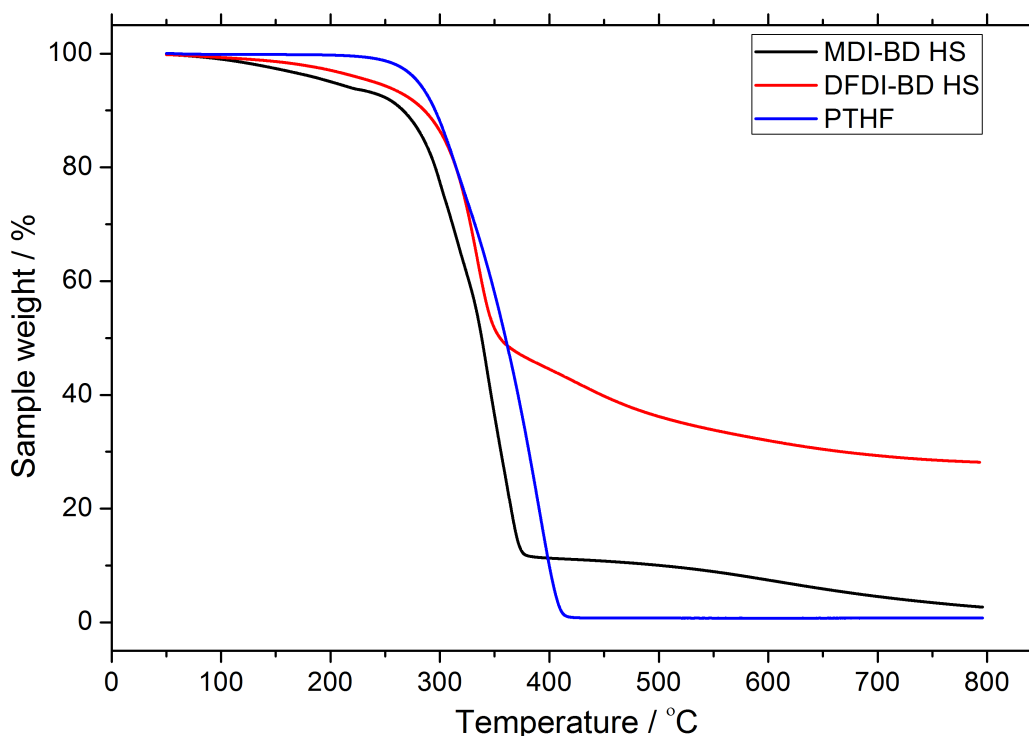
Figure 67: Sample weight as a function of temperature from TGA experiments for pure phases utilised in this chapter.

The onset of mass loss occurs cooler in DFDI based elastomers, and in this series it is noticeable that mass loss occurs marginally cooler at lower Mwt SS.

The mass loss at 800ºC shows no variance for the MDI series, the DFDI series however displays a lower mass loss for shorter soft segments. This coincides with more phase mixing as seen in AFM images, more significantly the furanic content falls throughout the series (a consequence of maintaining consistent overall HS fractions with varying SS).

Isocyanate	SS Mwt	Onset of mass loss / ºC	Mass loss at 800ºC / %
DFDI	1k	284	86.8
DFDI	2k	304	91.0
DFDI	2.9k	312	92.6
MDI	1k	325	96.0
MDI	2k	325	96.3
MDI	2.9k	325	96.5

Table 21: Weight loss % and mass loss for varying SS Mwt of DFDI and MDI based elastomers. The error on temperatures is ±2ºC.

Pure phase	Onset of mass loss / °C	Mass loss at 800°C / %
PTHF	247	99.3
MDI-BD	266*	97.0
DFDI-BD	280*	72.0

*Table 22: Weight loss % and onset of mass loss for pure phases. The error on temperatures is ±2°C. * Mass loss is evident at a slow rate immediately, the temperature reported is that of the more severe mass loss.*

Boufi[21] has previously shown that furanic content in a polyurethane elastomer can protect against mass loss. This observation matches the trends seen in this chapter. A more thorough comparison to relevant literature can be found in the previous chapter.

Chapter 6. Polyurethaneureas based on DFDI/MDI and their precursor diamines

Introduction

Solution cast elastomers with hard segments composed of diisocyanates and the diamine precursors of those diisocyanates were synthesised following the method described in the experimental section at 20%HS.

The ability to form strong bidentate hydrogen bonds allows PUU elastomers to form very tough elastomers when highly segregated morphologies are achieved[45e]. Phase separation in PUU elastomers is often reported as being higher than in analogous PU systems[37a, 45e] when elastomers are solvent cast.

In some systems the strong interactions between hard segments can lead to vitrification and arrest the development of higher order. Garrett[72] reported a decrease in phase separation at high hard segment contents in an MDI-ED-PTHF system, and suggested that the strong hydrogen bonds were hindering phase separation.

The solvent evaporation rate can influence the degree of phase separation, Ikeda[41] reports a higher degree of phase separation was observed in PU elastomers cast using a slower evaporation rate of the solvent. In this work the films were formed slowly due to a high boiling solvent and a low level of vacuum.

Results

Both MDI and DFDI derived PUU elastomers were tough and elastomeric. The MDI based film was optically clear, analogous to previously reported elastomers the DFDI based PUU was red in colour.

AFM

AFM images of the solution cast film surfaces are reported in figure 68.
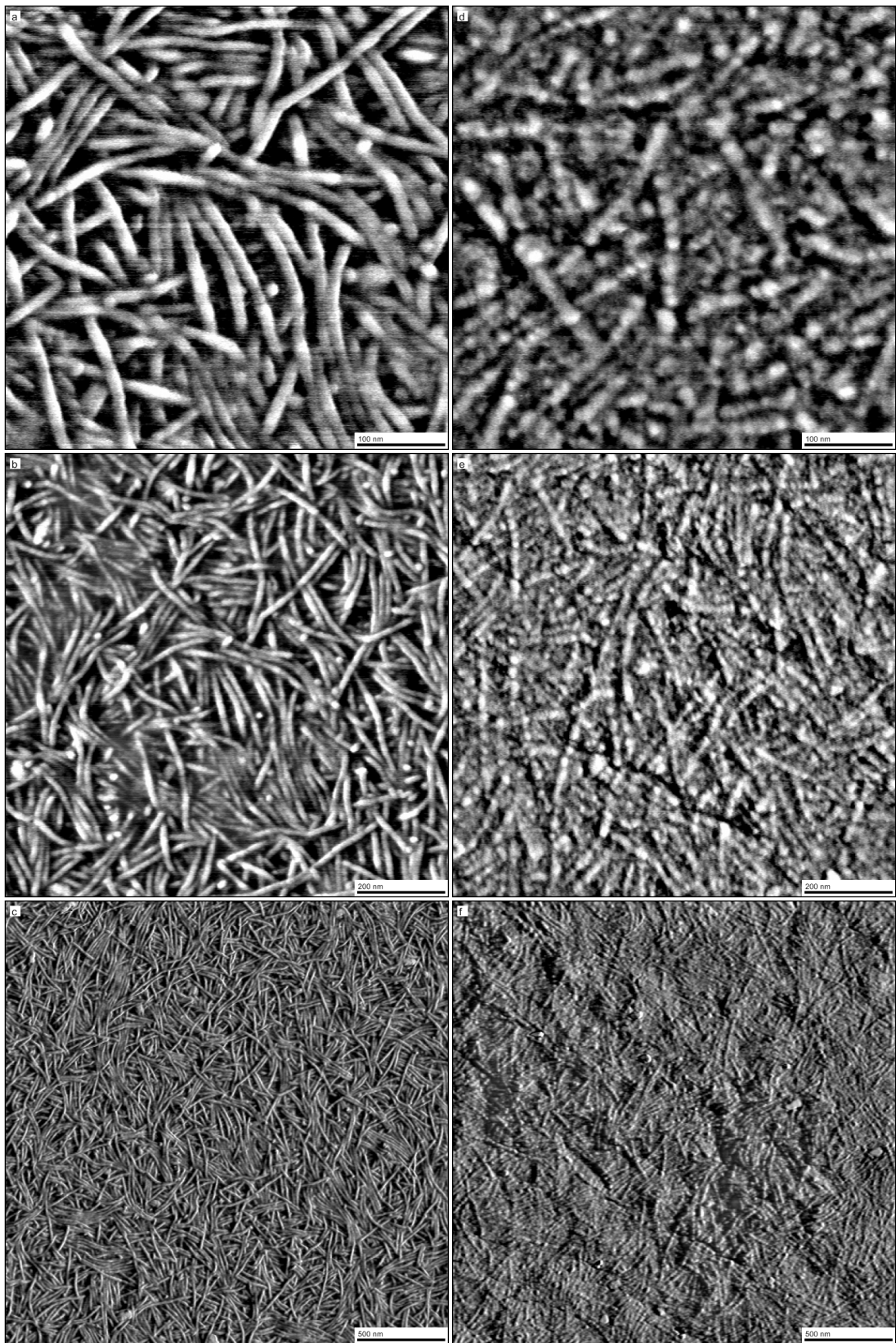
Figure 68: AFM phase images at different length scales of solvent cast DFDI-DFDA (a-c) and MDI-MDA (d-f) based PUU elastomers.

The AFM phase images of DFDI-DFDA based PUU elastomers show a strong rod like structure consistent over large length scales, the rods have an average diameter of 16nm. The MDI-MDA based elastomers show a similar structure at the same average diameter but the rod structures appear far less defined.

No literature presenting images of MDI-MDA based HS elastomers was found; although it is a common HS in foam systems, the structure of foams makes them difficult to image by AFM.

The lower degree of observed order in the MDI based PUU is likely due to the decrease in flexibility around the diisocyanate compared to DFDI. Another possible explanation could be the partial arresting of phase separation due to the π stacking interactions possible with benzene rings, although the WAXS data (reported later) does suggests there is little crystallinity within the HS.

SAXS

Both systems display a clear peak consistent with a 13nm domain spacing as seen in figure 69 with results from SAXS and AFM summarised in table 23. The significant discrepancy between domain spacing measured by SAXS and AFM techniques is only mirrored in the 0%HS DFDI PU elastomer reported in chapter 4.

The invariant suggests a low degree of phase separation in both PUU elastomers synthesised compared to the PU elastomers in previous chapters. The contribution of the electron density difference term to the invariant affects this and may account for the discrepancy between SAXS data and other results. AFM, DSC and DMTA data all indicate a high degree of phase separation in line with or greater than that observed in the PU elastomers reported in previous chapters.

WAXS and DSC data (reported below) shows the degree of crystallinity within the SS is higher in DFDI based PUU. As discussed before, this increases the density of the SS phase, narrowing the gap between the electron density difference between the two phases and thus reducing the observed scattering intensity, explaining the lower invariant presented in the DFDI SAXS data.
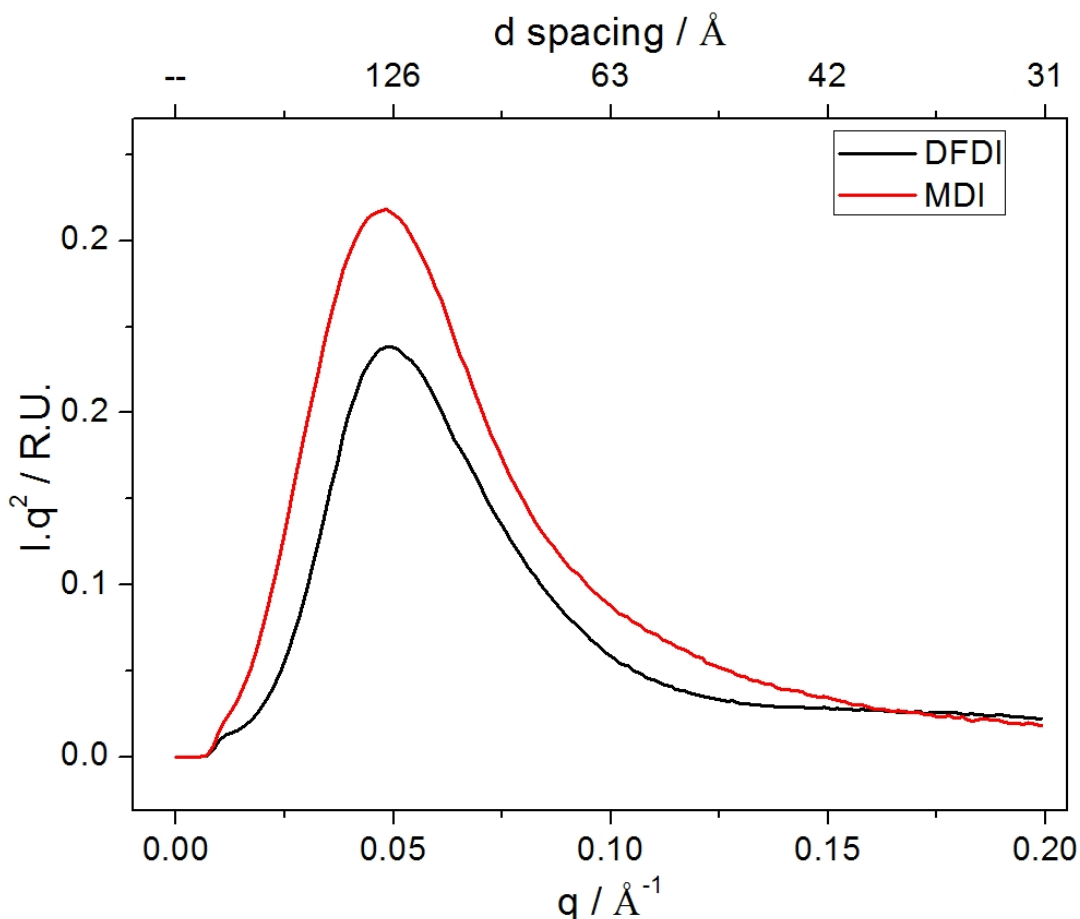
Figure 69: SAXS Lorrentz corrected intensity versus q for DFDI and MDI based PUU elastomers.

Isocyanate	d-spacing / nm			Relative invariant	
	Iq² Peak	Correlation function	AFM	Iq² Peak	Correlation function
DFDI	13 ± 0.3	12 ± 0.5	16 ± 1	1.0	1.0
MDI	13 ± 0.4	13 ± 0.5	16 ± 1	1.5	1.4

Table 23: Domain spacing (from SAXS and AFM experiments) and relative invariant (SAXS).

WAXS

Both PUU elastomers display crystalline PTHF SS when cooled and kept at 0°C. The degree of crystallinity (normalised) for the MDI based elastomer is 6%, while the DFDI elastomer is calculated to be 9% crystalline. These values are in line with AFM images which show a more ordered structure in the DFDI elastomer. WAXS frames are presented in figure 70.

The room temperature DFDI sample exhibits a broad peak centred at 21° consistent with amorphous PTHF seen in other samples. A second weaker peak observed at 17° is

attributed to single isocyanate units and has been observed in other frames from this work and in literature[85].

Scortanu[102] has previously reported the WAXS frame for an MDI-MDA (methylene dianiline) based PUU with the frame matching the room temperature WAXS frame from thesis exactly.
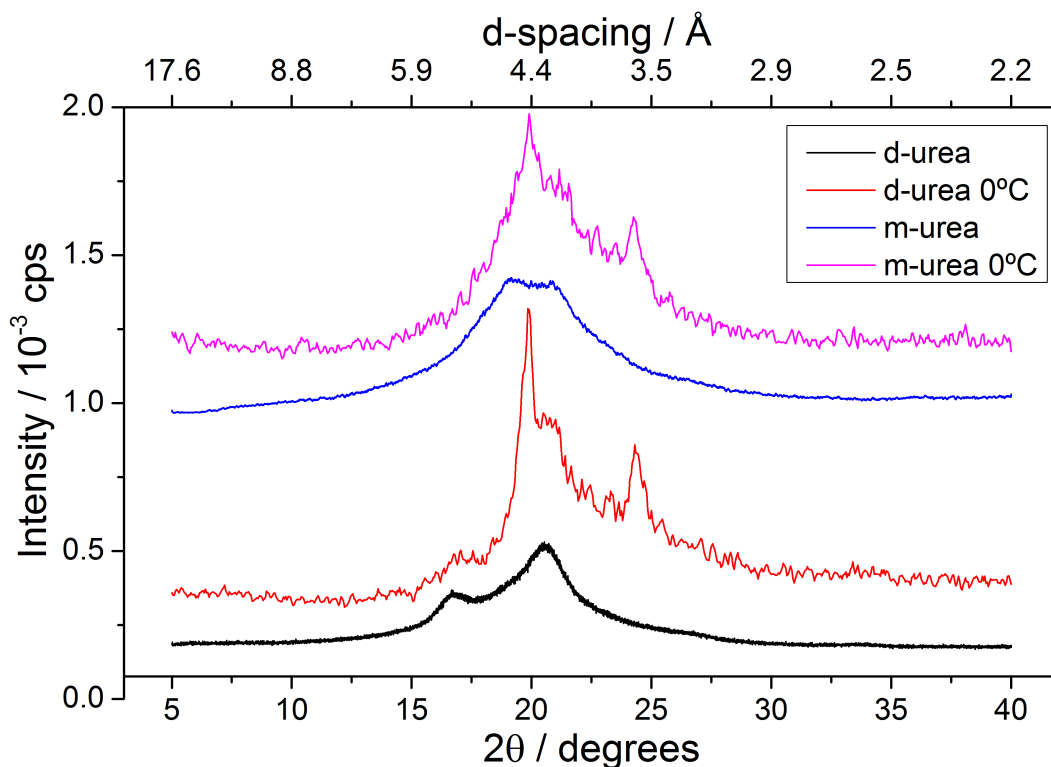
Figure 70: WAXS intensity as a function of scattering angle for PUU elastomers. Series are offset on the Y axis for clarity.

DSC

Both elastomers display clear SS melting and crystallisation transitions and weak glass transitions. Both PUU elastomers undergo crystallisation upon cooling, a property not observed in the bulk cast MDI based elastomers in previous chapters. DSC traces are presented in figure 71, temperatures and associated enthalpies can be found in table 24.

The extent of phase separation allows for crystallisation upon cooling in both elastomers. The SS Tg for the MDI elastomer (-73ºC) is lower than any observed in the previous two series', the MDI based elastomer displaying the next lowest Tg (m-2.9k at -72ºC) also begins to show crystallisation upon cooling.
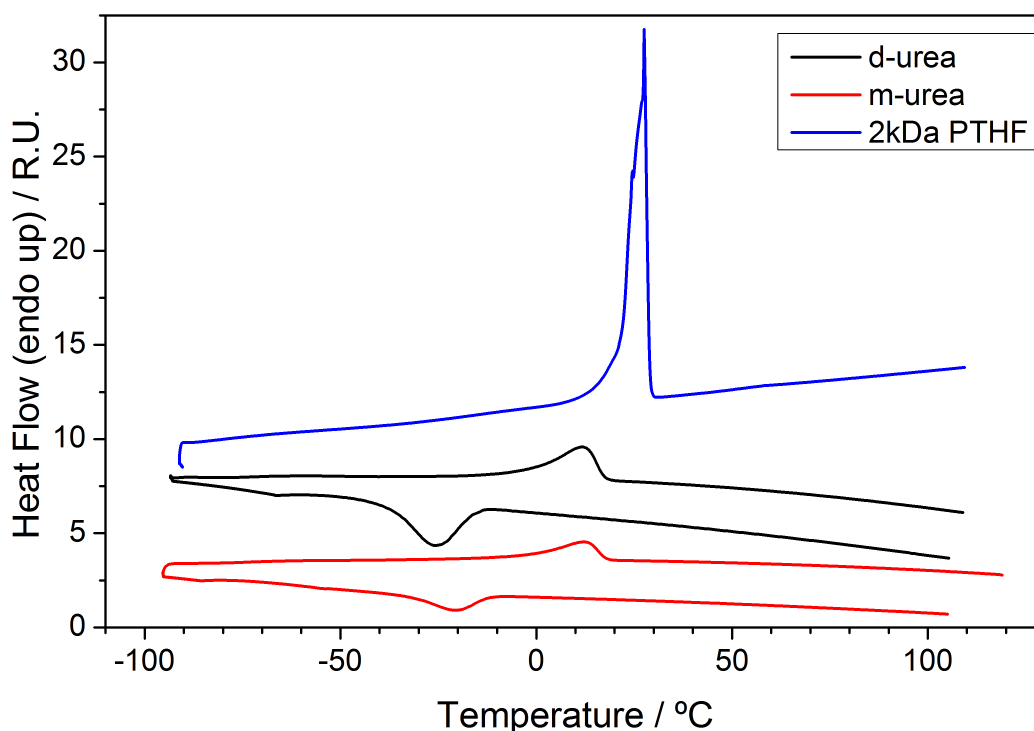
Figure 71: DSC traces for the PUU elastomers and the melting of the pure SS.

The weak enthalpy associated with the Tg is consistent with all other samples displaying SS crystallinity and is due to more of the SS being crystalline and reducing the amount of material capable of undergoing a glass transition.

Isocyanate	Experiment phase	Tg_{SS} / °C	ΔH / $J\,g^{-1}$°C-1	$Tcrys_{SS}$ / °C	ΔH / $J\,g^{-1}$	$Tmelt_{SS}$ / °C	ΔH / $J\,g^{-1}$
MDI	Cool cycle			-21	-15.42		
	Heat cycle	-73	0.09			9	16.43
DFDI	Cool cycle			-26	-22.10		
	Heat cycle	-72	0.13			13	22.60

Table 24: Temperatures and associated enthalpies of transitions observed in DSC traces for PUU elastomers. The error on temperatures is ±1°C.

DMTA

Both elastomers present broad tanδ peaks and steady decays in the storage modulus as seen in figure 72, consistent with previous samples also displaying SS crystallinity. Transition temperatures are compiled alongside results from DSC experiments in table 25.

The modulus at room temperature is significantly higher at room temperature in the DFDI based elastomer, and is likely due to the increased hydrogen bonding potential of the furan groups compared to the phenyl groups in MDI. The difference in modulus is

126

eliminated at -100ºC as all material becomes glassy and stiff.
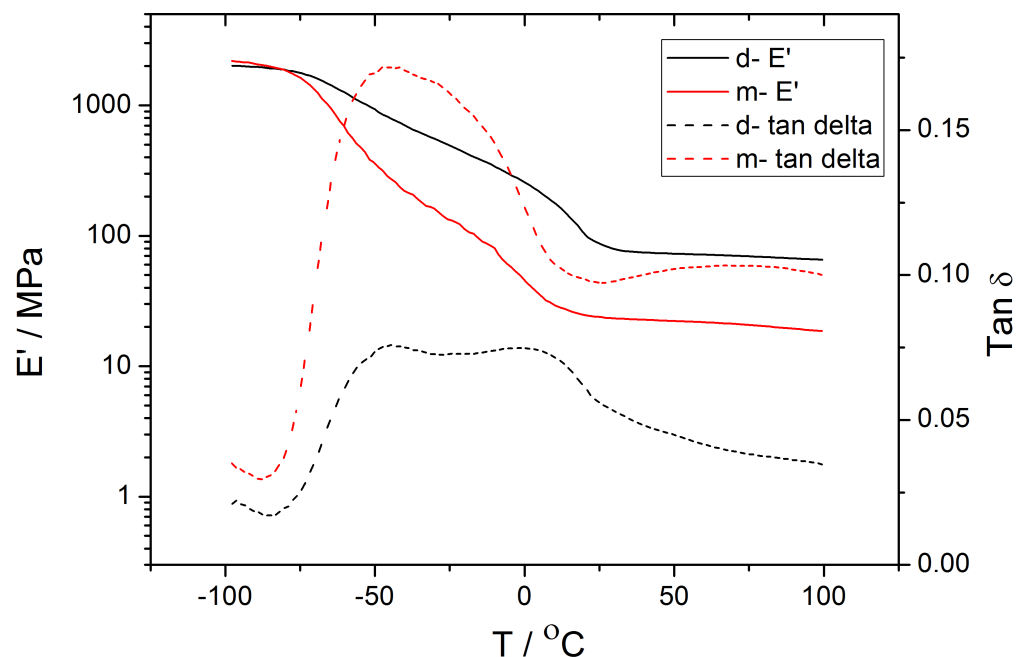
Figure 72: Storage modulus (E') and mechanical damping (tanδ) as a function of temperature for PUU elastomers.

The tanδ curve of the DFDI elastomer appears to be two overlapping broad peaks associated with the Tg and melting of the SS. The distinction between the two peaks suggests a more monodisperse crystal size in these samples compared to samples in the previous series.

Isocyanate	DSC	DMTA			
	Tg / °C	Tg (tanδ onset) / °C	Δ (to DSC) / °C	Tg (E' decay) / °C	Δ (to DSC) / °C
DFDI	-72	-78	6	-73	1
MDI	-73	-76	3	-65	8

Table 25: Comparison of Tg as calculated from DSC and DMTA experiments. The error on temperatures from DSC measurements is ±1ºC while the error on DMTA measurements is ±2ºC.

TGA

Figures 73 and 74 show the mass loss curves for the PUU elastomers and the pure phases used.
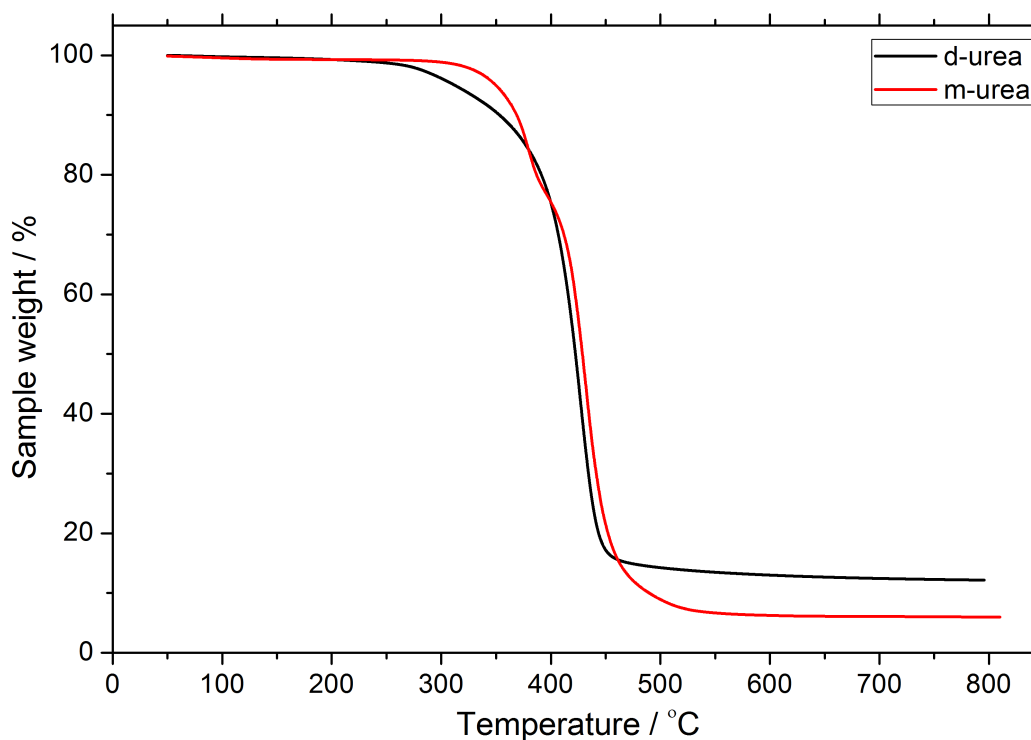
Figure 73: Sample weight as a function of temperature from TGA experiments for PUU elastomers.

Consistent with data presented in the previous chapters, furan containing material retains more mass at higher temperatures. The pure hard phases display a clear stepwise nature in the mass loss curves, a property not mirrored in the BD based hard segments studied. The DFDI-DFDA hard segment has a less clear second decay and the mass loss is much more gradual. The MDI based PUU has two noticeable decays, the DFDI elastomer presents a change in rate of mass loss though two discrete mass loss transitions can not be seen.
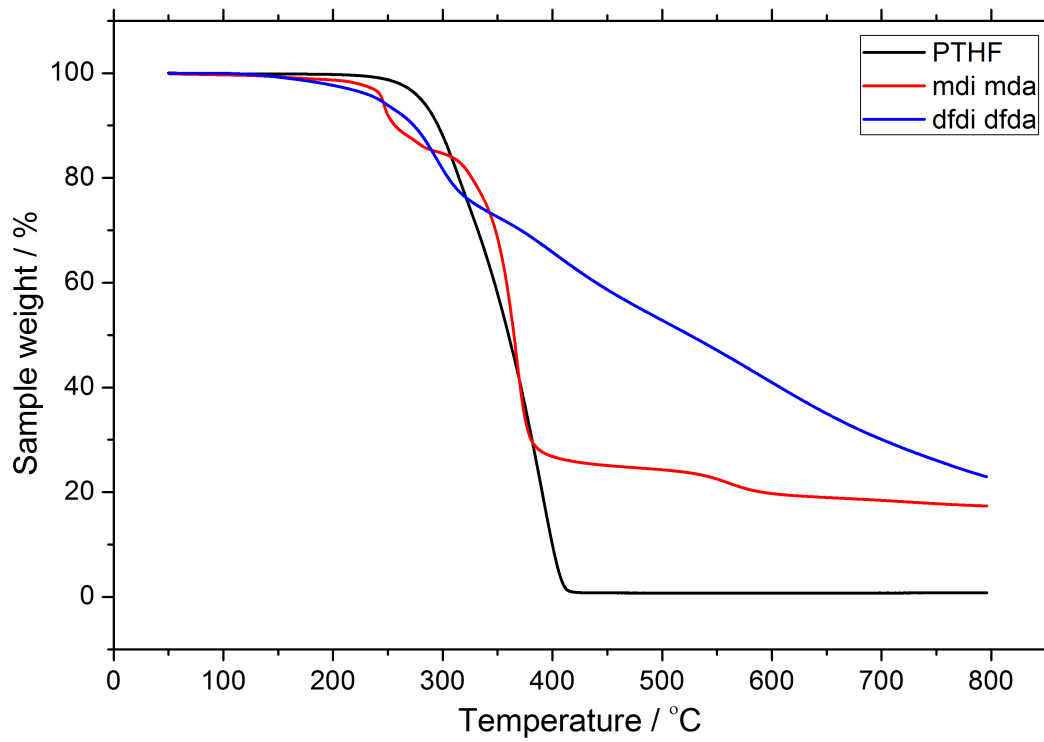
Figure 74: Sample weight as a function of temperature from TGA experiments for the pure phases used in PUU elastomers.

Chapter 7. Summary of conclusions

Introduction

A renewable sourced diisocyanate has been synthesised using a previously published procedure that was modified to increase the safety of the phosgenation reaction.

DFDI presents a significant decrease in reactivity compared to MDI, though as shown previously and in this work; tough, resilient and well phase separated elastomers can be formed using a standard pre-polymer route.

The structure property relationships of DFDI based elastomers have been explored in detail and compared to those of analogous MDI based PU and PUU.

SAXS and AFM data were shown to be consistent in determining the domain spacing in samples. WAXS, DSC and DMTA provided information into the thermo-mechanical properties and crystallinity observed in samples.

Synthesis and kinetics

DFDI was synthesised as per the method published by Cawse[19a] in 1984, with a modification of the phosgenation step to use triphosgene rather than phosgene.

The four step synthesis was accomplished with an overall yield of only 14.4% (yields of 91, 40, 88 and 45%), unconverted hydrochloride salt of the diamine may be salvaged in the final step however.

The kinetics of the reaction between the diisocyanates and primary alcohols was assessed using an adiabatic temperature rise experiment. Stoichiometric equivalent reactions were used to follow the second order kinetics. The solvents used were DMF and diglyme and the primary alcohols used were methanol and methyl-diglycol. Diglyme and methyl-diglycol are polyether like and allow the following of reaction kinetics in an analogous (bulk-like) environment.

The apparent rate constant was found to be between 12 and 18 times greater in MDI systems, consistent with previously reported values. A longer pre-polymer (end-capping) time was used in the synthesis of PU and PUU elastomers when using DFDI

for this reason. All elastomers cured well to form tough and rubbery polymers.

Elastomers

PU based elastomers within the increasing HS% series (static 2kDa SS) increased in modulus with increasing HS% as expected. The 0%HS elastomers were transparent as the slower reacting systems allowed enough time for a vacuum to be applied to removed dissolved air, other elastomers were translucent.

Domain spacing was found to decrease within the DFDI series from 20%HS (15, 14, and 13nm), the 0%HS elastomer displayed a lower domain spacing (11nm) due to the lower degree of phase separation interfering with SS crystallisation. AFM images show that crystallisation within the SS is pronounced and dominates the morphology.

The AFM images for the MDI based series match those most commonly reported in literature of an amorphous SS with dispersed hard domains, and phase inversion at c.50%HS. Domain spacing therefore increases from 20 to 40%HS and then drops in the 60%HS elastomer (13, 16 and 15nm (no phase separation in the 0%HS elastomer)).

Crystallinity was observed in the HS of 40 and 60%HS MDI based elastomers, and matches WAXS data published previously. The PTHF SS was observed to crystallise in all DFDI elastomers, with purer crystals at lower HS%. MDI based elastomers displayed crystallinity within the SS of only 0 and 20%HS elastomers and the crystals were less pure and not observable by room temperature tapping mode AFM. Calculations of the degree of crystallinity was achieved by both DSC and WAXS, values generally agree well.

TGA data shows that hard segments are more resistant to mass loss at higher temperatures, this effect is much more pronounced in furan based hard segments.

Elastomers within the SS Mwt series (static 20%HS) showed that SS crystallinity was much more pronounced with greater SS Mwt, as expected. MDI based elastomers displayed stable SS crystals only at 2.9kDa Mwt SS. The 2kDa SS displayed crystalline SS only in experiments where the elastomer was cooled (DSC, DMTA and WAXS). The shore A hardness measurements mirror this effect as the hardness falls, but then increases (as SS crystals are stable at RT) across the increasing SS Mwt MDI series.

The domain spacing increases with increasing SS Mwt in both MDI and DFDI based elastomers. SAXS frames also showed that the domains became more monodisperse, in agreement with AFM images.

The SS Tg decreases with increasing SS Mwt (DFDI -49, -71, -72, MDI -36, -67, -72ºC) indicating a purer phase, though the SAXS invariant suggests the overall degree of phase separation changes little throughout the series.

PUU elastomers were cast using the diamine precursor to the diisocyanate as the chain extender in order to investigate the property and morphology in samples with hard segments analogous to those found in water blown foams. Elastomers were cast from solution to yield very tough and transparent films.

AFM images show a very clear interwoven rod structure in the DFDI-DFDA elastomer, with a similar though less defined structure in the MDI-MDA elastomer.

DSC and DMTA data shows the SS Tg is very low in both samples (-73 and -72ºC MDI, DFDI) indicating a high degree of phase separation. The SAXS invariant is very low, though the increased electron density of a crystalline SS phase may account for this.

Chapter 8. Suggestions for future work

Improvements to work presented here

Synthesis of DFDI

There was no focus on improving the yields of the steps leading to the diamine in this work. While the yield of the phosgenation is low, the hydrochloride salt is salvageable with no real losses otherwise. Improving the yields in steps leading up to the diamine would lead to a significant reduction in the cost of DFDI.

AFM

Using tapping mode AFM at elevated temperatures may be able to reveal any hidden morphology due to the hard segments, rather than the crystalline SS morphology that dominated most images. Though no peaks due to HS crystallites were discernible in WAXS frames, a separated but non crystalline phase may exist. This structure would be useful in predicting the properties of elastomers with non-crystalline soft segments.

SAXS

A synchrotron x-ray source would allow the kinetics of phase separation to be followed which would provide useful information into the way morphology develops in these systems. All polymers were annealed at high temperatures ruling out SS crystallisation as the driving force for phase separation in the curing elastomer. Time resolved SAXS would allow the mechanism to be followed.

To complement this thesis

Stress-strain behaviour

It would be advantageous to assess both the tensile strength and elongation at break (EAB) in DFDI based elastomers, these values would be useful in determining the potential use of DFDI in real world applications.

These measurements require the casting of near perfect elastomers, any trapped air

bubbles would lead to propagation of tears (and lower results of EAB) and incorrect measurements of cross section (and therefore reduced measured stress). The lab equipment used in this thesis comprised a mechanical stirrer for mixing the chain extender and pre-polymer, which mixes significant amounts of air into the viscous pre-polymer. A solution would be to use a lab scale RIM machine using a static mixer and vacuumed storage tanks for the pre-polymer and chain extender.

DMTA data suggests that the modulus is higher in most DFDI based elastomers so a higher tensile strength may be assumed, though as only a 1% strain was applied a full stress/strain curve would be much more useful.

EAB could be assumed to be higher in DFDI based PU as the degree of phase separation is greater, meaning a purer SS contributes to the rubbery properties of the elastomer. Crystallinity within the SS however may drastically reduce EAB, though Sonnenchein[76] has reported that crystallinity within the SS of PTHF based SPU elastomers did not reduce the value of EAB.

Other soft segments

Using PPO or PEO end-capped PPO soft segments would allow the synthesis of elastomers with SS much less likely to crystallise. Differences between the elastomers would then be due to the HS, with no contribution from SS crystallinity which had a large effect on elastomers in the series of this work.

Costing

A significant factor into any potential real world use would be the bulk cost of DFDI. A prohibitive cost would lead to DFDI only being considered in niche (green) applications. An estimation of the cost was not possible as the cost of raw materials when purchased in bulk can vary dramatically based upon not only the quantities ordered, but also the buying power of the customer. As the synthesis follows a similar route to that of MDI, any plant capable of processing MDI would be expected to be able to switch over to production of DFDI with very few issues.

New areas to research

Coatings

The reduced reactivity of DFDI compared to MDI would allow for greater stability of pre-polymers. This would be advantageous in some situations as alongside their light stability, low reactivity is another reason that HDI and IPDI are often used in one component coatings. A detailed look into weathering via UV and hydrolysis would be useful to determine the potential for use in such applications.

Electrospinning DFDI based PU fibres

If the bulk price of DFDI is significantly more expensive than that of MDI, for its use to be justified the products it is used in must have a high added value. One example of a PU based product with a high added value is Lycra.

Attempts were made to electrospin fibres of DFDI based PU elastomers from solution. MDI based elastomers can be electrospun from solutions of DMF/THF blends with relative ease to produce aligned fibres or a non-woven mesh. Difficulties were encountered with DFDI based elastomers due to the hydrogen bonding possible with furan groups. Attempts to introduce salts to disrupt hydrogen bonds were unsuccessful, though it is expected that further research may result in a working method.

Other renewable soft segments

Though PTHF has a renewable source, it is not the primary synthetic route. Other polyols are available that are completely bio-sourced. Examples include soy-bean oil polyols which have been used within this group before. Investigation into the structure-property relations in systems utilising DFDI and soy based polyols would be an interesting topic as the elastomers would (depending on the choice of chain extender), be renewable derived elastomers as opposed to the "potentially" renewable derived elastomers of this work.

References

1.   Bayer, O., Polyurethanes. *Modern Plastics* **1947,** *24* (No. 10), 149-52,250,252,254,256,260,262.

2.   Herrington, R.; Hock, K., *Dow Polyurethanes, Flexible foams*. Dow chemical company: Michigan, 1997.

3.   Pinner, S. H., Chemistry and technology of organic isocyanates. *Plastics (London)* **1947,** *11*, 206-11,215,257.

4.   Ozaki, S., Recent Advances in Isocyanate Chemistry. *Chem. Rev.* **1972,** *72* (5), 457.

5.   Randall, D., *The Polyurethanes Book*. Wiley: 2002.

6.   Rosu, D.; Rosu, L.; Cascaval, C. N., IR-change and yellowing of polyurethane as a result of UV irradiation. *Polymer Degradation and Stability* **2009,** *94* (4), 591-596.

7.   Winkler, J., Aging of urethan foams. *SPE Journal* **1956,** *12* (No. 11), 23-5.

8.   (a) Yilgor, I.; Yilgor, E.; Guler, I. G.; Ward, T. C.; Wilkes, G. L., FTIR investigation of the influence of diisocyanate symmetry on the morphology development in model segmented polyurethanes. *Polymer* **2006,** *47* (11), 4105-4114; (b) Sheth, J. P.; Unal, S.; Yilgor, E.; Yilgor, I.; Beyer, F. L.; Long, T. E.; Wilkes, G. L., A comparative study of the structure-property behavior of highly branched segmented poly(urethane urea) copolymers and their linear analogs. *Polymer* **2005,** *46* (23), 10180-10190; (c) Schneider, N. S.; Paiksung, C. S.; Matton, R. W.; Illinger, J. L., Thermal Transition Behavior of Polyurethanes Based on Toluene Diisocyanate. *Macromolecules* **1975,** *8* (1), 62-67; (d) Mormann, W.; Zhang, C. X., Ternary phase separation in polyurethane elastomers with immiscible soft segments. *Macromol. Symp.* **2003,** *198*, 271-281.

9.   Wilson, W. C., Furan. *Organic Syntheses* **1927,** *7*, 40-41.

10.   Ryan, A. J. Structure-property relations in Poly(Urethane-Urea)s and Polyureas formed by reaction injection moulding, RIM. University of Manchester, Manchester, 1988.

11.   Priester, R. D., Jr.; McClusky, J. V.; O'Neill, R. E.; Turner, R. B.; Harthcock, M. A.; Davis, B. L., FTIR - a probe into the reaction kinetics and morphology development of urethane foams. *Proceedings of the SPI Annual Technical/Marketing Conference* **1990,** *33rd*, 527-39.

12.   Lovering, E. G.; Laidler, K. J., Thermochemical Studies of Some Alcohol-Isocyanate Reactions. *Canadian Journal of Chemistry* **1962,** *40* (1), 26-30.

13.   Baker, J. W.; Holdsworth, J. B., Mechanism of aromatic side-chain reactions with special reference to the polar effects of substituents. XIII. Kinetic examination of the reaction of aryl isocyanates with methyl alcohol. *Journal of the Chemical Society* **1947**, 713-26.

14.   Farkas, A.; Strohm, P. F., Mechanism of the amine-catalyzed reaction of isocyanates with hydroxyl compounds. *Industrial & Engineering Chemistry Fundamentals* **1965,** *4* (1), 32-8.

15.   (a) Peebles, L. H., Jr., Sequence length distribution in segmented block copolymers. *Macromolecules* **1974,** *7* (6), 872-81; (b) Peebles, L. H., Jr., Hard block length distribution in segmented block copolymers. *Macromolecules* **1976,** *9* (1), 58-61.

16.   Gandini, A., Polymers from Renewable Resources: A challenge for the future of macromolecular materials. *Macromolecules* **2008,** *41* (24), 9491-9504.

17.   Pande, C. D.; Kapoor, S. K.; Bajaj, I.; Venkataramani, B., Polyurethan foams. II. Influence of different surfactants, catalysts, and fillers on castor oil prepolymer foams. *Indian Journal of Technology* **1966,** *4* (4), 109-13.

18.   (a) Ferrer, C. C. Natural Oil polyol. University of Sheffield, Sheffield, 2007; (b) Ferrer, M. C. C.; Babb, D.; Ryan, A. J., Characterisation of polyurethane networks based on vegetable derived polyol. *Polymer* **2008,** *49*, 3279-3287; (c) Mortamet, A.-C. Soy bean polyols in polyurethane elastomers. University of Sheffield, Sheffield, 2011.

19.   (a) Cawse, J. L.; Stanford, J. L.; Still, R. H., Polymers from Renewable Sources . 1. Diamines and Diisocyanates Containing Difurylalkane Moieties. *Makromolekulare Chemie-Macromolecular Chemistry and Physics* **1984,** *185* (4), 697-707; (b) Cawse, J. L.; Stanford, J. L.; Still, R. H., Polymers from Renewable Sources .2. Kinetics and Polyurethane Formation from Furan-Based Diisocyanates. *Makromolekulare Chemie-*

Macromolecular Chemistry and Physics **1984,** *185* (4), 709-723; (c) Quillerou, J.; Belgacem, M. N.; Gandini, A.; Rivero, J.; Roux, G., Urethanes and Polyurethanes Bearing Furan Moieties .1. Synthesis and Characterization of Monourethanes. *Polymer Bulletin* **1989,** *21* (6), 555-562; (d) Belgacem, M. N.; Quillerou, J.; Gandini, A.; Rivero, J.; Roux, G., Urethanes and Polyurethanes Bearing Furan Moieties .2. Comparative Kinetics and Mechanism of the Formation of Furanic and Other Monourethanes. *European Polymer Journal* **1989,** *25* (11), 1125-1130; (e) Belgacem, M. N.; Quillerou, J.; Gandini, A., Urethanes and polyurethanes bearing furan moieties. 3. Synthesis, characterization and comparative kinetics of the formation of diurethanes. *European Polymer Journal* **1993,** *29* (9), 1217-24; (f) Boufi, S.; Gandini, A.; Belgacem, M. N., Urethanes and polyurethanes bearing furan moieties: 5. Thermoplastic elastomers based on sequenced structures. *Polymer* **1995,** *36* (8), 1689-96; (g) Quillerou, J. Syntheses et caracterisations d'urethanes et polyurethanes furaniques. PhD, De l'institut national polytechnique de grenoble, Grenoble, 1988.

20.   Gandini, A.; Belgacem, M. N., Furans in polymer chemistry. *Progress in Polymer Science* **1997,** *22* (6), 1203-1379.

21.   Boufi, S.; Belgacem, M. N.; Quillerou, J.; Gandini, A., Urethanes and polyurethanes bearing furan moieties. 4. Synthesis, kinetics and characterization of linear polymers. *Macromolecules* **1993,** *26* (25), 6706-6717.

22.   (a) Stanford, J. L., Polyurethanes from Renewable Resources. *Abstracts of Papers of the American Chemical Society* **1987,** *194*, 80-CELL; (b) Stanford, J. L.; Still, R. H.; Cawse, J. L.; Donnelly, M. J., Polyurethanes from Renewable Resources. *Acs Symposium Series* **1989,** *385*, 424-442.

23.   Burkus, J.; Eckert, C. F., The Kinetics of the Triethylamine-Catalyzed Reaction of Diisocyanates with 1-Butanol in Toluene. *J. Am. Chem. Soc.* **1958,** *80* (22), 5948-5950.

24.   Macosko, C. W., *RIM, Fundamentals of reaction injection molding*. Hanser: Munich, Vienna, New York, 1989.

25.   Flory, P. J., Molecular size distribution in three dimensional polymers. I. Gelation. *J. Am. Chem. Soc.* **1941,** *63*, 3083-3090.

26.   Stockmayer, W. H., Theory of molecular size distribution and gel formation in

branched polymers II. General cross linking. *The Journal of Chemical Physics* **1944,** *12*, 125.

27.   Macosko, C. W.; Miller, D. R., New Derivation of Average Molecular-Weights of Nonlinear Polymers. *Macromolecules* **1976,** *9* (2), 199-206.

28.   (a) Lopez-serrano, F.; Castro, J. M.; Macosko, C. W.; Tirrell, M., Recursive Approach to Copolymerization Statistics. *Polymer* **1980,** *21* (3), 263-273; (b) Elwell, M. J. Structure development during the reactive processing of flexible polyurethane foam. PhD, University of Manchester, 1993.

29.   Lyman, D. J., Polyurethanes. *Polym. Rev.* **1966,** *1* (1), 191-237.

30.   Keller, A., Morphology of Polymers. *Pure and Applied Chemistry* **1992,** *64* (2), 193-204.

31.   Ryan, A. J.; Macosko, C. W.; Bras, W., Order-disorder transition in a block copolyurethane. *Macromolecules* **1992,** *25* (23), 6277-83.

32.   Sperling, L. H., *Introduction to Physical Polymer Science*. Wiley-Interscience: 2006.

33.   Jones, R. A. L., *Soft Condensed Matter*. Oxford university press: 2002; p 195.

34.   Flory, P. J., *Principles of polymer chemistry*. Cornell Univ Pr: 1953.

35.   Leibler, L., Theory of Microphase Separation in Block Co-Polymers. *Macromolecules* **1980,** *13* (6), 1602-1617.

36.   Benoit, H.; Hadziioannou, G., Scattering-Theory and Properties of Block Copolymers with Various Architectures in the Homogeneous Bulk State. *Macromolecules* **1988,** *21* (5), 1449-1464.

37.   (a) Paiksung, C. S.; Hu, C. B.; Wu, C. S., Properties of Segmented Poly(Urethaneureas) Based on 2,4-Toluene Diisocyanate .1. Thermal Transitions, X-Ray Studies, and Comparison with Segmented Poly(Urethanes). *Macromolecules* **1980,** *13* (1), 111-116; (b) Paiksung, C. S.; Smith, T. W.; Sung, N. H., Properties of Segmented Polyether Poly(Urethaneureas) Based on 2,4-Toluene Diisocyanate .2. Infrared and Mechanical Studies. *Macromolecules* **1980,** *13* (1), 117-121.

38.   Bras, W.; Derbyshire, G. E.; Bogg, D.; Cooke, J.; Elwell, M. J.; Komanschek, B.

U.; Naylor, S.; Ryan, A. J., Similtaneous studies of reaction kinetics and structure development in polymer processing. *Science* **1995,** *267*, 996-999.

39.   ASTM, D4274 - Standard Test Methods for Testing Polyurethane Raw Materials: Determination

of Hydroxyl Numbers of Polyols. Philadelphia, 1990.

40.   ASTM, D5155 - 10 Standard Test Methods for Polyurethane Raw Materials Determination of the Isocyanate Content of Aromatic Isocyanates. **2012**.

41.   Ikeda, Y.; Tabuchi, M.; Sekiguchi, Y.; Miyake, Y.; Kohjiya, S., Effect of Solvent Evaporation Rate on Microphase-Separated Structure of Segmented Poly(Urethane-Urea) Prepared by Solution Casting. *Macromolecular Chemistry and Physics* **1994,** *195* (11), 3615-3628.

42.   (a) Pannone, M. C.; Macosko, C. W., Kinetics of Isocyanate Amine Reactions. *Journal of Applied Polymer Science* **1987,** *34* (7), 2409-2432; (b) Pannone, M. C.; Macosko, C. W., Reaction-Kinetics of a Polyurea Reaction Injection-Molding System. *Polymer Engineering and Science* **1988,** *28* (10), 660-669; (c) Sun, X. D.; Toth, J.; Lee, L. J., Chemorheology of poly(urethane/isocyanurate) formation. *Polymer Engineering and Science* **1997,** *37* (1), 143-152; (d) Li, W.; Ryan, A. J.; Meier, I. K., Effect of Chain Extenders on the Morphology Development in Flexible Polyurethane Foam. *Macromolecules* **2002,** *35* (16), 6306-6312.

43.   Smith, H. A., Effect of Urethane Groups on Reaction of Alcohols with Isocyanates. *Journal of Polymer Science Part a-1-Polymer Chemistry* **1968,** *6* (5PA1), 1299-&.

44.   Reifer, D.; Windeit, R.; Kumpf, R. J.; Karbach, A.; Fuchs, H., AFM and TEM investigations of polypropylene/polyurethane blends. *Thin Solid Films* **1995,** *264* (2), 148-52.

45.   (a) Garrett, J. T.; Siedlecki, C. A.; Runt, J., Microdomain Morphology of Poly(urethane urea) Multiblock Copolymers. *Macromolecules* **2001,** *34* (20), 7066-7070; (b) Aneja, A.; Wilkes, G. L., Hard segment connectivity in low molecular weight model trisegment' polyurethanes based on monols. *Polymer* **2004,** *45* (3), 927-935; (c) De, D.; Gaymans, R. J., Thermoplastic polyurethanes with TDI-based monodisperse

hard segments. *Macromolecular Materials and Engineering* **2009,** *294* (6-7), 405-413; (d) McLean, R. S.; Sauer, B. B., Tapping-Mode AFM Studies Using Phase Detection for Resolution of Nanophases in Segmented Polyurethanes and Other Block Copolymers. *Macromolecules* **1997,** *30* (26), 8314-8317; (e) Klinedinst, D. B.; Yilgor, E.; Yilgor, I.; Beyer, F. L.; Wilkes, G. L., Structure-property behavior of segmented polyurethaneurea copolymers based on an ethylene-butylene soft segment. *Polymer* **2005,** *46* (23), 10191-10201; (f) Waletzko, R. S.; Korley, L. T. J.; Pate, B. D.; Thomas, E. L.; Hammond, P. T., Role of Increased Crystallinity in Deformation-Induced Structure of Segmented Thermoplastic Polyurethane Elastomers with PEO and PEO-PPO-PEO Soft Segments and HDI Hard Segments. *Macromolecules (Washington, DC, United States)* **2009,** *42* (6), 2041-2053; (g) Godinho, M. H.; Melo, L. V.; Brogueira, P., Atomic force microscopy evidence of patterning urethane/urea copolymers. *Materials Science & Engineering, C: Biomimetic and Supramolecular Systems* **2003,** *C23* (6-8), 919-922.

46.   Grandy, D. B.; Hourston, D. J.; Price, D. M.; Reading, M.; Silva, G. G.; Song, M.; Sykes, P. A., Microthermal characterization of segmented polyurethane elastomers and a polystyrene-poly(methyl methacrylate) polymer blend using variable-temperature pulsed force mode atomic force microscopy. *Macromolecules* **2000,** *33* (25), 9348-9359.

47.   Bowen, W. R., Hilal, N, Atomic force microscopy in process engineering. Butterworth-Heinemann: 2009; p 304.

48.   Aneja, A.; Wilkes, G. L., A systematic series of 'model' PTMO based segmented polyurethanes reinvestigated using atomic force microscopy. *Polymer* **2003,** *44* (23), 7221-7228.

49.   Menard, K. P., *Dynamic mechanical analysis*. CRC Press, Taylor & Francis group: 2008.

50.   Fox, T. G.; Flory, P. J., 2nd-Order Transition Temperatures and Related Properties of Polystyrene .1. Influence of Molecular Weight. *Journal of Applied Physics* **1950,** *21* (6), 581-591.

51.   ASTM, D2240 - Standard Test Method for Rubber Property 8212 - Durometer Hardness **2010**.

52.   Glatter, O.; Kratky, O.; Editors, *Small Angle X-ray Scattering*. 1982; p 515.

53.   (a) Vanbogart, J. W. C.; Gibson, P. E.; Cooper, S. L., Structure-Property Relationships in Polycaprolactone-Polyurethanes. *J. Polym. Sci. Pt. B-Polym. Phys.* **1983,** *21* (1), 65-95; (b) Li, Y.; Ren, Z.; Zhao, M.; Yang, H.; Chu, B., Multiphase structure of segmented polyurethanes: effects of hard-segment flexibility. *Macromolecules* **1993,** *26* (4), 612-22; (c) Parnell, A. J.; Cadby, A. J.; Mykhaylyk, O. O.; Dunbar, A. D. F.; Hopkinson, P. E.; Donald, A. M.; Jones, R. A. L., Nanoscale Phase Separation of P3HT PCBM Thick Films As Measured by Small-Angle X-ray Scattering. *Macromolecules* **2011,** *44* (16), 6503-6508; (d) Chu, B.; Gao, T.; Li, Y. J.; Wang, J.; Desper, C. R.; Byrne, C. A., Microphase Separation Kinetics in Segmented Polyurethanes - Effects of Soft Segment Length and Structure. *Macromolecules* **1992,** *25* (21), 5724-5729.

54.   Cullity, B. D.; Stock, S. R., *Elements of X-ray Diffraction*. Prentice Hall Upper Saddle River, NJ: 2001; Vol. 3.

55.   (a) Debye, P.; Anderson, H. R.; Brumberger, H., Scattering by an Inhomogeneous Solid .2. The Correlation Function and Its Application. *Journal of Applied Physics* **1957,** *28* (6), 679-683; (b) Strobl, G. R.; Schneider, M., Direct Evaluation of the Electron-Density Correlation-Function of Partially Crystalline Polymers. *J. Polym. Sci. Pt. B-Polym. Phys.* **1980,** *18* (6), 1343-1359; (c) Ryan, A. J.; Stanford, J. L.; Tao, X. Q., Morphology and Properties of Novel Copoly(Isocyanurate Urea)S Formed by Reaction Injection-Molding. *Polymer* **1993,** *34* (19), 4020-4031.

56.   Ranney, M. W., *Isocyanates Manufacture, 1972 (Chemical Process Review No. 63)*. 1972; p 258.

57.   Clayden, J.; Greeves, N.; Warren, S.; Wothers, P., *Organic Chemistry*. Oxford University Press: New York, 2001; p 1073.

58.   Cotarca, L., *Phosgenations--a handbook*. Vch Verlagsgesellschaft Mbh: 2004.

59.   Sayigh, A. A. R.; Ulrich, H.; Farrissey, W. J., Jr., Diisocyanates. *High Polymers* **1972,** *27*, 369-476.

60.   Eckert, H.; Forster, B., Triphosgene, a Crystalline Phosgene Substitute. *Angew. Chem.-Int. Edit. Engl.* **1987,** *26* (9), 894-895.

61.   Charalambides, Y. C.; Moratti, S. C., Comparison of Base-Promoted and Self-

Catalyzed Conditions in the Synthesis of Isocyanates from Amines Using Triphosgene. *Synthetic Communications* **2007,** *37* (6), 1037 - 1044.

62.   Twitchett, H. J., Chemistry of the production of organic isocyanates. *Chemical Society Reviews* **1974,** *3* (2), 209-30.

63.   Holfinger, M. S.; Conner, A. H.; Holm, D. R.; Hill, C. G., Synthesis of Difurfuryl Diamines by the Acidic Condensation of Furfurylamine with Aldehydes and Their Mechanism of Formation. *J. Org. Chem.* **1995,** *60* (6), 1595-1598.

64.   Davis, T. L.; Farnum, J. M., Relative velocities of reaction of alcohols with phenyl isocyanate. *J. Am. Chem. Soc.* **1934,** *56*, 883-885.

65.   Verhoeven, V. W. A.; Padsalgikar, A. D.; Ganzeveld, K. J.; Janssen, L., A kinetic investigation of polyurethane polymerization for reactive extrusion purposes. *Journal of Applied Polymer Science* **2006,** *101* (1), 370-382.

66.   (a) Draye, A. C.; Tondeur, J. J.; Tiger, R. P., Solvent effects on an organotin-catalyzed alcohol-isocyanate reaction. *Main Group Met. Chem.* **1999,** *22* (6), 367-372; (b) Draye, A.-C.; Tondeur, J.-J., Temperature effect on alcohol - isocyanate kinetics. *React. Kinet. Catal. Lett.* **1999,** *66* (Copyright (C) 2010 American Chemical Society (ACS). All Rights Reserved.), 319-324; (c) Cordeiro, N.; Belgacem, M. N.; Gandini, A.; Neto, C. P., Urethanes and polyurethanes from suberin .1. Kinetic study. *Industrial Crops and Products* **1997,** *6* (2), 163-167; (d) Zaverkina, M. A.; Lodygina, V. P.; Komratova, V. V.; Stovbun, E. V.; Badamshina, E. R., Kinetics of diisocyanate reactions with chain-extending agents. *Polymer Science Series A* **2006,** *48* (4), 382-387.

67.   (a) Sivakamasundari, S.; Ganesan, R., Kinetics and Mechanism of the Reaction between Phenyl Isocyanate and Alcohols in Benzene Medium. *J. Org. Chem.* **1984,** *49* (4), 720-722; (b) Lovering, E. G.; Laidler, K. J., Kinetic Studies of Some Alcohol-Isocyanate Reactions. *Can. J. Chem.-Rev. Can. Chim.* **1962,** *40* (1), 31-&.

68.   Yang, W. L. P.; Macosko, C. W., Phase-Separation during Fast (Rim) Polyurethane Polymerization. *Makromolekulare Chemie-Macromolecular Symposia* **1989,** *25*, 23-44.

69.   Cooper, S. L.; Tobolsky, A. V., Properties of Linear Elastomeric Polyurethanes. *Journal of Applied Polymer Science* **1966,** *10* (12), 1837.

70.   (a) Koberstein, J. T.; Galambos, A. F.; Leung, L. M., Compression-Molded Polyurethane Block Copolymers .1. Microdomain Morphology and Thermomechanical Properties. *Macromolecules* **1992,** *25* (23), 6195-6204; (b) Koberstein, J. T.; Leung, L. M., Compression-Molded Polyurethane Block Copolymers .2. Evaluation of Microphase Compositions. *Macromolecules* **1992,** *25* (23), 6205-6213.

71.   (a) Speckhard, T. A.; Hwang, K. K. S.; Yang, C. Z.; Laupan, W. R.; Cooper, S. L., Properties of Segmented Polyurethane Zwitterionomer Elastomers. *Journal of Macromolecular Science-Physics* **1984,** *B23* (2), 175-199; (b) Fu, B.; Macknight, W. J.; Schneider, N. S., Structure-Property Relationships of Segmented Polyurethanes Containing Monodisperse 2,4-Toluene Diisocyanate Butanediol Hard Segments. *Rubber Chemistry and Technology* **1986,** *59* (5), 896-911.

72.   (a) Garrett, J. T.; Runt, J.; Lin, J. S., Microphase separation of segmented poly(urethane urea) block copolymers. *Macromolecules* **2000,** *33* (17), 6353-6359; (b) Garrett, J. T.; Lin, J. S.; Runt, J., Influence of preparation conditions on microdomain formation in poly(urethane urea) block copolymers. *Macromolecules* **2002,** *35* (1), 161-168.

73.   Wang, C.-S.; Kenney, D. J., Effect of hard segments on morphology and properties of thermoplastic polyurethanes. *Journal of Elastomers & Plastics* **1995,** *27* (2), 182-99.

74.   Cawse, J. L.; Stanford, J. L.; Still, R. H., Novel Precursors Suitable for Rim Polyurethane Networks. *British Polymer Journal* **1985,** *17* (2), 233-238.

75.   Christenson, C. P.; Harthcock, M. A.; Meadows, M. D.; Spell, H. L.; Howard, W. L.; Creswick, M. W.; Guerra, R. E.; Turner, R. B., Model Mdi Butanediol Polyurethanes - Molecular-Structure, Morphology, Physical and Mechanical-Properties. *J. Polym. Sci. Pt. B-Polym. Phys.* **1986,** *24* (7), 1401-1439.

76.   Sonnenschein, M. F.; Lysenko, Z.; Brune, D. A.; Wendt, B. L.; Schrock, A. K., Enhancing polyurethane properties via soft segment crystallization. *Polymer* **2005,** *46* (23), 10158-10166.

77.   Blackwell, J.; Nagarajan, M. R.; Hoitink, T. B., Structure of polyurethane elastomers: effect of chain extender length on the structure of MDI/diol hard segments. *Polymer* **1982,** *23* (7, Suppl.), 950-6.

78.   Zdrahala, R. J.; Gerkin, R. M.; Hager, S. L.; Critchfield, F. E., Polyether-Based Thermoplastic Polyurethanes .1. Effect of the Hard-Segment Content. *Journal of Applied Polymer Science* **1979,** *24* (9), 2041-2050.

79.   Szycher, M., Biostability of Polyurethane Elastomers: A Critical Review *Journal of Biomaterials Applications* **1988,** *3* (2), 297-402.

80.   Tsuchiya, M.; Kojima, T., Melting behavior of poly(tetrahydrofuran)S and their blends. *Journal of Thermal Analysis and Calorimetry* **2003,** *72* (2), 651-655.

81.   (a) Yilgor, E.; Isik, M.; Yilgor, I., Novel Synthetic Approach for the Preparation of Poly(urethaneurea) Elastomers. *Macromolecules* **2010,** *43* (20), 8588-8593; (b) Unsal, E.; Yalcin, B.; Yilgor, I.; Yilgor, E.; Cakmak, M., Real time mechano-optical study on deformation behavior of PTMO/CHDI-based polyetherurethanes under uniaxial extension. *Polymer* **2009,** *50* (19), 4644-4655; (c) De, D.; Gaymans, R. J., Polyurethanes with Narrow- and Polydisperse Hard Segment Distributions. *Macromolecular Materials and Engineering* **2008,** *293* (11), 887-894.

82.   Willkomm, W. R.; Chen, Z. S.; Macosko, C. W.; Gobran, D. A.; Thomas, E. L., Properties and Phase-Separation of Reaction Injection Molded and Solution Polymerized Polyureas as a Function of Hard Block Content. *Polymer Engineering and Science* **1988,** *28* (14), 888-900.

83.   Krijgsman, J.; Husken, D.; Gaymans, R. J., Synthesis and properties of thermoplastic elastomers based on PTMO and tetra-amide. *Polymer* **2003,** *44* (25), 7573-7588.

84.   Schon, P.; Bagdi, K.; Molnar, K.; Markus, P.; Pukanszky, B.; Vancso, G. J., Quantitative mapping of elastic moduli at the nanoscale in phase separated polyurethanes by AFM. *European Polymer Journal* **2011,** *47* (4), 692-698.

85.   Li, F. K.; Hou, J. N.; Zhu, W.; Zhang, X.; Xu, M.; Luo, X. L.; Ma, D. Z.; Kim, B. K., Crystallinity and morphology of segmented polyurethanes with different soft-segment length. *Journal of Applied Polymer Science* **1996,** *62* (4), 631-638.

86.   Christenson, E. M.; Anderson, J. M.; Hiltner, A.; Baer, E., Relationship between nanoscale deformation processes and elastic behavior of polyurethane elastomers. *Polymer* **2005,** *46* (25), 11744-11754.

87. Camberlin, Y.; Pascault, J. P., Phase Segregation Kinetics in Segmented Linear Polyurethanes - Relations between Equilibrium Time and Chain Mobility and between Equilibrium Degree of Segregation and Interaction Parameter. *J. Polym. Sci. Pt. B-Polym. Phys.* **1984,** *22* (10), 1835-1844.

88. Bowman, I. J. W.; Brown, D. S.; Wetton, R. E., Crystal Density, Crystallinity and Heat of Fusion of Poly (Tetramethylene Oxide). *Polymer* **1969,** *10* (8), 715-&.

89. Vandenberg, E. J., Mechanism Aspects of Ring-Opening Polymerization of Episulfides Compared to Epoxides. *Journal of Polymer Science Part a-1-Polymer Chemistry* **1972,** *10* (2), 329-&.

90. Neff, R.; Adedeji, A.; Macosko, C. W.; Ryan, A. J., Urea hard segment morphology in flexible polyurethane foam. *Journal of Polymer Science, Part B: Polymer Physics* **1998,** *36* (4), 573-581.

91. Sun, Y. S.; Jeng, U. S.; Huang, Y. S.; Liang, K. S.; Lin, T. L.; Tsao, C. S., Complementary SAXS and SANS for structural characteristics of a polyurethethane elastomer of low hard-segment content. *Physica B* **2006,** *385*, 650-652.

92. (a) Turley, J. W.; JCPDS--International Centre for Diffraction Data., *X-ray diffraction patterns of polymers*. International Centre for Diffraction Data (12 Campus Blvd., Newtown Square, 19073-3273): Newtown Square, PA, 1994; p 22, 78; (b) Hwang, K. K. S.; Hemker, D. J.; Cooper, S. L., Phase-Diagrams and Morphology of a Urethane Model Hard Segment and Polyether Macroglycols. *Macromolecules* **1984,** *17* (3), 307-315; (c) Williams, S. R.; Wang, W.; Winey, K. I.; Long, T. E., Synthesis and Morphology of Segmented Poly(tetramethylene oxide)-Based Polyurethanes Containing Phosphonium Salts. *Macromolecules* **2008,** *41* (23), 9072-9079.

93. (a) Martin, D. J.; Meijs, G. F.; Renwick, G. M.; McCarthy, S. J.; Gunatillake, P. A., The effect of average soft segment length on morphology and properties of a series of polyurethane elastomers .1. Characterization of the series. *Journal of Applied Polymer Science* **1996,** *62* (9), 1377-1386; (b) Martin, D. J.; Meijs, G. F.; Renwick, G. M.; Gunatillake, P. A.; McCarthy, S. J., Effect of soft-segment CH2/O ratio on morphology and properties of a series of polyurethane elastomers. *Journal of Applied Polymer Science* **1996,** *60* (4), 557-571; (c) Blackwell, J.; Lee, C. D., Hard-Segment Polymorphism in Mdi Diol-Based Polyurethane Elastomers. *J. Polym. Sci. Pt. B-Polym.*

Phys. **1984,** *22* (4), 759-772; (d) Quay, J. R.; Sun, Z.; Blackwell, J.; Briber, R. M.; Thomas, E. L., The Hard Segment Unit-Cell for Mdi Bdo-Based Polyurethane Elastomers. *Polymer* **1990,** *31* (6), 1003-1008; (e) Bonart, R., X-ray investigations concerning the physical structure of cross-linking in segmented urethane elastomers. *Journal of Macromolecular Science, Part B* **1968,** *2* (1), 115-138; (f) Koberstein, J. T.; Galambos, A. F., Multiple Melting in Segmented Polyurethane Block Copolymers. *Macromolecules* **1992,** *25* (21), 5618-5624.

94.   Yeh, F.; Hsiao, B. S.; Sauer, B. B.; Michel, S.; Siesler, H. W., In-situ studies of structure development during deformation of a segmented poly(urethane-urea) elastomer. *Macromolecules* **2003,** *36* (6), 1940-1954.

95.   (a) Brandrup, J.; Immergut, E. H.; Grulke, E. A.; Abe, A.; Bloch, D. R., *Polymer handbook*. Wiley New York: 1999; Vol. 1999; (b) Faucher, J. A.; Koleske, J. V., Estimation of Glass Transition of Polyethylene by Extrapolation of a Series of Polyethers. *Polymer* **1968,** *9* (1), 44-&; (c) Miller, G. W.; Saunders, J. H., Thermal Analyses of Polymers .2. Thermomechanical Analyses of Segmented Polyurethane Elastomers. *Journal of Applied Polymer Science* **1969,** *13* (6), 1277-&.

96.   Kretz, M.; Meurer, B.; Lotz, B.; Weill, G., Plastic-Deformation of Polytetramethylene Oxide .1. Influence of Molecular-Weight Distribution, Crystallinity, and Structure. *J. Polym. Sci. Pt. B-Polym. Phys.* **1988,** *26* (3), 663-675.

97.   Hu, C. B.; Ward, R. S.; Schneider, N. S., A New Criterion of Phase-Separation - the Effect of Diamine Chain Extenders on the Properties of Polyurethaneureas. *Journal of Applied Polymer Science* **1982,** *27* (6), 2167-2177.

98.   Rueda-Larraz, L.; d'Arlas, B. F.; Tercjak, A.; Ribes, A.; Mondragon, I.; Eceiza, A., Synthesis and microstructure-mechanical property relationships of segmented polyurethanes based on a PCL-PTHF-PCL block copolymer as soft segment. *Eur. Polym. J.* **2009,** *45* (7), 2096-2109.

99.   (a) Zdrahala, R. J.; Hager, S. L.; Gerkin, R. M.; Critchfield, F. E., Polyether Based Thermoplastic Polyurethanes Effect of the Soft Segment Molecular-Weight. *Journal of Elastomers and Plastics* **1980,** *12* (4), 225-244; (b) Takahara, A.; Tashita, J.; Kajiyama, T.; Takayanagi, M.; Macknight, W. J., Microphase Separated Structure and Blood Compatibility of Segmented Poly(Urethaneureas) with Different Diamines in the

Hard Segment. *Polymer* **1985,** *26* (7), 978-986; (c) Velankar, S.; Cooper, S. L., Microphase separation and rheological properties of polyurethane melts. 1. Effect of block length. *Macromolecules* **1998,** *31* (26), 9181-9192.

100.   Das, S.; Yilgor, I.; Yilgor, E.; Inci, B.; Tezgel, O.; Beyer, F. L.; Wilkes, G. L., Structure-property relationships and melt rheology of segmented, non-chain extended polyureas: Effect of soft segment molecular weight. *Polymer* **2007,** *48* (1), 290-301.

101.   Pukanszky, B.; Bagdi, K.; Tovolgyi, Z.; Varga, J.; Botz, L.; Hudak, S.; Doczi, T., Nanophase separation in segmented polyurethane elastomers: Effect of specific interactions on structure and properties. *European Polymer Journal* **2008,** *44* (8), 2431-2438.

102.   Scortanu, E.; Prisacariu, C.; Caraculacu, A. A.; Bruma, M.; Sulitanu, N., New heterocyclic polyurethane-ureas based on 4,4 '-dibenzyl diisocyanate, Part 1: Influence of oxadiazole structure on mechanical properties. *High Performance Polymers* **2006,** *18* (2), 127-143.